Title

A comprehensive review of proppant embedment in shale reservoirs: Experimentation, modeling and future prospects

Authors

Katende, Allan

O'Connell, Lisa

Rich, Ashley

et al.

Publication Date

2021-11-01

DOI

10.1016/j.jngse.2021.104143

A comprehensive review of proppant embedment in shale reservoirs: Experimentation, modeling and future prospects

Allan Katende[a], Lisa O'Connell[b], Ashley Rich[c], Jonny Rutqvist[d], Mileva Radonjic[a,e,*]

[a]*School of Chemical Engineering, Oklahoma State University, 420 Engineering North: Stillwater, Oklahoma(OK) 74078, United States of America (USA).*
[b]*Stim-Lab Inc. Core Laboratories, Duncan, Oklahoma(OK),73533, United States of America (USA).*
[c]*PropTester Inc, 17222 Huffmeister Road Cypress, Texas(TX) 77429, United States of America (USA).*
[d]*Energy Geosciences Division, Lawrence Berkeley National Laboratory, Berkeley, California(CA) 94720, United States of America (USA).*
[e]*Boone Pickens School of Geology, Oklahoma State University, 105 Noble Research Center, Stillwater, OK 74075, United States of America (USA).*

Abstract

This paper provides a comprehensive review on the application of proppants to maintain fracture permeability over the lifetime of a well based on published observations from experiments and modeling. The review identifies and describes important processes occurring during proppant embedment, during hydraulic fracturing, laboratory testing of fracture conductivity, proppant embedment and modeling of proppant embedment. Finally, this paper identifies the challenges and knowledge gaps that also provide future avenues of research and opportunities for collaborative technological development which requires an interdisciplinary approach of science, engineering in academia, government, and private sector.

Keywords: Shale Gas, Tight oil, Hydraulic Fracturing, Proppant Embedment, Fracture Conductivity, Horizontal drilling.

Contents

*Corresponding author: Dr. Mileva Radonjic(mileva.radonjic@okstate.edu)is a Samson Chair at the School of Chemical Engineering, Oklahoma State University, 420 Engineering North: Stillwater, Oklahoma(OK) 74078, United States of America (USA).
Email address: mileva.radonjic@okstate.edu (Mileva Radonjic)

1. Introduction

Among the twenty two largest gas fields based on recoverable reserves worldwide, six are located in North American shale reservoirs with average recovery factors of approximately 20% (Rogers, 2011). At present, innovations in horizontal well drilling and completion supported by 3-D seismic, microseismic, formation microimager (FMI)/formation microscanner (FMS), and other measurements are unlocking supplies of natural gas throughout North America for the decades ahead (Clarkson et al., 2013; Curtis et al., 2011, 2014; Dindoruk et al., 2020; Eren and Suicmez, 2020; Kang et al., 2020; Pan et al., 2015; Rutqvist et al., 2013; Sharma and Livescu, 2020; Soeder, 2018; Soeder and Borglum, 2019; Wang and Li, 2017).

Figure 1 shows the technically proven shale hydrocarbon resources worldwide whereas Figure 2 shows the natural gas producing plays in the United States; the major shale plays are the Antrim, Barnett, Haynesville and Marcellus Shales. The United States Energy Information Administration suggests that the USA possesses more than three thousand trillion ft^3 of recoverable reserves, of which more than 30% is contained within shale formations (Boardman and Puckette, 2006; Li et al., 2016; Wang and Li, 2017).

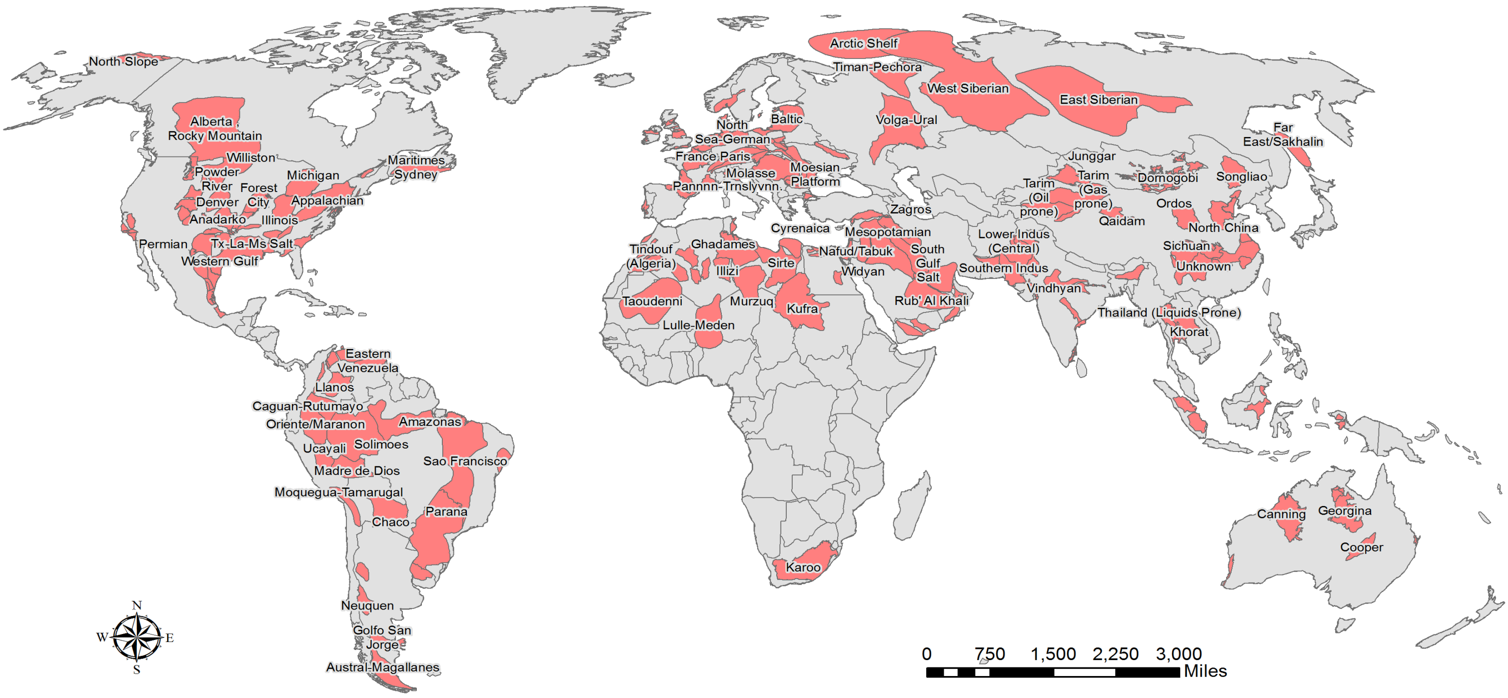

Figure 1: Geographical map showing the location of proven technically recoverable Shale hydrocarbon resources world-wide(GIS-Data obtained from EIA)

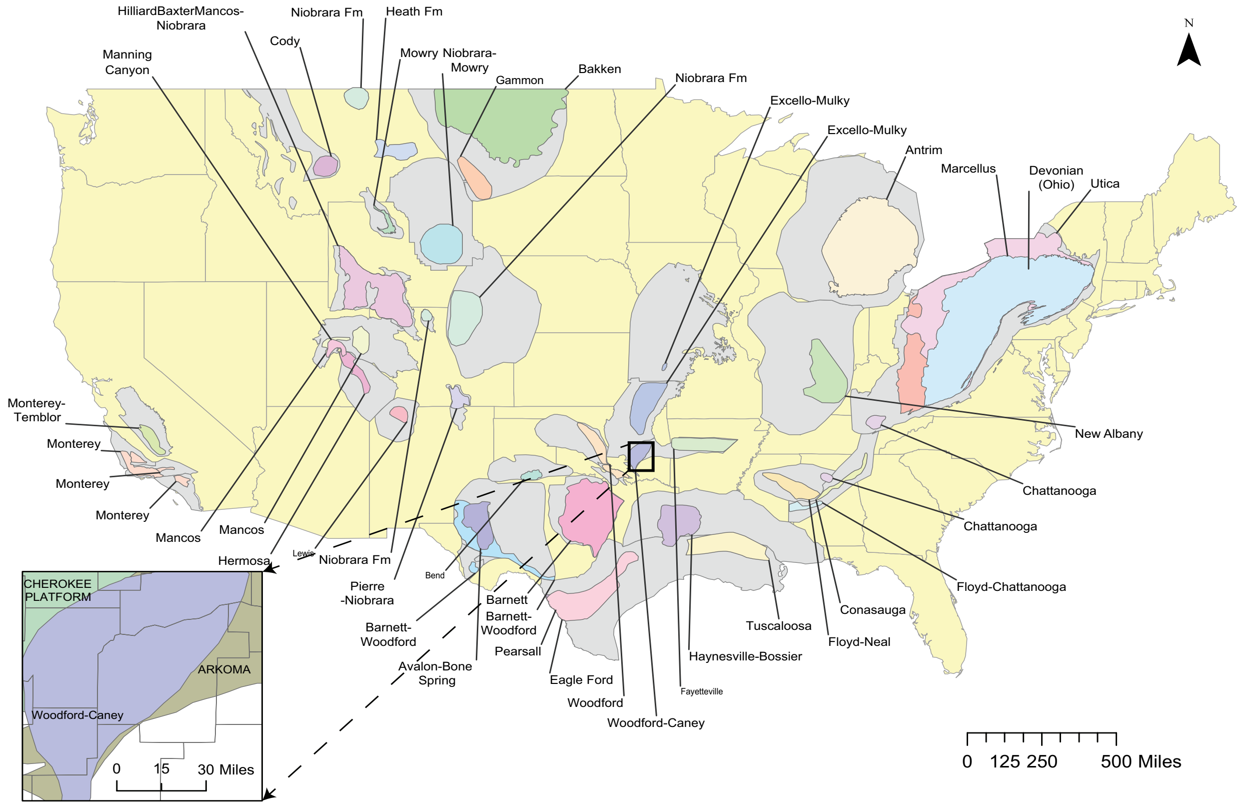

Figure 2: Shale producing plays in the United States. The figure on the bottom left shows the map of the Caney shale part of which lies in the Arkoma basin and the rest in the Anadarko basin within the Oklahoma county .

However, considerable variability in well production, even within the same field, continues to challenge our intuition about the simple and consistent nature of shale formations, the oil condensate and gas within (Bilgen and Sarikaya, 2016).

Thus, for the exploration and exploitation of the advantages of shale reservoirs, it is important to have a good understanding of its governing parameters and shale characterization demands; seismic, sonic log, and laboratory-based data (Du et al., 2021; Froute and Kovscek, 2020; Gokaraju et al., 2020; He et al., 2019; Radonjic et al., 2020; Sambo et al., 2020; Wei et al., 2019).

Through a combination of technological developments and active learning, operators are beginning to develop a mastery of the fracturing approaches employed in shale reservoirs (Ghofrani and Atkinson, 2020; Leimkuhler and Leveille, 2012; Yang et al., 2013). However, even in situations in which it is possible to complete a massive hydraulic fracture treatment (Zeng et al., 2020a), sustained production rates of the well cannot be guaranteed (Asadi et al., 2020; Dejam, 2019; Nobakht et al., 2013; Ramandi et al., 2021; Zhang et al., 2018). A significant reduction in the amount produced from the well can be observed as a result of low in-situ formation permeability (Clarkson et al., 2011; Dejam et al., 2018; Pan et al., 2015). In the case of hydraulically fractured wells, proppant failure can also lead to a rapid reduction in production (Bandara et al., 2020b; Ding et al., 2020; Tan et al., 2018). Due to higher fracture closure pressures (Wang et al., 2018a; Zhuo et al., 2020), and with the current ability to stimulate greater-depth treatments (Sutra et al., 2017), studies relating to proppant embedment are becoming increasingly relevant. Proppant embedment (Bandara et al., 2021; Maslowski and Labus, 2021) represents a particularly pressing issue in terms of low permeability reservoirs because of the marginal profits produced by wells of this nature (Chuprakov et al., 2021).

Wide and long fractures are typically required to ensure the economic viability of low-permeability candidate formations (Huang et al., 2021b; Mahrer, 1999; Torsaeter et al., 1987). Multiple propped fractures are critical for long-term production in shale formations (Buenrostro et al., 2019; Krishnan et al., 2021; Michael et al., 2020). However, it is to be expected that a substantial area of a given fracture is supported by a monolayer (Khanna et al., 2015) of proppant or less (Chuprakov et al., 2021; Huang et al., 2019; Luo et al., 2020b; Xiao et al., 2021). In situations such as this, the fracture conductivity is directly influenced by proppant embedment (Elsarawy and Nasr-El-Din, 2019; Voltolini and Ajo-Franklin, 2020; Zhi and Elsworth, 2020). Fracture closure stress will further increase during production as a result of the pressure drawdown (Alramahi and Sundberg, 2012). These pressures may increase in response to an intensification of the pressure drawdown (Zheng and Tannant, 2019) and this causes additional proppant embedment and could even cause -proppant failure in cases of high closure stress (Alramahi and Sundberg, 2012; Legarth et al., 2005).

Wang et al. (2020b) studied the correlation between particle migration, embedment, and proppant breakage on fracture diversion. They assessed the impact that fracture conductivity had on particle migration by varying the closing pressure and injection velocity. The produced fluid was obtained at various experimental stages, and the particle morphology was subsequently investigated. The outcomes revealed that particle migration, embedding, and proppant breakage all have a negative impact on fracture conductivity that correlates with flow rate and closing pressure, and a rise in fluid injection velocity exacerbates the particle migrations blocking effect.

Liu et al. (2021) examined embedment and deformation within a framework that was designed to determine the best packing ratio for proppant placement. The outcomes revealed that a lower proppant elastic modulus or rock elastic modulus causes a larger optimal proppant packing ratio and lower permeability correction factor. The conductivity correction factor-based optimal proppant packing ratio is more closely aligned with the findings of previous studies than the permeability correction factor-based value. The findings of their work also indicated that with regard to proppant deformation, the optimal proppant packing ratio is substantially greater, the optimal proppant intensities at various phases of graded proppant injection are appropriately greater, and the anticipated folds of productivity rise after stimulation is much less. Liu et al. (2021) also described how there have been some inconsistencies between the experimental and modelling results by previous scholars. They highlighted how one potential cause of the variation could be the neglectfulness of proppant deformation and proppant embedment into the walls of the hydraulic fracture. These factors may have a significant impact in soft or unconsolidated formations like ductile shales, coal bed methane, geothermal reservoirs, etc. because rigid proppants can be readily embedded within the walls of the fracture whereas soft proppants can be deformed easily, all of which can reduce the fracture aperture.

The conductivity of propped and unpropped fractures determines the effectiveness of the hydraulic fracturing process however the impairment to fracture conductivity is proppant embedment (Fan et al., 2021; Li et al., 2021; Liu et al., 2021; Maslowski and Labus, 2021; Song et al., 2021a). Studies being conducted at present are deeply focused on increasing the effectiveness of fracturing fluids, mitigating proppant embedment and raising the fracture conductivity.

Contemporary reviews on fracturing technologies, proppants and materials for coating proppants used in hydraulic fracturing have been attempted in previous studies (Ahamed et al., 2019; Barboza et al., 2021; Barree et al., 2019; Danso et al., 2021; Duenckel et al., 2016; Isah et al., 2021; Liang et al., 2016; Liew et al., 2020; Michael et al., 2020; Ramlan et al., 2021). However, substantial progress has occurred in the last decade and proppant embedment in shale has not been extensively documented. This paper has therefore focussed(see Figure 3) on proppant embedment in shale reservoirs with details on the; proppants used during hydraulic fracturing, proppant embedment with a focus on factors affecting proppant embedment and fracture conductivity while also detailing the laboratory testing of proppant embedment and fracture conductivity and finally the modeling of proppant embedment during hydraulic fracturing. To-date, there is a lack of understanding on how proppant embedment can be mitigated in ductile formations such as shale and in soft unconsolidated formations. Therefore we hope that this review can enhance our knowledge on mitigating proppant embedment and ensuring that constant production rates can always be achieved after hydraulic fracturing and well completion.

2. Methodology

This review has been based on original research articles on the evaluation and optimization design of long-term conductivity of propped fractures in shale reservoirs during hydraulic fracturing. The review process followed a reiterative process where search items were updated as the review process progressed. The selection of literature to include was based on peer reviewed journal articles as well as peer reviewed conference proceedings. The literature search was done based on scientific databases that include; Scopus, ScienceDirect, Taylor & Francis, Springer. Where previous databases listed were limited, Google Scholar was used to expand the search process. To include several keywords in a single search, the boolean operator ”AND” was used during the search. Where necessary; the literature search was confined to articles published within the last decade. An exception was made in areas with limited peer reviewed articles available. There wasn't any geographical limit that was applied during the review process. A total of 260+ references were reviewed where the majority are peer reviewed journal articles. Figure 3 shows the scope and structure of this review.

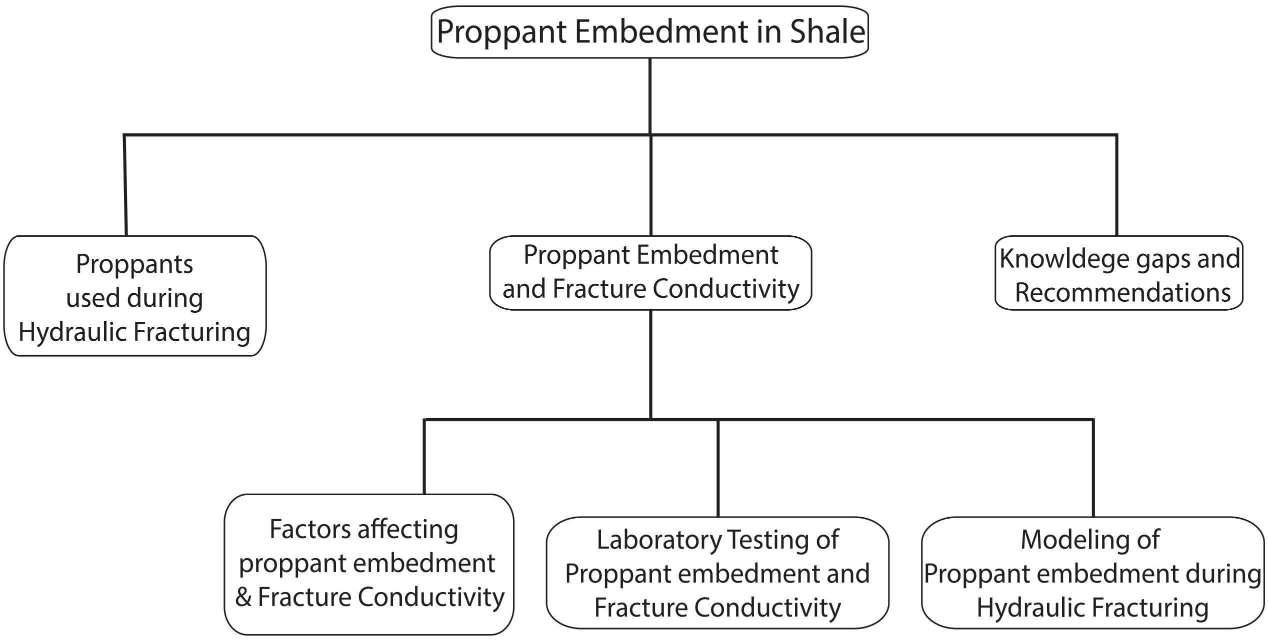

Figure 3: Scope and structure of the review problem.

3. Proppants: history, source, mineralogy, shape & size, mechanical and chemical stability

The purpose of proppants, such as sand, is to hold the fractures open after the drilling fluid flows back into the wellbore(Nimerick et al., 1992; Sinclair et al., 1983). Polymers have been used extensively in the petroleum industry to optimize the drilling of wells. More recently, they have been used for proppant coating during hydraulic fracturing in order to improve their strength (Dewprashad et al., 1993; Michael et al., 2020; Zoveidavianpoor et al., 2018). Proppants illustrated in figure 4 are similar in nature to spheres that are small enough with sufficient strength to resist the large stresses in the well and rock formation. Proppants coated with thin layers of polymer in general result in high fracture conductivity, which improves the quality of the hydraulic fracturing treatment.

Proppants may be grouped into conventional and advanced propppants. Conventional proppants include sand, ceramics, nutshells, and glass beads, whereas polymer coated proppants are advanced proppants. Conventional proppants work fairly well and are much cheaper than advanced proppants. However, ceramics are the advanced proppants, resin coated proppants are not widely used in shale wells due to problems with low permeability. The cost of RCP or ceramics is much higher than 100 mesh sand, and with the volumes of sand proppant increasing, the well cost tends to be dominated by proppant cost. Smaller unpropped fracture systems do not perform well. (Besler et al., 2007; Melcher et al., 2020; Zoveidavianpoor et al., 2018).

Sand was the first proppant to be utilized in hydraulic fracturing, but it was not able to endure the high stresses of deeper rock formations. Consequently, ceramics were introduced, as they are able to withstand high stresses; however, due to their high specific gravity, their utilization has been restricted. Glass beads were subsequently suggested, but their high cost of production and relatively low resistance to closure stresses limited their applications as well. To combat these problems, polymer coating was proposed. A polymer coating can provide adequate resistance to closure stresses and prevent flowback, allowing the formation to be cleaned up with ease and also hinder settling of proppants (Beckwith, 2011; Zoveidavianpoor et al., 2018).

The fracture walls are held open by proppants, thereby forming a conductive path that connects the reservoir to the wellbore after pumping and fracturing fluid leak-off. Successful hydraulic fracturing treatment demands the right proppant type at the right concentration. Most treatments use sand as the proppant due to its obtainability, cost-effectiveness, and adequate fracture conductivity at closure stresses up to 6000 psi,(Table 1) Furthermore, sand can be strengthened through the addition of a resin coating (e.g. Northern White Sand), which, depending on the type of resin, allows its use with closure stresses up to 8000 psi,(Table 1), enhances the proppant strength, and decreases flowback during production. Coating sand with resin also increases its conductivity for closure stresses above 4000 psi while not affecting the resins fluid effects (Krishnan et al., 2021; Melcher et al., 2020). Despite their reliability and versatility, some components of resin-coated proppants (RCPs) can negatively interact with some of the common additives of fracturing fluids, e.g. organometallic crosslinkers, and oxidative breakers (Norman et al., 1992). According to Assem and Nasr-El-Din (2015); Chuprakov et al. (2021); Deng et al. (2014); Iriarte and Tutuncu (2018); Michael et al. (2020); Nimerick et al. (1992); Norman et al. (1992); Songire et al. (2019), this affects organometallic crosslinking, hinders the bonding of the proppant pack, and reduces the clean-up of fracturing fluid, thereby increasing proppant crushing and affecting flowback and reducing permeability. However, issues with proppant flowback can also be addressed using fiber technology, which is chemically compatible and does not require special curing in terms of temperature or time. (Chuprakov et al., 2020; Sallis et al., 2014)

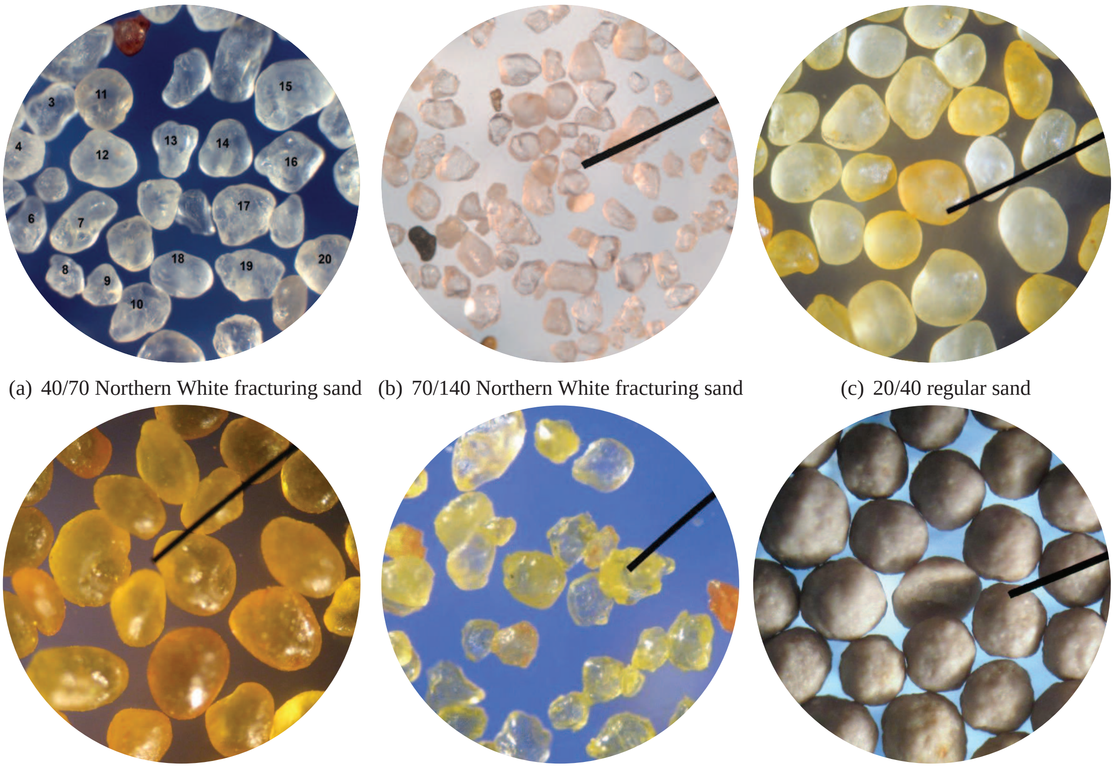

(a) 40/70 Northern White fracturing sand (b) 70/140 Northern White fracturing sand (c) 20/40 regular sand

(d) 20/40 Resin coated sand (e) 40/70 Resin coated sand (f) 20/40 Ceramic proppant

Figure 4: Optical micro-graphs illustrating commonly used proppants taken at 40X.

Table 1: Comparisons of embedment influencing properties for different types of proppants(Zoveidavianpoor et al., 2018)

Properties	**Chemically Modified Reinforced Composite Proppant**	**Frac Sand**	**Resin Coated Sand**	**Ceramic**	**Light weight ceramic**	**Coated ceramic**	**Medium strength ceramic**	**Medium strength coated ceramic**
Roundness	0.8	0.7	0.8	0.9	0.9	0.9	0.9	0.9
Sphericity	0.8	0.7	0.8	0.9	0.9	0.9	0.9	0.9
Bulk Density, g/cm^3	0.68	1.54	1.46	1.56	1.55	1.5	1.55	1.5
Solubility in HCl/HF	1.8	4.59	0.3	5.89	<2%	<2%	<2%	<2%
Crush, wt% fines generated at 8000 psi	0.1622	9.5	0.8	5.2	–	0.57	–	0.37
Turbidity (FTU)	38	<100		80	<100	<100	<100	<100
Specific gravity	1.42	2.66	2.8		2.8	3.2	3.2	3.4
Pressure (psi)	<8000	<5000	<8000	>10,000	>10,000	>10,000	>10,000	>10,000
Temperature (^{o}F)	<300	<200	<250	>300	>300	>300	>300	>300

4. Proppant Embedment and Fracture Conductivity

Proppant embedment is a vital step in drilling reservoirs with low permeability (Atteberry et al., 1979; Cooke, 1977; Coulter and Wells, 1972; Holditch and Ely, 1973; Tan et al., 2020; Wang et al., 2020c). Proppants hold fractures open, allowing oil and gas to be produced. However, many issues arise when transporting proppants (Barboza et al., 2021; Clark, 2006; Isah et al., 2021; Li et al., 2021; Luo et al., 2020b; Wen et al., 2007; Zhang et al., 2015). Proppants are meant to keep complex fractures open (Maslowski et al., 2018), but those proppants do not travel as far into the fracture network as expected before stopping due to excessive roughness and the fracture geometry (Ma et al., 2020b; Sahai and Moghanloo, 2019). Subsequent closure of those fractures diminishes production (Wang et al., 2018a; Zhuo et al., 2020).

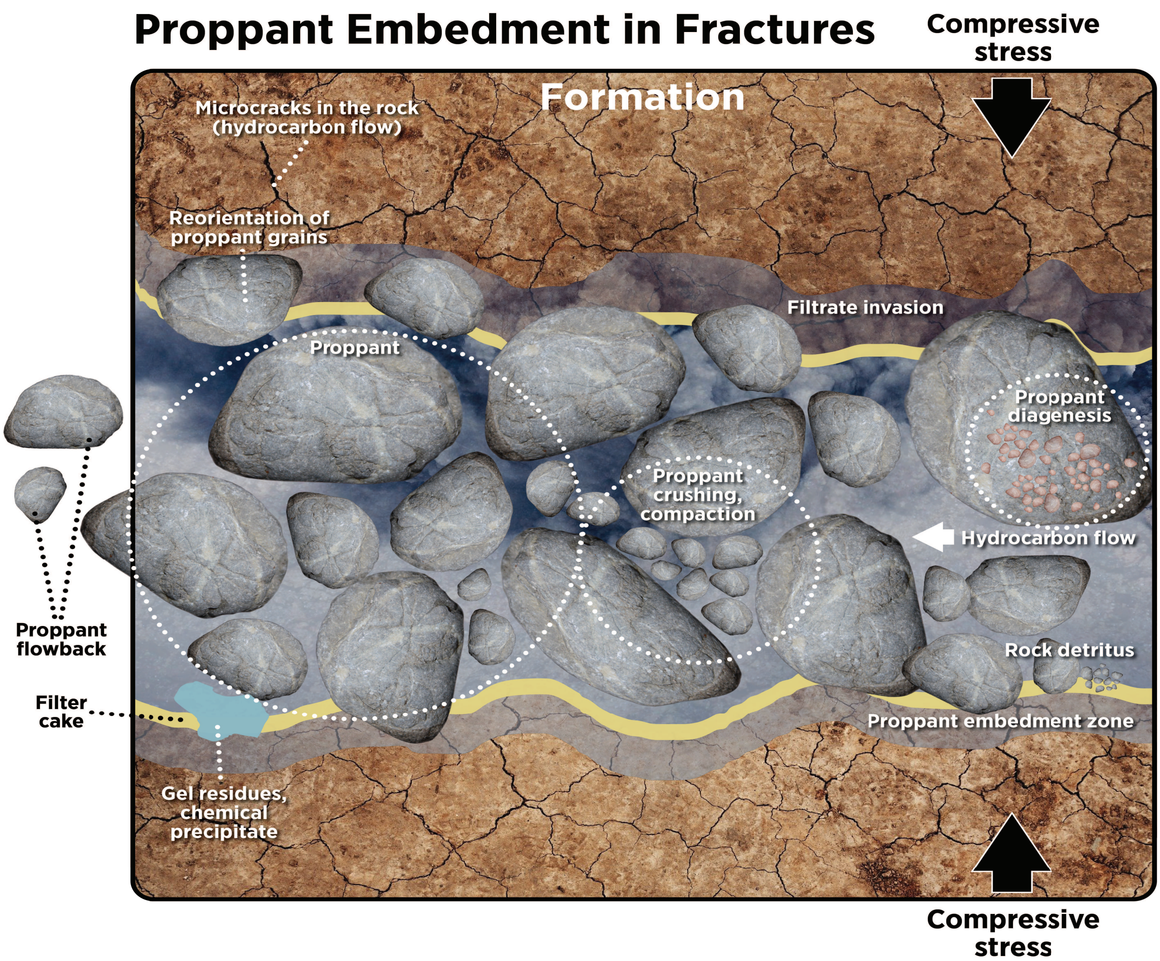

Figure 5: Illustration of physical phenomena that affect an effectively packed fracture due to proppant embedment after the hydraulic fracturing of a shale reservoir.

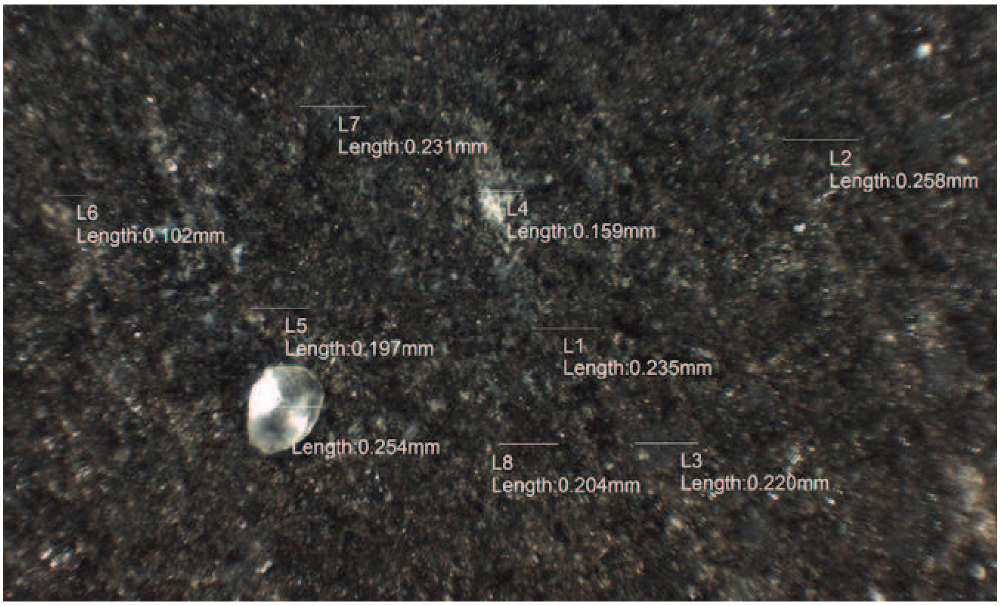

Figure 6: Optical micro-graphs showing northern white proppant embeded in a shale core.

After stimulating a well, the conductivity and porosity of the well will decline because of proppant embedment as well as deformation (Bandara et al., 2020a; Hou et al., 2020; Wang and Elsworth, 2018; Wang et al., 2018b). As the closure pressure increases, proppants will deform the fractures and impede the porosity of the formation (Alramahi and Sundberg, 2012; Zheng and Tannant, 2019). Figure 5 shows how proppants are deformed by one another and how the formation is similarly changed by the proppants. In addition to the damage mechanisms outlined in Figure 5, breakdown of the fracture faces from proppant creates additional fines which are an additional source of material occluding pore throats and damaging porosity as shown in Figure 6.

Many studies are ongoing to determine what influences the embedment of proppants and they are demonstrating that the major influencing factors are the; closure stress, particle size, and proppant concentration(Li et al., 2018; Voltolini and Ajo-Franklin, 2020; Wang and Elsworth, 2020, 2018; Wang et al., 2018a; Zheng et al., 2020). Simulations of proppant embedment are also ongoing as curtailed in section 6; the proppants are being modeled as regular spheres and arranged in a diamond shape between particles (Li et al., 2018). The simulations show that under a closure stress, proppants become embedded into the rock, changing its porosity (Gu et al., 2015; Li et al., 2018; Osiptsov et al., 2020; Zhang and Hou, 2015). After the fracturing fluid is withdrawn from the wellbore, the mechanical properties of the shale are also modified (Bai et al., 2020; Zhao et al., 2020). Youngs modulus and Poissons ratio predicted in the simulations as well as measureed in experimental data indicate that as the proppant embedment depth increases, Youngs modulus decreases, and poissons ratio increases (Chen et al., 2019; Zhong et al., 2019), this is more closely related to the affected zone.

Table 2 illustrates a summary of the previous studies investigating proppant embedment.

4.1. Factors Influencing proppant embedment and fracture conductivity

Lee et al. (2016) argues that well productivity is impacted by conductivity losses in a fracture network. Cooke (1973b); Gaurav et al. (2012); Lee et al. (2016); Lehman et al. (1999); Miskimins and Alotaibi (2019); Schubarth and Tayler (2004) have examined the proppant pack conductivity for material selection purposes. According to Lehman et al. (1999), reference conductivity data can be considered quite optimistic; in fact, the actual conductivity of the fractures is typically lower than the expected fracture conductivity. As such, all of the detrimental effects from downhole scenarios should be taken into consideration when defining the proppant conductivity (Hlidek and Duenckel, 2020; Ning et al., 2020).

The following factors affect proppant conductivity.

4.1.1. Proppant Quality

Several scholars Luo et al. (2020b); Sookprasong (2010); Volk et al. (1981); Zhang et al. (2015) have examined the in situ closure stresses on proppant-induced fractures. Their work involved conducting experiments and mathematical modeling of the permeability, the closure stresses, the closure of fractures and the pressures around the fracture and the wellbore. Their results demonstrated that the type of closure stress in response to the proppant in the fracture will result in both elastic and nonelastic deformation. Moreover, Alramahi and Sundberg (2012) , Lee and Yasuhara (2013), Lee et al. (2009) have stated that an evolving stress field also impacts both the proppant placed within hydraulic fractures and the changes in the chemical compositions of the fluids present in the porosity. To determine the treatment quality, it is essential to select the proper type of proppant since the final fracture conductivity would be primarily a result of the treatment quality (Montgomery and Steanson, 1985; Terracina, 2011; Vincent and Huckabee, 2007).

Below are some of the factors that affect proppant quality.

4.1.1.1. Type

After the injection phase ceases, to keep the fractures open, different types of proppants can be used (Xu et al., 2020). As shown in Figure 4 and table 1 the main proppant types are lightweight ceramics (LWC), high-strength proppants (HSP), natural sands, resin-coated sand (RCS) and RCP, and intermediate-strength proppants (ISP).

The most popular and commonly used proppant is natural sand (quartz sand) due to its widespread availability and low cost but it results in a significant loss of fracture conductivity and a reduction in estimated ultimate recovery (Syfan and Anderson, 2011).

Bandara et al. (2020c) performed experiments to evaluate the type of proppants on the general quality of proppants. Their study involved using; resin coated sand, sintered bauxite ceramic, and natural sand as proppant test specimens. Their results in figure 7 indicated that a great amount of fines were generated from sand in comparison to resin-coated proppants and ceramic proppants. They also observed a great increase in compaction and proppant porosity for all proppants indicating that whatever the type of proppant used, proppant pack porosity and compaction reduction is expected under a higher stress confinement.

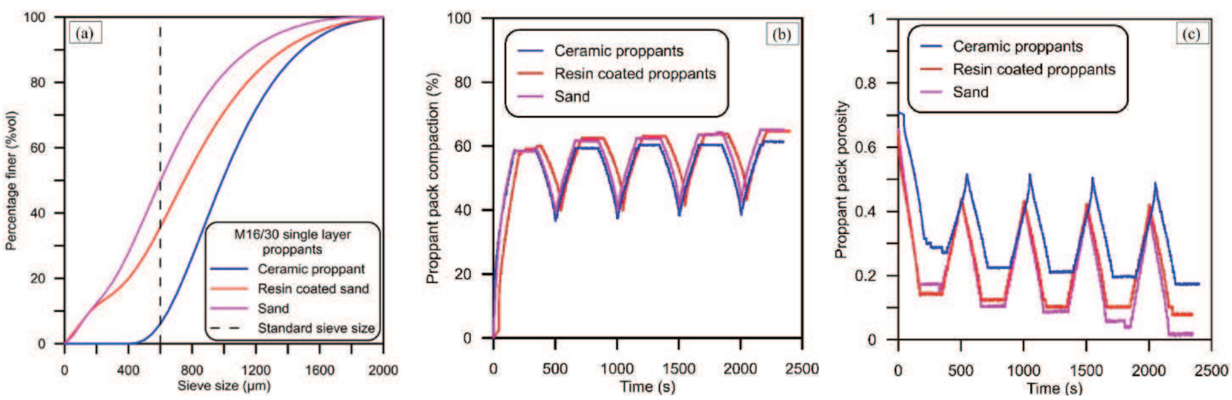

(a) The effect of particle size on varying types of proppants

(b) How compaction of the proppant pack varies with types of proppants

(c) Porosity of the proppant pack varies with proppant type.

Figure 7: Investigating the effect of proppant type (Bandara et al., 2020c).

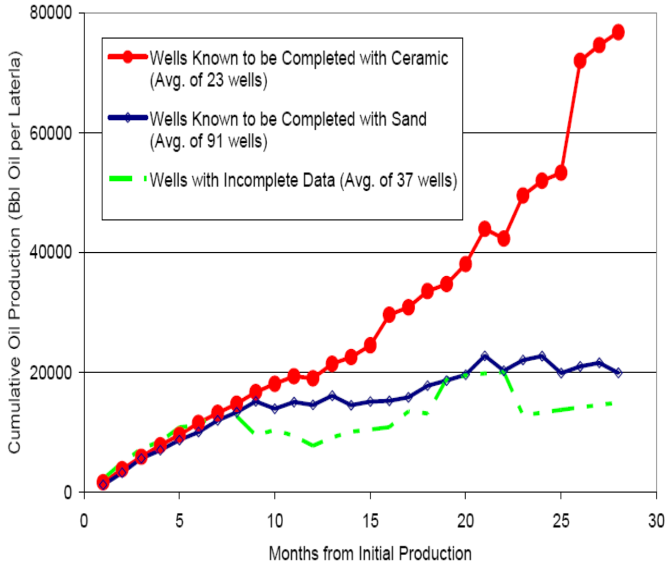

Figure 8: Effect of proppant type on cumulative oil production per lateral for Ceramic, Sand proppants and an unknown completions in North Dakota (Besler et al., 2007)

Besler et al. (2007) observed based on figure 8 that long-term production was sustained from wells where ceramic proppants were used as compared to conventional sand implying that the type of proppants used can significantly affect production.

4.1.1.2. Size

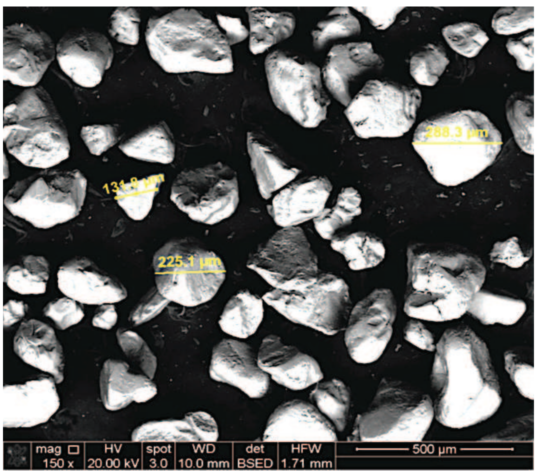

Figure 9: SEM Optical micro-graph of the 40/70 Northern White fracturing sand taken at the Venture I facility at Oklahoma State University Laboratory. This micro-graph shows a variation in proppant size as well as sphericity even within the same batch of proppants.

Many scholars have deduced that in hydraulic fracture treatments, the proppants size range is imperative and typically lies between 8 and 140 mesh (0.0937 in and 0.0041 in). The number of protrusions across one linear inch of screen specifies the mesh size (Bandara et al., 2020c; Guo et al., 2012; Schmidt et al., 2014). The term 'sieve cut' refers to the proppant when detailing the proppant size (Barree et al., 2019). For instance, 20/40 mesh is labelled 0.0331 in and 0.0165 in; 40/70 mesh is 0.0165 in and 0.0083 in; and 70/140 mesh is 0.0083 in and 0.0041 in.

As it is evident in figure 9, that proppant size and sphericity can vary implying that proppants are available in various sizes (Schmidt et al., 2014). Fracture conductivity is typically a function of particle size, wherein a larger particle size leads to a higher fracture conductivity (Huckabee et al., 2005). The near-wellbore conductivity can be maximized with the traditional fracture treatment: initially utilizing a relatively small-size proppant tailored with a larger-size proppant (Guo et al., 2012). Improved permeability and a correspondingly improved conductivity have been noted with proppants comprising larger grain sizes. However, due to their greater contact area with the fracture, proppants with large particles tend to be weaker and more easily crushed because they support a larger load. Conversely, regarding the occurrence of crushing and invasion of fines, although smaller grains demonstrate higher strength and resistance, they have less permeability (Bandara et al., 2020c). As such, a constant proppant grain size can be achieved by minimizing the mesh range to attain a better permeability. Commonly, proppant particles with a variety of sizes are mixed in hybrid completion designs based on the assumptions and criteria of the stimulation design. Correspondingly, permeability can be potentially reduced in stimulation treatments by mixing various proppant sizes (Schmidt et al., 2014). For instance, relative to 20/40 proppant, the application of 100 mesh is likely problematic, as the 100 mesh can invade and occupy pore space (Dontsov and Peirce, 2014).

Carroll and Baker (1979), Schmidt et al. (2014) explored the performance of a variety of proppant sizes on tail-in mixing and on the mixing of a variety of proppant sizes; their studies revealed that the conductivity of proppant-filled fractures is significantly impacted by higher concentrations of high-conductivity proppant. For instance, irrespective of the proppant concentration, the conductivity of the overall proppant pack is significantly improved by mixing large-size lightweight ceramic(LWC) proppant and 40/70 sand. Similarly, the same conductivity can be achieved at high concentrations of 40/80 LWC proppant mixed with larger LWC proppant particles and at low concentrations of 40/70 sand mixed with larger LWC proppant particles.

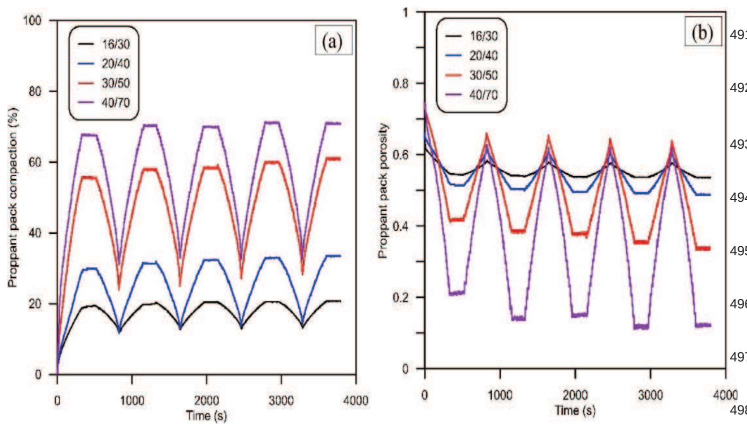

Figure 10: (a) Variation in compaction of the proppant pack and (b) porosity of proppant pack with proppant size (Bandara et al., 2020c).

To progressively evaluate the effect of proppant size, Bandara et al. (2020c) used only ceramic proppants from sizes, 16/30, 20/40, 30/50 and 40/70 at a constant maximum stress of 70 MPa packed in three layers and loaded for five cycles. Their results in figure 10 indicated that when the proppant size decreases, there is an increase in proppant pack compaction which leads to a reduction in proppant pack porosity and they hypothesised that larger proppants are generally recommended for well stimulation.

4.1.1.3. Roundness and Sphericity

Sphericity and the smoothness of edges refer to the roundness of the grains and indicate how closely their shape resembles a sphere (Elochukwu and KhaiKiat, 2021; Lyu et al., 2019). El-Kader et al. (2020) contends that proppants in general must have a certain roundness in order to maintain their mechanical strength and the roundness and sphericity of most proppants is about 0.9. Tang et al. (2017) observed that, the higher the roundness and sphericity, the better the proppant transportation in cracks was and that little fracturing fluid was needed.

The proppant pack porosity is directly proportional to the roundness or sphericity of the grains. Furthermore, round and spherical grains that are similar in size demonstrate increased strength due to the even distribution of stress (He et al., 2020).

Hao et al. (2020), Xu et al. (2020) have compared ceramic proppants against quartz sand and deduce that the uniformity in size and shape contributes to a higher sphericity and roundness which in turn contributes to a higher porosity and permeability during hydraulic fracturing. Round proppant flows out of the fracture more easily during cleanup than does proppant with sharper edges that tends to lock in place.

4.1.1.4. Strength

A comparison of the most popular commercial proppants is presented in Figure 4 and table 1. The closure stress or minimum horizontal stress illustrated in Figure 5 represents the pressure exerted by the formation on the proppant. Proppant grains must be sufficiently strong to withstand this pressure (Tang and Ranjith, 2018; Wu et al., 2017). According to Haoze et al. (2021); Huckabee et al. (2005); Ma et al. (2020a); Naima et al. (2020), an inadequate proppant strength may cause the proppant to be crushed under the closure stress; as a result, due to the creation of fines, the proppant pack will suffer reduced conductivity and permeability. Smaller proppant has more load support area and is much stronger than larger proppant of the same type (Song et al., 2021b). Thus, a higher proppant strength would result in a better retained conductivity at the closure pressure (Cooke, 1977; Cooke et al., 1977; Melcher et al., 2020; Tasque et al., 2021).

4.1.2. Proppant Pack Damage

Proppant pack damage is a serious problem during hydraulic fracturing (Huang et al., 2021a; Tandon et al., 2018; Weaver et al., 2009b). In-situ stresses and temperature can lead to damage of the proppant pack which results in reduced porosity of the proppant pack (Han et al., 2016; Luo et al., 2020b; Raysoni and Weaver, 2012). As a result of mechanical damage, there is; proppant embedment, proppant flowback, proppant crushing and proppant pack diagenesis as illustrated in figure 5 and figure 11.

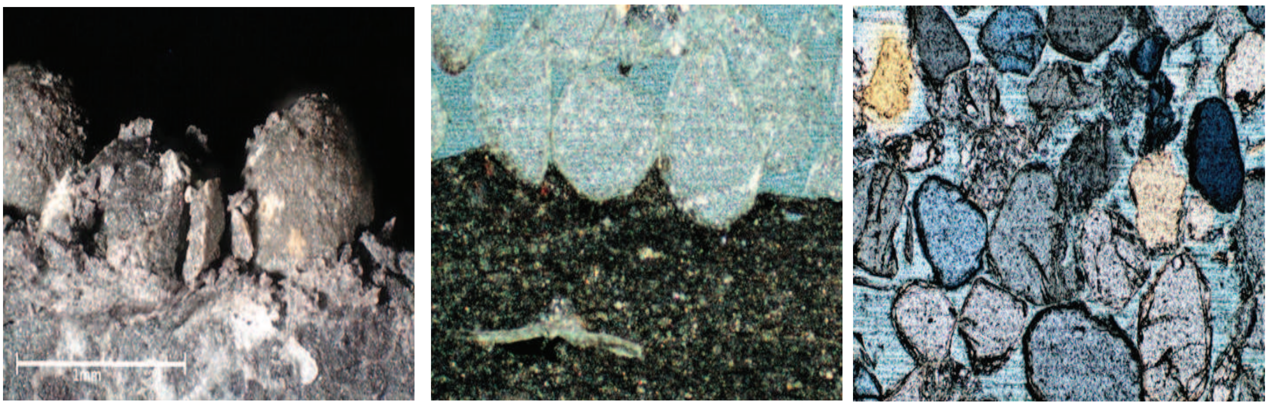

(a) (b) (c)

Figure 11: Optical micro-graphs showing: (a)Fractured High Strength Proppant in the Niobrara Shale (b)Proppant embedment of regional sand in the woodford shale. (c)Proppant crushing of regional sand

Below is a discussion on the factors resulting in proppant pack damage;

4.1.2.1. Proppant Embedment

As shown in Figures 5, due to the reduced width of the proppant pack when embedding proppants into the fracture walls, there is a reduction in conductivity (Luo et al., 2020b).

Arshadi et al. (2017) studied the effect of deformation on two phase flow using middle east proppant(generally sand grains used in the Bakken shale) packed shale samples and visualised the effects using X-ray microtomography. Their results denoted that when closure stress conditions remained constant, proppant packs in the fracture prevented deformation and the degree of embdement was dependent on the amount of clay and quartz present in the shale.

Osiptsov et al. (2020) looked at how fracture conductivity was affected by proppant embedment. Their study involved using a coupled finite element model in which the geomechanics were treated in combination with the fluid displacement model in the fracture. Their results revealed that proppant pack compaction greatly influenced conductivity and the decrease in embedment had an insignificant effect on well production.

Moreover, Voltolini and Ajo-Franklin (2020) conducted an experimental study to investigate the development of propped fractures by using an in-situ microtomography.

Their study involved using; ottawa sand and ceremic ball blasting beads as proppants on three different formations ie; Eagle-ford shale, Marcellus shale & Niobrara shale . Results revealed that ceramic proppants performed better than ottowa sand because the roundness reduced conductivity losses in the fracture and their high strength reduced proppant pack damage. Furthermore, their results revealed that ceramic propped fractures remained optimal over a range of closure pressures. They also observed partial embedment in all shales when quartz grains were intact.

Embedment also results in spalling, as the failure of the reservoir rock will generate fine particles (Osiptsov et al., 2020; Terracina, 2011; Terracina et al., 2010). When using smaller proppants, because of the better load distribution, less embedment is typically observed (Bandara et al., 2020c).

4.1.2.2. Proppant Geochemical Diagenesis

Weaver et al. (2005) coined the term "proppant diagenesis" after observing mineral precipitates during the rock-fluid and proppant interaction. Later on; Duenckel et al. (2012, 2011) , Elsarawy and Nasr-El-Din (2018) defined diagenesis that; when crystalline precipitation is observed in laboratory observations of proppants, this precipitation is referred to as diagenesis. Diagenesis shown in figure 5 entails a series of three processes (Ghosh et al., 2014; LaFollette and Carman, 2010; Lee et al., 2010)

(1) impinging of the grain-grain contact leads to dissipation,
(2) the interfacial water film that distinguishes the grains leads to dissipation,
(3) precipitates at the walls of the pore.

The loss of porosity is observed during diagenesis from proppant dissolution, followed by subsequent remineralization along the pack, resulted in a direct damage of pack permeability (Ghosh et al., 2014; Gupta et al., 2019; Karazincir et al., 2018, 2019).

Weaver et al. (2005, 2006, 2007) looked at the impact of fracture conductivity due to diagenesis and reported that when the strength of the proppants was high, porosity filling reactions were exasperated due to the formation of minerals akin to clay.

Correspondingly, Elsarawy and Nasr-El-Din (2018, 2020) have studied diagenesis of the eagle ford shale by aging the sand, ceramic and resin coated proppants together with the shale samples using de-ionised water for a period of three weeks at 325^{o}F and 300psia. Their results revealed that because of the dissolution reactions of the shale with de-ionised water, calcium sulphate and calcium zeolite precipitated from the shale samples with ceramic proppants. Sand and resin coated proppants had no effect of precipitation but changed the composition of the elements of zeolite precipiate due to the rock fluid-interaction. This dissolution was due to the presence of silicon(Si) ions. Thereofre the presence of Si–ions is believed to be a major contributing factor to diagenesis and needs to be addressed during hydraulic fracturing.

4.1.2.3. Proppant Crushing

Formation closure (Shuang et al., 2020) is the major source of crushing, specifically in cases where the proppant is not well distributed (Palisch et al., 2009). Commonly, crushing is less prevalent towards the pack center and more prevalent at the interface (Han and Wang, 2014). Previous scholars (Barree and Conway, 2000; Dusterhoft et al., 2004; Schubarth and Tayler, 2004) have also reported that depending on the amount of stress induced on the proppant pack, the grain to grain contact may be increased leading to crushing and fracture conductivity reduction due to deformation.

Bandara et al. (2020c) looked at a series of parameters such as; proppant size, type, and concentration and they analysed results of particle size with a Mastersizer 2000 optical analyzer. The authors suggested that proppant crushing occurred when the highest stress levels were induced and this led to proppant pack damage. Their results also showed that a large quantity of fines were generated by sand compared to ceramic proppants and resin coated proppants.

It is therefore important to improve crushing resistance of proppants and reduce the impact of formation damage, this is particularly true for large grain proppant less so for the 100 mesh sizes..

4.1.2.4. Proppant Flowback

In the petroleum industry, choking and proppant flowback are eminent and are considered to be potentially bothersome (Terracina et al., 2000). Proppant back-flow on cleanup is a significant problem because most proppant flow is seen before the fracture closes which can take days in an ultra-low permeability formation like shale. There are still debates (Frederic et al., 2011) that flowback would not be a problem during production, however, these controversies have limited validity due to the following;

1. displacing proppants horizontally from the wellbore leaves an inadequately propped zone or channel around the well.
2. dynamic pressure redistribution or unintentional hydraulic fracturing when the well is shut in as well as during its operation can be the cause of this overflushing.

Likewise, any intentional or unintentional flowback can re-introduce proppants back into a well. This may take place after hydraulic fracturing, during production, during a hard shutdown, which would send a pressure signal into and out of a fracture, and during pressure redistribution when the well is shut–in (Trela et al., 2008; van Batenburg et al., 1999).

Almond et al. (1995) have studied RCP and what factors would impact their flowback. Their laboratory studies involved; varying the pH of the fluid from 7 to 12, using potassium chloride fluid, seawater and borate fracturing fluid; varying the closure stress; stress cycling and finally looked at the bottom-hole circumstances during proppant flow-back. Their work exemplified that; when pH was increased, the resin removal percentage increased and correspondingly UCS decreased, with borate fracturing fluid, there was a reduction in UCS compared to samples immersed in potassium chloride.

Shor and Sharma (2014) conducted modeling of proppant transport considering movements of discrete particles and provided an explanation to parameters that would lead to an increased rate of flow back and these include; closure stress, fluid velocity, cohesion between contacting of proppants and fracture width. Their work demonstrated that the width of the fracture was a function of closure stress and fluid velocity whereas the proppant flowback was a function of cohesion between particles that could be enhanced in resin coated proppants. High production flow rate would impact the fracture as high fluid velocity tended to loosen particles and destabilized the proppant pack. Shor and Sharma (2014) therefore recommended gradual flow rate buildup to ensure confining stress on proppant pack before imposing high fluid velocity.

4.1.3. Shale rock susceptibility to proppant embedment as a result of Geomechanical Properties

The influence of rock mineralogy on the shale's geomechanical properties has been studied extensively by Cheng and Bunger (2015); Detournay and Cheng (1993); Dewhurst et al. (2013); Dong et al. (2017, 2018); Eshkalak et al. (2014); Jacobi et al. (2009); Lawal and Mahmoud (2020); LeCompte et al. (2009); Yang et al. (2015, 2018), who indicated that Youngs modulus, brittleness, and hardness usually rise with a reduction in the fraction of clay minerals or an increase in the fraction of carbonate minerals. Furthermore, Dong et al. (2018) , Ghanizadeh et al. (2015) , Vafaie and Kivi (2020) , Yang et al. (2018) demonstrated that increased brittleness is caused by a high fraction of carbonate minerals, while biogenic quartz improves brittleness. Moreover, the Total organic content only slightly impacts the geomechanical properties of high thermal maturity shales.

Abousleiman et al. (2007) has evaluated the geomechanical properties of the woodford shale(whose clay content is mainly illite and chlorite) using a triaxial cell, a brazillian test on samples exposed to drilling and fracturing fluids and finally correlating the parameters to field log data. Their results postulated isotropic that drilling or fracturing fluids have a great significance on compressive stress and tensile stress. Young's modulus of elasticity, poisson's ratio and other mechanical properties correlated to log data were found to be largely isotropic.

Sierra et al. (2010) made a follow-up study on the mechanical properties and the effects of lithofacies on the woodford shale and their results revealed that the upper woodford which is lower in clay content had a much higher fracture toughness in comparison with the lower and middle woodford.

Ma and Zoback (2018) studied Bakken core samples subjected to recurring hydrostatic loads and observed that the cyclic mechanical response were indicative of consistent results after seasoning but variability and uncertainties in experimental data were lost due to seasoning because seasoning closed micro-cracks and constricted soft parts. The question that remained to be pursued was; can seasoning be representative of a material in in-situ state?

It is difficult to quantify geomechanical properties (Iferobia and Ahmad, 2020; Rezaei et al., 2020) that would lead to inefficient fracture conductivity and eventually proppant damage. Many studies have been carried out involving laboratory equipment such as; triaxial cell (Frash et al., 2019; Islam and Skalle, 2013), X-ray Computed tomography (Voltolini, 2021), unconfined compressive stress measurements (Rezaei et al., 2020) and based proppant strength tests (Bandara et al., 2020c) acquired under ideal laboratory conditions, which are API RP 19D (Duenckel et al., 2016) compliant using one-and-a-half inch wide and one-tenth inch long conductivity cell that accommodates sandwiched rock-proppant-rock samples and it is utilized for the analysis of fracture conductivity loss and proppant pack damage.

4.1.4. Shale rock/hydraulic fracturing fluid interaction and its impact on proppant embedment

Selecting the right fracturing fluid is essential to hydraulic fracturing. The fluid is primarily used to maintain an open fracture as well as to convey the propping agent along the fracture. Fluid selection generally considers viscosity (Yang et al., 2020) as this affects proppant transport, fluid loss, and fracture geometry, as well as cleanliness following flowback to ensure maximum conductivity after the fracture. Certain cases may require other fluid characteristics to be taken into account, such as whether it is compatible with other materials, e.g. resin-coated proppants, and the rock, fluids and pressure of the reservoir; for example, the use of foams can facilitate flowback in reservoirs under low pressure. In addition, the choice of fluid is further conformed by; environmental, safety, and cost factors as well as pipe friction and surface pump pressure.

A large quantity of fluid makes contact with the rock formation during hydraulic fracturing, giving rise to physical and chemical interactions (Alagoz and Sharma, 2021; Edgin et al., 2021; Jeffry et al., 2020; Khan et al., 2021; Qingyun et al., 2020; Xiong et al., 2020; Zeng et al., 2020b). The chemical equilibrium of the rock, hydrocarbon, and connate water system is disrupted by the treatment fluid (Gundogar et al., 2021; Khan et al., 2021). This leads to the physical and chemically alteration of a zone of rock directly adjacent to the fracture face (Bremer et al., 2010; Lyu et al., 2020; Weaver et al., 2009b). Many factors can influence fracture-face permeability, such as rock softening, water retention, chemical scale formation, and proppant embedment (Jacobi et al., 2009; Rutqvist, 2015; Wang et al., 2015; Weaver et al., 2008, 2009a, 2010; Wick et al., 2020; Xiong et al., 2020).

Yiman et al. (2017) studied the geochemistry during hydraulic fracturing and their work involved conducting experiments on water-rock interactions using Longmaxi shale samples. Their results indicated an increase in total dissolved solids in the fluid obtained during flowback. They also observed a dominant increase in SO_4^{2-}, Ca^{2+}, K^+, Na^+, Cl^-. These were attributed to oxidation of pyrite (equations: 1,2,3), dissolution of plagioclase (equation: 6), dolomite (equation: 5) & calcite (equation: 4).

$$FeS_2 + 2.5O_{2(aq)} + H_2O \rightarrow Fe^{2+} + 2SO_4^{2-} + 2H^+, \quad (1)$$

$$12Fe^{2+} + 3O_2 + 6H_2O \rightleftharpoons 8Fe^{3+} + 4Fe(OH)_3, \quad (2)$$

$$SO_4^{2-} + 2C + 2H_2O \rightleftharpoons H_2S + 2HCO_3^-. \quad (3)$$

$$CaCO_3 + H^+ \rightleftharpoons Ca^{2+} + HCO_3^-, \quad (4)$$

$$CaMg(CO_3)_2 + 2H^+ \rightleftharpoons Ca^{2+} + Mg^{2+} + 2HCO_3^-. \quad (5)$$

$$2KAlSi_3O_8 + 2H^+ + H_2O \rightleftharpoons Al_2(Si_2O_5)(OH)_4 + 2K^+ + 4SiO_2. \quad (6)$$

Qingyun et al. (2020) has deduced that a critical role is played by matrix bulk mineralogy and the mineral distribution in the formation in water-surface interactions, thereby influencing a variety of mechanisms.

Zeng et al. (2020b) have studied the effect of fracturing fluids on Eagle Ford, Marcellus and Barnette shales using imbibition with de-ionised water. They monitored the ion concentration, pH and electrical conductivity during inhibition for a period of four weeks. Their results revealed that samples that had a highest calcite content and lowest organic carbon imbibed much more water and this was true for Barnett shale followed by Marcellus shale and finally Eagle Ford shale. Figure 12 shows an SEM micrograph before and after imbibition for a period of one week showing that pyrite was oxidised and dissolved in water which generated H^+ and a reduced pH was seen. This is indicative that fluid-shale interactions are vital during hydraulic fracturing.

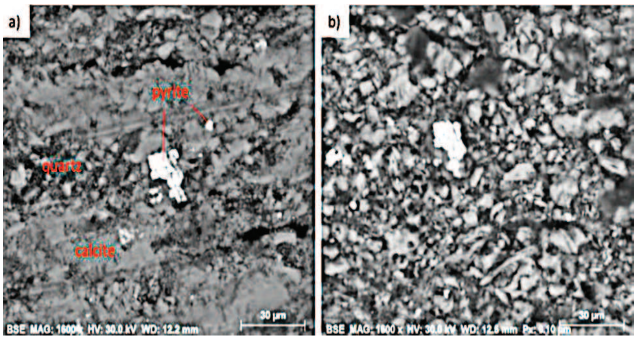

Figure 12: SEM micrograph of Marcellus shale; a) before imbibition b) after imbibition for one week at ambient conditions (Zeng et al., 2020b).

Lyu et al. (2020), Yuepeng et al. (2020) argue that chemical processes involving precipitation following calcite mineral dissolution can lead to further withering of the rock which results in reduced permeability and porosity. Formation mineral re-mineralization in the pack following dissolution could reduce pack permeability (Li et al., 2020; Zhong et al., 2019). Exposure to stress conditions and high temperatures (Voltolini, 2021) when proppants are transported into the hydraulic fracture support geochemical reactions, possibly resulting in the formation of pore-filling minerals and leading to a reduction in the proppant pack porosity (Shenggui et al., 2020; Wei et al., 2020). Proppant embedment is greatly affected by shear weakening in carbonates resulting from fluid saturation (Chuprakov et al., 2020; Hu et al., 2016).

5. Currently available laboratory testing techniques for proppant embedment and fracture conductivity

Testing proppants as a means of better understanding the permeability and conductivity at closure stress is important during the process of designing and evaluating hydraulic fractures. Fundamentally, there is a requirement for traditional proppants to provide and maintain conductive fractures within sites of production. It is typical for the well to experience downhole conditions. In such situations, there is a requirement to ensure the closure stress demands are fulfilled when also maintaining the resistance to diagenesis during the production process. Some of the methods that are used for proppant embedment and fracture conductivity testing are presented below.

5.1. American Petroleum Institute(API) Conductivity Cell

The conductivity cell was the first industry standard used in testing proppant pack conductivity.

Figure 13 shows the traditional API fracture conductivity unit that was designed to be used with de-ionised and distilled water. In this test, samples are cut to fit a cell size of 1.5-inches in width and 7.0-inches in length. A proppant concentration of 2lb/ft^2 is used and proppant confinement is by the steel platens at confinement stresses from 1psi to 14,000psi where proppant is held at any stress for a fifteen minute period and all experiments are conducted at ambient conditions.

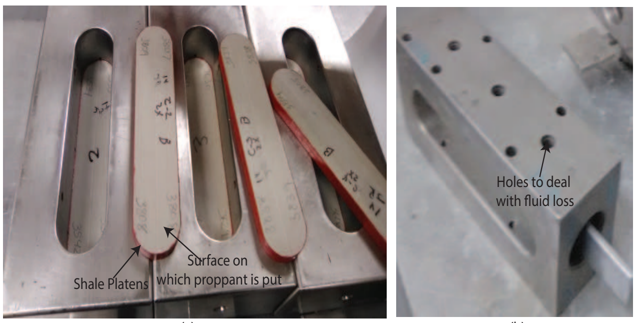

(a) (b)

Figure 13: (a)Linear flow conductivity test cell. (b) Linear flow conductivity cell modified to deal with fluid loss.

The cell in figure 13(a) can be modified to look at proppant flowback under a multiphase flow condition. Shale has no nano-permeability and there will not be any fluid losses as it may be seen for sand stone and carbonate formations therefore, the industry modified figure 13(a) into figure 13(b) where there exists leakoff lines which you can also use to pump through the cell and leak off at the core sample in order to build a filter cake. The disadvantage of the conductivity cell testing method is that it is not designed to give accurate measurements of proppant conductivity under downhole conditions and the industry has now amalgamated this test into a fracture conductivity system.

5.2. Fracture Conductivity System

To overcome the limitations of the API conductivity cell, a fracture conductivity system shown in figure 14 was designed to be able to mimic reservoir conditions. Wang et al. (2020b,c) have used a fracture conductivity testing system to investigate; proppant breakage, embedment, particle migration, fracturing fluid on gel breaking performance and damage to fracture conductivity. The sample preparation requirements for the conductivity cell and the fracture conductivity system are the same. The advantage of the fracture conductivity system is that you can have closure pressures in the range of 0-20,000psi, with an accuracy of 0.04% on the set point, temparatures that range from ambient conditions to 177^{o}C, flow rates in the range of 0.001–50ml/min and you can use varying fracturing fluids as opposed to the conductivity cell shown in figure 13. The system can accommodate a variety of fracturing fluids ranging in composition and pH. It can go from two platens and four platens during the test.

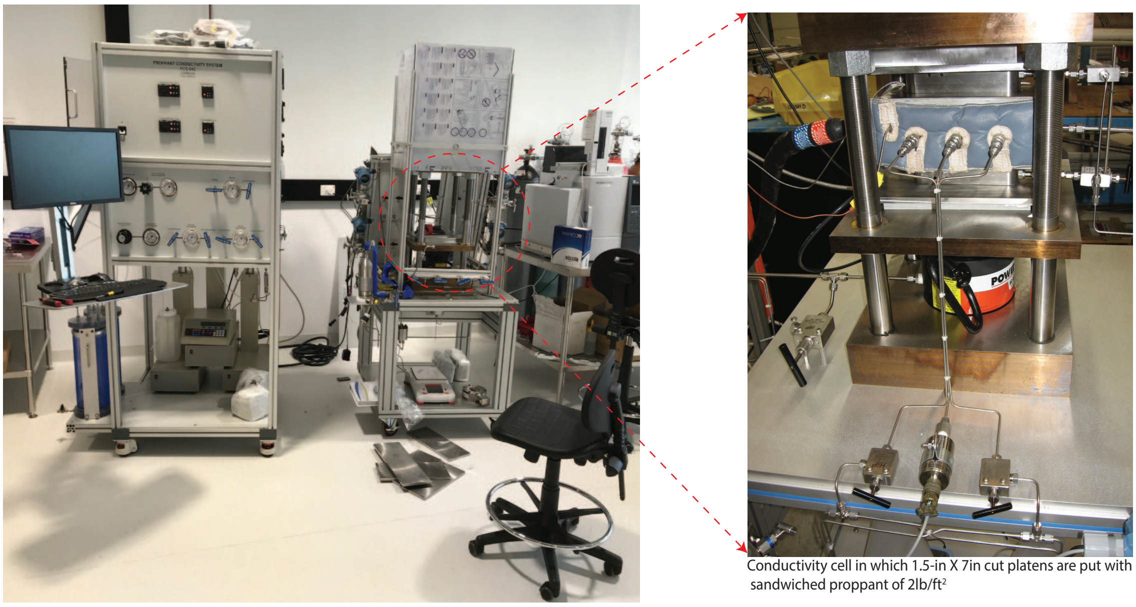

Figure 14: Illustration of the Fracture Conductivity System at the Corelab facility in Tulsa, Oklahoma.

5.3. *Laser surface Profilometry*

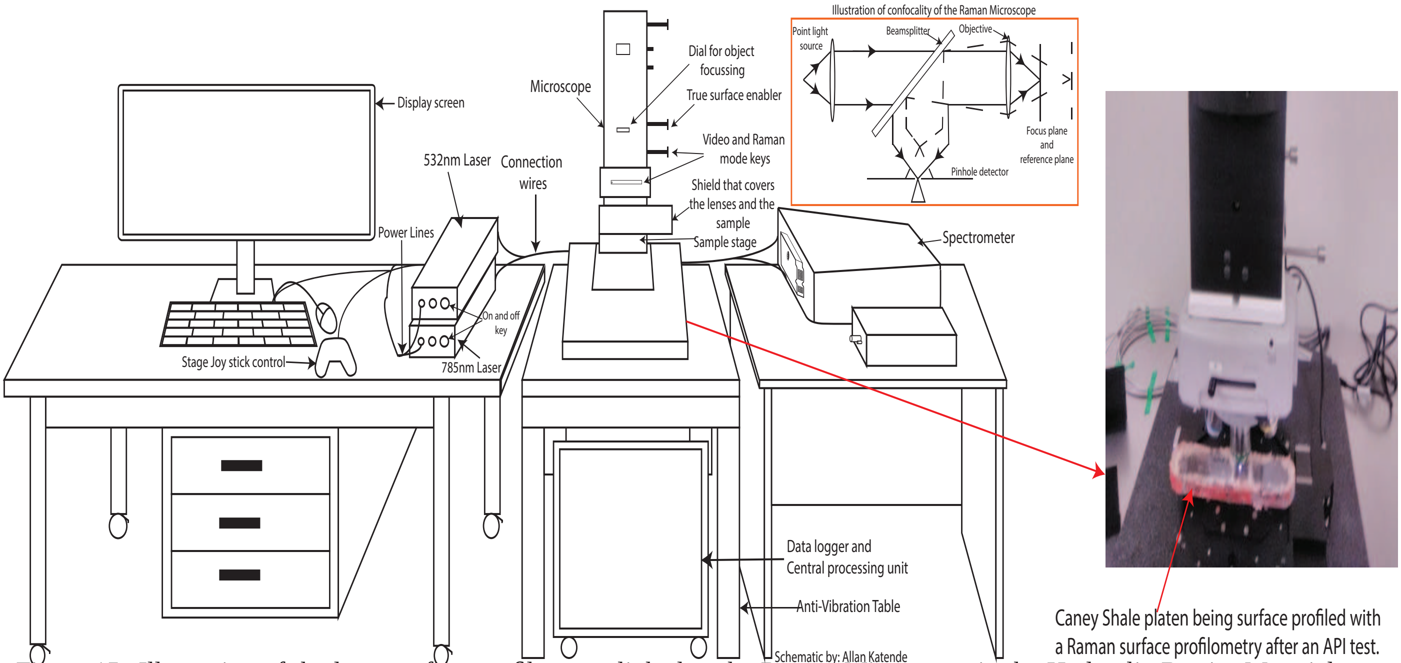

Figure 15: Illustration of the laser surface profilometry linked to the Raman Microscope in the Hydraulic Barrier Materials Laboratory at Oklahoma State University.

The laser surface profilometer linked to the Raman microscope shown in figure 15 was used for quantifying the proppant embedment depths on the Caney Shale samples after an API test. Samples were placed under a Raman microscope shown in figure 15. To obtain a surface profilometry map, the following parameters were used: 20X and 50X objective lenses, an excitation wavelength from the 532nm laser distributed by a 600 g/mm BLZ=500nm grating, a laser power between 0.55 mW. Figure 16 and Figure 17 illustrate how the surface profilometry was used to quantify proppant embedment on a a Caney Shale sample after an API test. Figure 17 shows an optical image in (a) that was used for surface profiling and upon the final surface profiling, cross-sectional lines are drawn in regions of interest to determine how deep the proppant embedments are as shown in Figure 17.

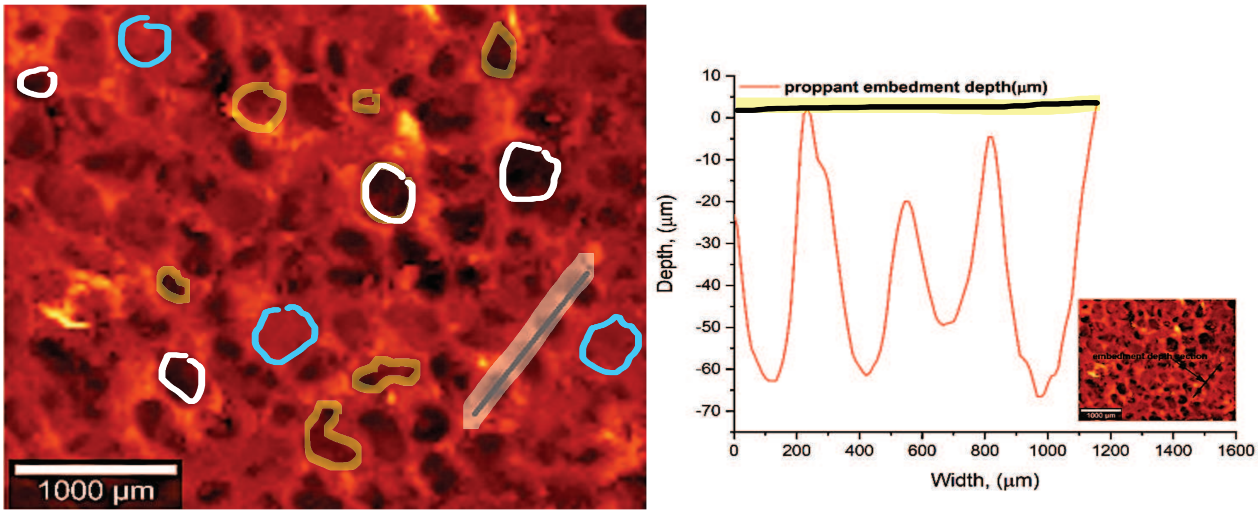

Figure 16: Proppant Embedment captured by Surface Profilometry of Caney Shale in contact with ceramic proppant at 12000psi and 95C, API19D. a) shallow embedment blue, up to 20micrometers, b)medium embedment yellow, up to 50micrometers c) deep embedment white up to 70micrometers

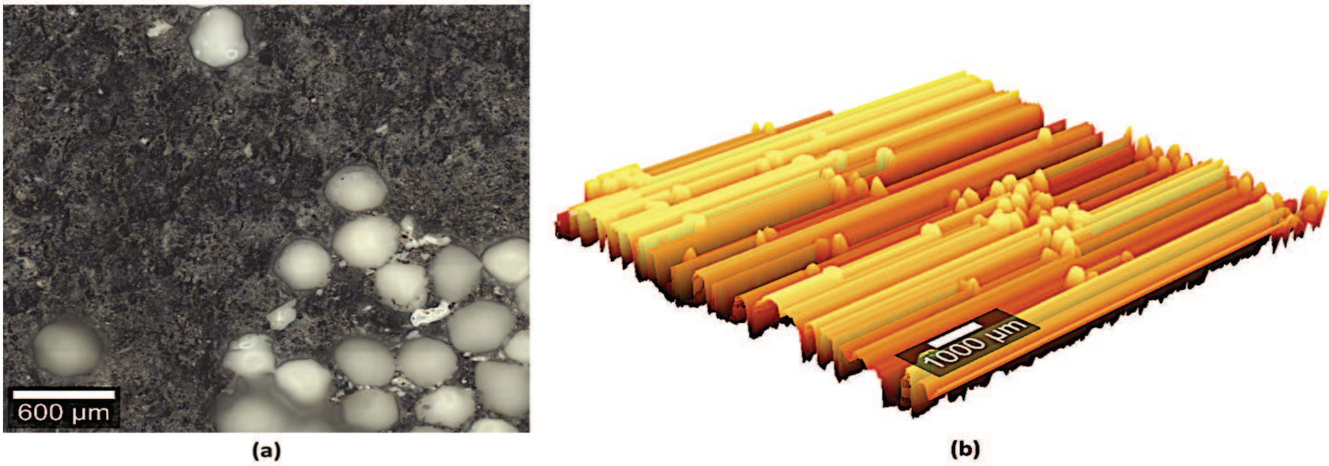

Figure 17: (a) Raman microscope image of the shale platelet surface. Ceramic proppants are visible on the surface of the shale sample (b) 3D-Surface profilometer image obtained from the Raman Microscope. The surface profilometer image obtained from the Raman microscope was used to determine the embedment depth along the profile.

5.4. Indentation Testing

Indentation testing can provide a good indication in predicting proppant embedment. Figure 18 shows how the Indenter can can be used to determine hardness and elastic modulus. hardness provides a good indication in predicting proppant embedment while elastic modulus provides a good indication in predicting fracture aperture. These two properties can only be achieved through indentation testing. After indention testing is complete, post analysis is done using scanning electron microscopy and energy dispersive spectroscopy. Figure 19 shows an SEM micro-graph and an EDS micro-graph of a Caney shale sample indicating heterogeneity in both the micro-structure and surface chemistry. The hardness and elastic modulus values obtained from indentation testing can provide insight into proppant embedment and fracture aperture generation.

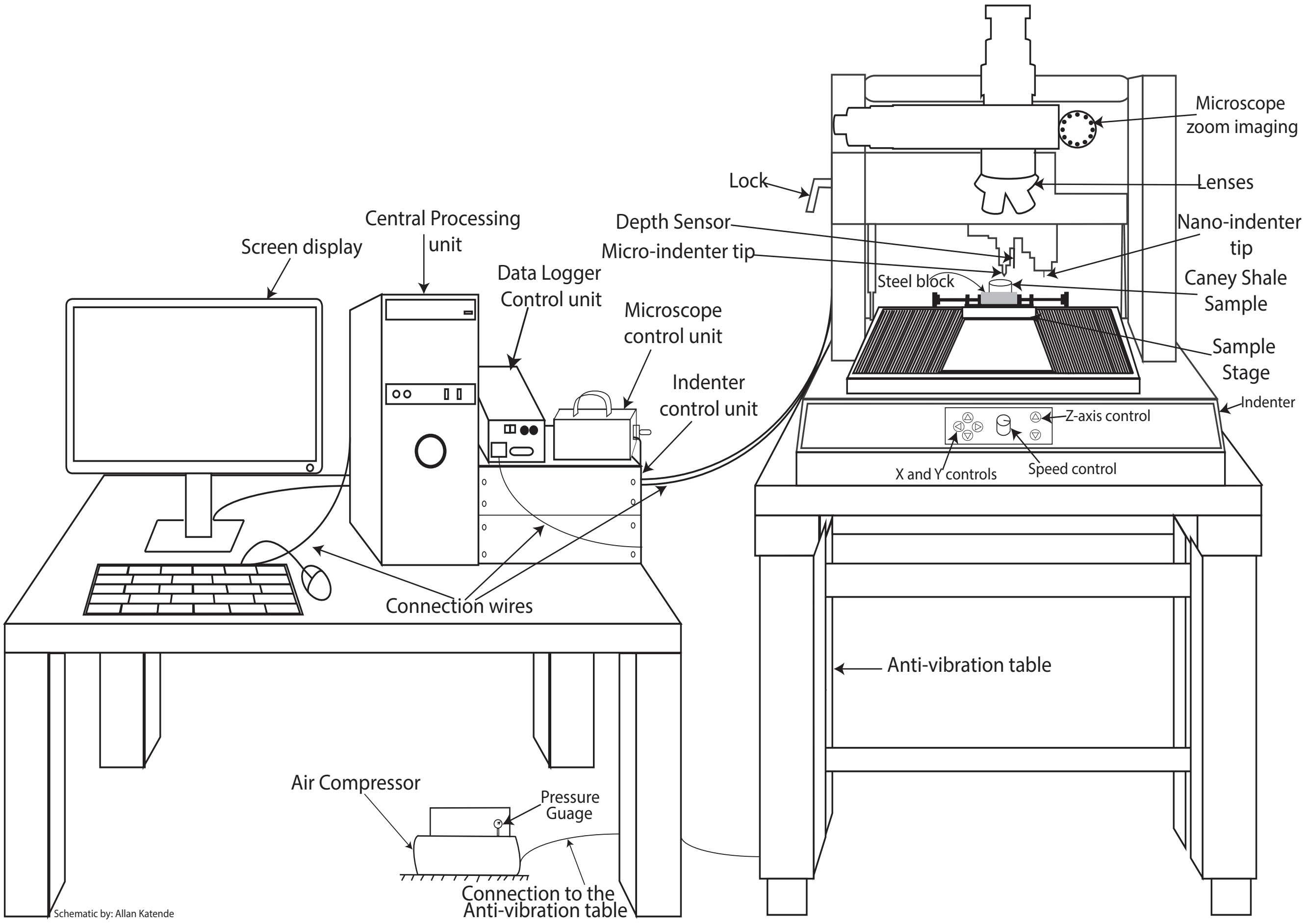

Figure 18: Schematic of the Indenter in the Hydraulic Barrier Materials Laboratory at Oklahoma State University.

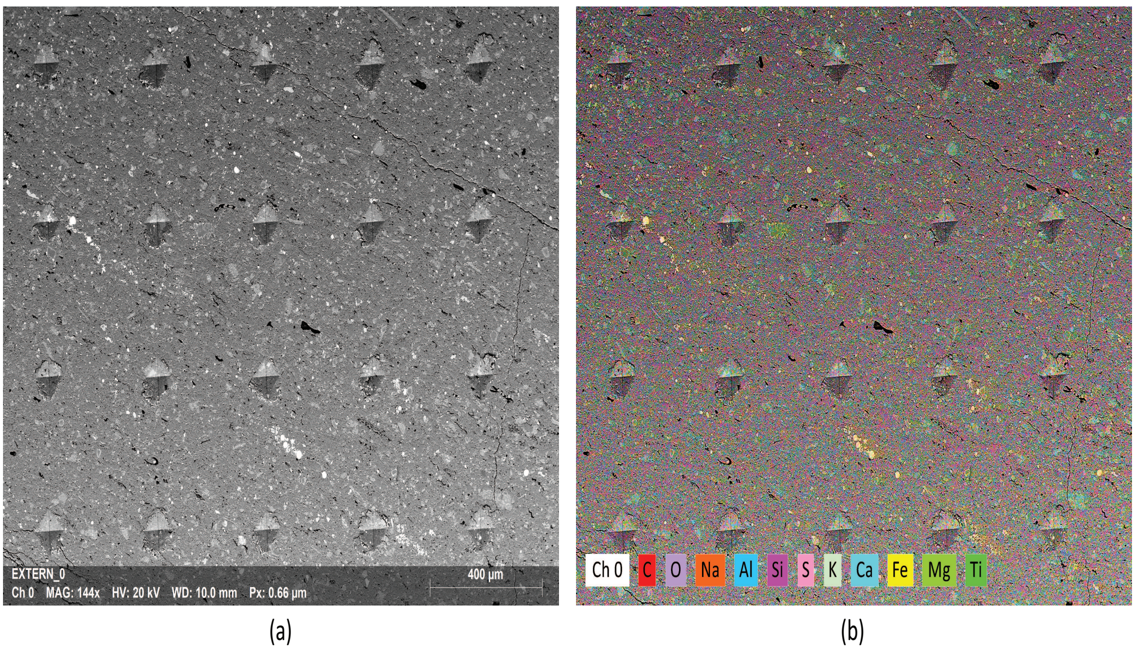

Figure 19: (a) SEM micrograph of showing indents on Caney Shale Sample. (b) Energy Dispersive Spectroscopy showing the surface chemistry of the indented Caney Shale sample

5.5. Flow-through Testing coupled with X-ray Computed Tomography

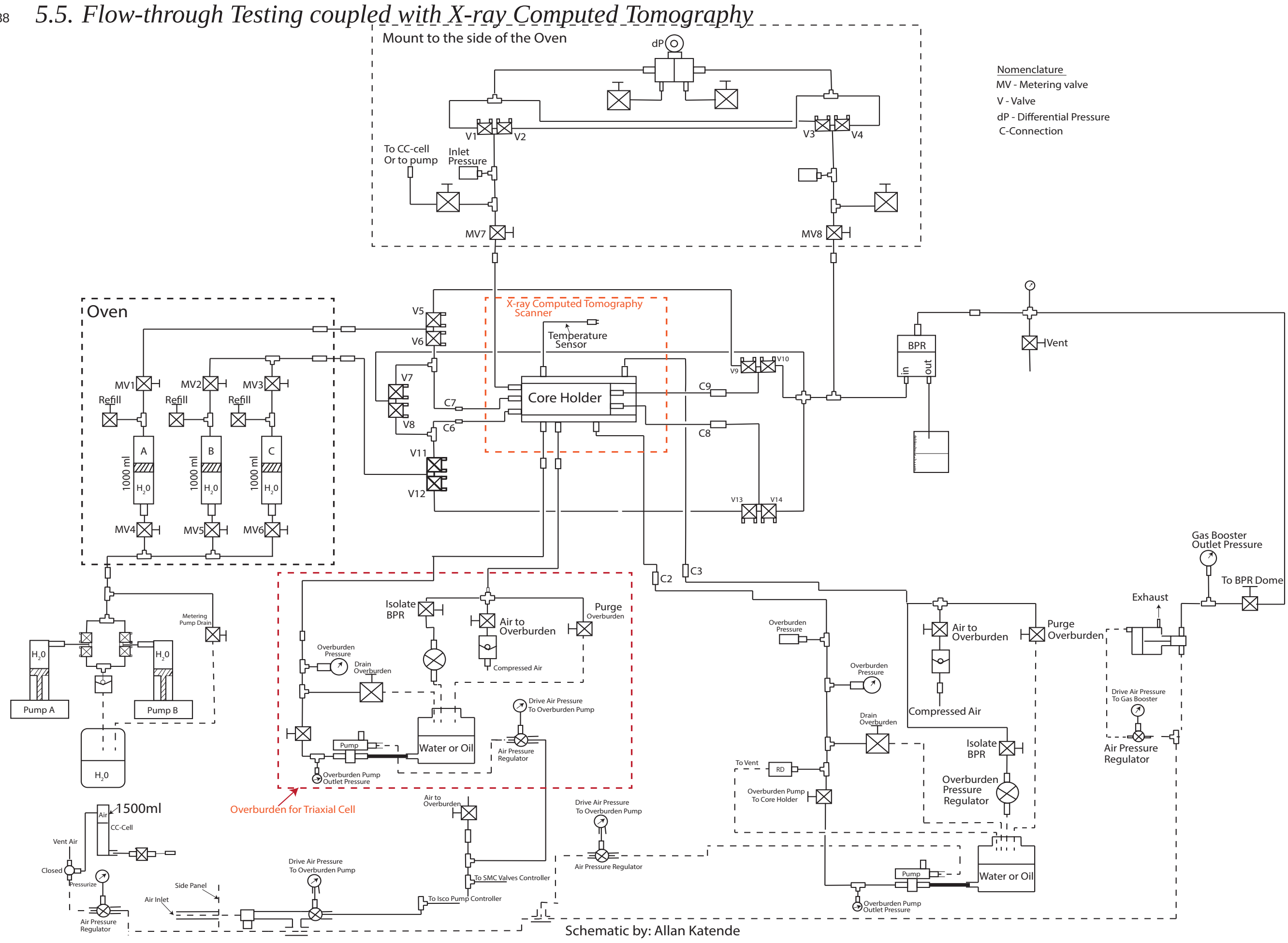

Figure 20: Schematic of the flow-through system coupled with the X-ray computed tomography and a Tri-axial cell in the Hydraulic Barrier Materials Laboratory at Oklahoma State University.

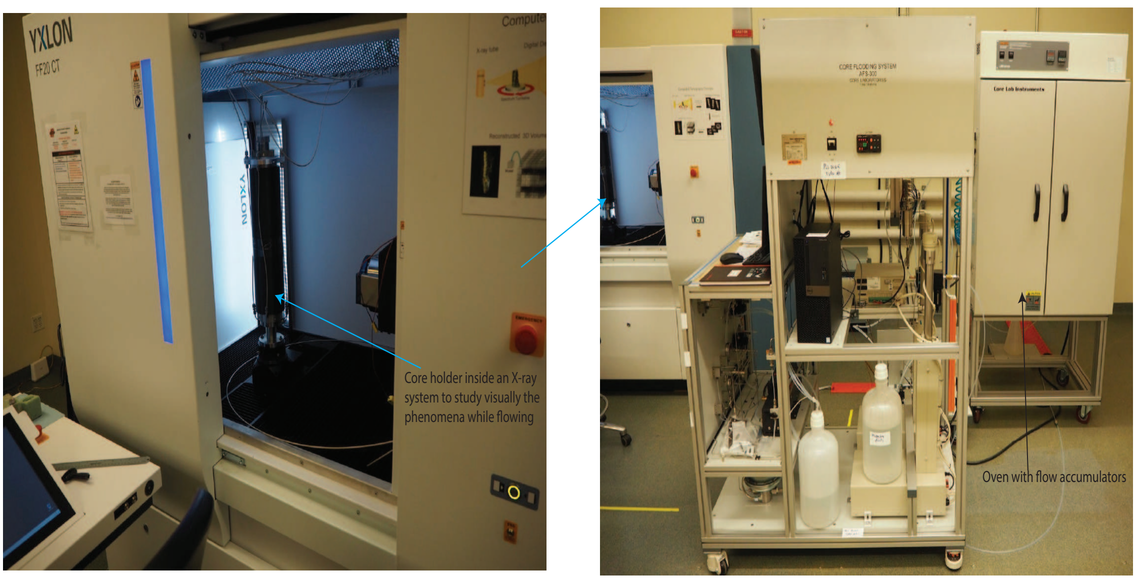

Figure 21: Visual representation of the flow-through system coupled with the X-ray computed tomography and a Tri-axial cell in the Hydraulic Barrier Materials Laboratory at Oklahoma State University.

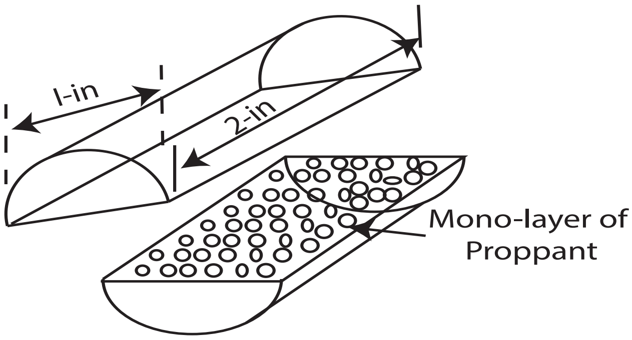

Figure 22: Sliced shale sample indicating how proppant is spread onto the sample surface prior to flow through testing.

The flow through system shown in figure 20 and figure 21 is used to investigate fracture permeability and proppant embedment up to closure stress of 6,000psi. To achieve this, a sample is sliced into two halves as shown in figure 22. Proppant is then spread onto the sample surface and the sample is made intact with the use of teflon tape and two filter papers on both sides so as to prevent fines migration during the actual flow-through experiments. Before experiments can begin and after experiments, the sample is scanned using an X-ray coupled with the flow through system as shown in figure 20 and figure 21. This enables the visualisation of the internal micro structure properties of the shale sample as seen in figure 23. After the experiment is done, the sample is scanned using a laser profilometer described in section 5.3 and an SEM system in-order to visualize and quantify the effect of embedment.

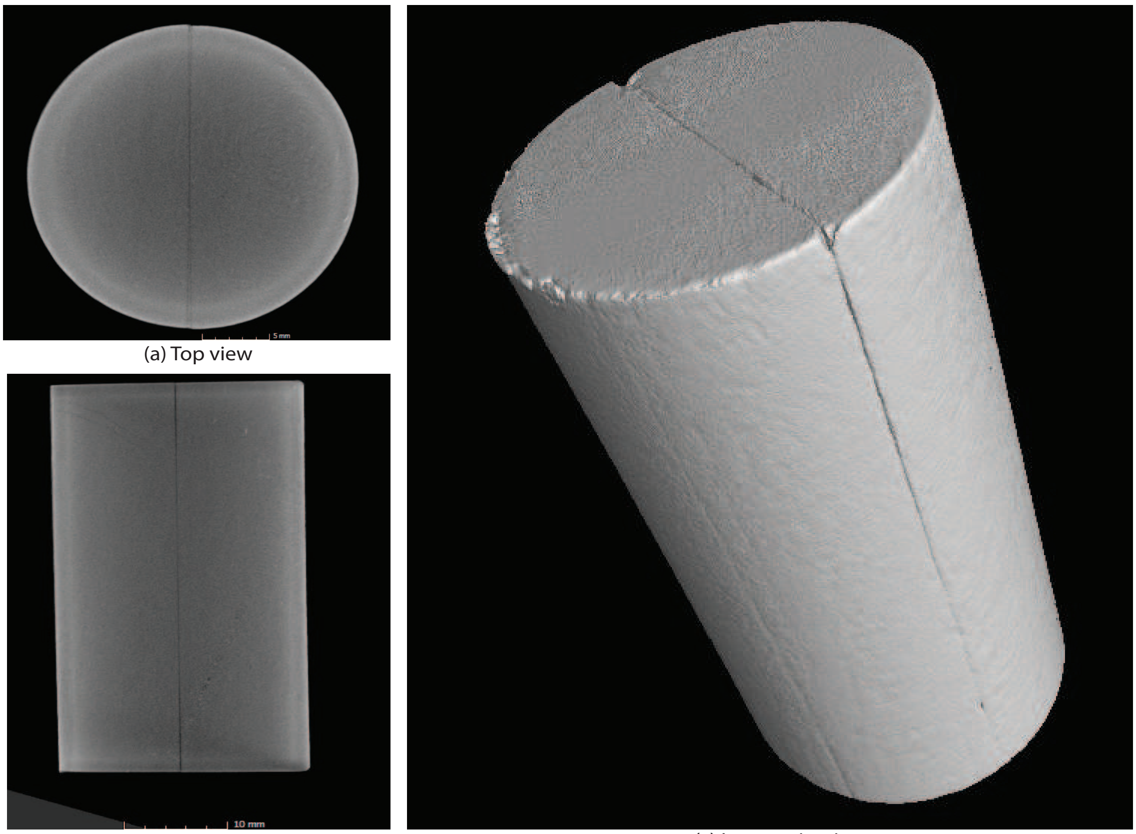

(a) Top view

(b) Side view

(c) Iso-metric view

Figure 23: Visualization of the micro structure of the proppant sand wiched shale sample using a flow-through system coupled with the X-ray computed tomography and a Tri-axial cell in the Hydraulic Barrier Materials Laboratory at Oklahoma State University.

6. Modelling of Proppant embedment during hydraulic fracturing and production

As the fracture is created and packed with proppant, a series of physical and chemical processes happen and change the characteristics of the hydraulic fracture (Hosseini and Khoei, 2020; Shi, 2021; Wang et al., 2020a; Yue et al., 2020). A major concern regarding these fracture character changes is related to the fracture conductivity (Wang et al., 2021; Wen et al., 2007). As compressive pressure acts on the fracture in conjunction with fluid-rock-proppant interaction, the fracture tends to close, and the fracture flow channel tends to be blocked. As a result, the fracture conductivity decreases (Alramahi and Sundberg, 2012; Cooke, 1973a; Li et al., 2015).

6.1. Proppant embedment modeling

The study of proppant embedment starts with a linear elastic model, and the classic Hertz (1896) contact model that is between an elastic semi-infinite half-space and a rigid spherical ball is used. The analytical solution is provided below:

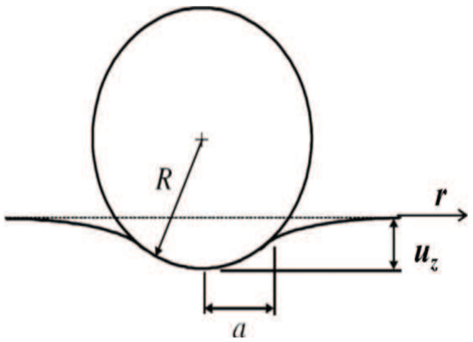

Figure 24: Hertz (1896) contact model between a rigid spherical ball and an elastic semi-infinite space.

$$u_z = \frac{1-\nu^2}{E} P_m \frac{\pi}{4a}\left(2a^2 - r^2\right); r \leqslant a \tag{7}$$

$$u_z = \frac{1-\nu^2}{E}\frac{3}{2} P_m \left[\left(2a^2 - r^2\right) sin^{-1}\frac{a}{r} + r^2\frac{a}{r}\left(1 - \frac{a^2}{r^2}\right)^{\frac{1}{2}}\right]; r \geqslant a \tag{8}$$

- $\nu \equiv$ poisson's ratio
- E $\equiv$ modulus of elasticity
- a is the radius of contact computed from Cripps (2007) equation 9.

$$a^3 = \frac{3}{4}\frac{PR}{E^*} \tag{9}$$

- P is the indenter load
- E^* $\equiv$ coalesced modulus of elasticity of the indenter and half-space computed by Cripps (2007) equation 10.

$$\frac{1}{E} = \frac{\left(1-\nu^2\right)}{E} + \frac{\left(1-\nu'^2\right)}{E'} \tag{10}$$

- ν'^2 $\equiv$ poisson's ratio.
- E' $\equiv$ youngs modulus of elasticity.

The degree of penetration often referred to in the Hertz (1896) contact theory, should be relatively small compared to the radius of the sphere indenter. In circumstances where proppant embedment is to a large degree, Chen et al. (2017) provided a power law correlation (Equation 11), which performs better than the Hertz (1896) model for shale rocks with a variety of clay minerals.

$$h = \eta\left(\sigma_e\right)^{\lambda} \tag{11}$$

- η and λ are fitted parameters from experimentation.

Jia et al. (2019) studied the rod-shaped proppant conductivity due to compaction and embedment. In their study, they considered two cylinders, as shown in Figure 25, and they summarized the following:

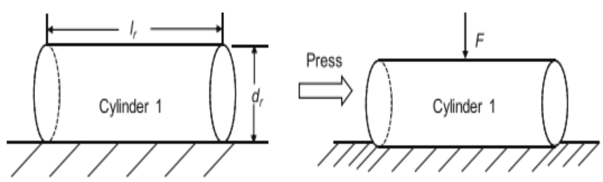

Figure 25: The mutually squeezed cylinder and plate(Jia et al., 2019).

$$\alpha' = \bar{F} \cdot (V_1 + V_2) \cdot \left[1 + ln \left\{ \frac{2l_r^2}{V_1 + V_2 \cdot \bar{F}} \cdot \left(\frac{1}{d_{r_1}} \right) \right\} \right] \quad (12)$$

- α' is dependent on embedment and deformation. For the illustration in figure 25, when the elastic modulus of the plane tends to infinity, cylinder 1 will not embed into the plane and α' is determined by only deformation.
- Deformation(β') is computed using equation 12 and has to satisfy the relation in equation 13

$$\beta' = \bar{F} \cdot V_1 \cdot \left[1 + ln \left\{ \frac{2l_r^2}{V_1 \cdot \bar{F}} \cdot \left(\frac{1}{d_{r1}} \right) \right\} \right] \quad (13)$$

The value of embedment(h') is computed from equation 14 and equation 15 below:

$$h' = \alpha' - \beta' \quad (14)$$

$$h' = \bar{F} \cdot \left\{ V_2 \left[1 + ln \left(\frac{2l_r^2}{(V_1 + V_2) \cdot \bar{F}} \cdot \frac{1}{d_{r1}} \right) \right] - V_1 \cdot ln \left(\frac{V_1 + V_2}{V_1} \right) \right\} \quad (15)$$

Shale formations contain a high clay content and undergo creep deformation. Several scholars have developed viscoelastic models to account for the creep deformation in proppant embedments. Guo and Liu (2012) used a Maxwell (1890) model to combine the elastic component and viscous component. These viscoelastic models include the Maxwell (1890) model and Burgers (1918) model. The details are listed in equation 16.

$$H = \frac{2P_c(t)(1 - \nu^2 a)}{E} + \frac{a}{2\eta_2} \left(1 + \frac{(1 - 2\nu)^2}{3} \right) \int_0^t P_c(t) dt \quad (16)$$

- q is the normal distributes stress, MPa
- a ≡ radius of q, mm
- E ≡ modulus of elasticity, MPa
- G_0 is the shear modulus, MPa
- H is the depth of embedment, mm
- K is the bulk modulus, MPa
- P_c is the closure pressure, MPa
- ν ≡ poisson's ratio
- η_{max} is the maximum vertical displacement on the boundary, mm
- η_2 ≡ shear coefficient during secondary creep, MPa

Ding et al. (2018) provided an analytical solution for the Maxwell (1890) model to describe viscoelastic deformation. The dimensionless depth is shown in equations 17&18 below for the fractional Maxwell (1890) model:

$$D(t) = \left\{ \frac{3\pi \left[5 + \frac{4E_2(1-\nu_1^2)}{E_1} - E_\alpha \left(- \left[\frac{E_2 t}{3\eta_2} \right]^\alpha \right) (1 - 2\nu_2)^2 - 4\nu_2 + \frac{E_2}{\eta_2} \frac{t^\alpha}{\Gamma(1+\alpha)} \right]}{16E_2} \right\}^{\frac{2}{3}} \quad (17)$$

And if $\alpha = 1$, equation 18 shows the dimensionless depth for the Maxwell (1890) model.

$$D(t) = \left\{ \frac{3\pi P_o \left[5 + \frac{4E_2(1-\nu_1^2)}{E_1} - e^{\frac{-E_2 t}{3\eta_2}} (1 - 2\nu_2)^2 - 4\nu_2 + \frac{E_2 t}{\eta_2} \right]}{16E_2} \right\}^{\frac{2}{3}} \quad (18)$$

- D is the deformation.
- P_o is the closure stress, Pa.
- ν ≡ poisson's ratio.
- E is the elastic modulus.

Luo et al. (2020b) applied a modified Burgers (1918) model to quantify the viscoelastic deformations by ignoring viscous flow. The corresponding total embedment of proppants into the fractures could generally be expressed by equation 19

$$\varepsilon(t) = \frac{\sigma}{E_{r0}} + \frac{\sigma}{E_{r1}} \left(1 - e^{\frac{-E_{r1}}{\eta_{r1}} t} \right) \quad (19)$$

- $\varepsilon(t)$ is the embedment depth.
- $\sigma \equiv$ applied stress.
- $E_{r1}\&E_{r0} \equiv$ creep and elastic modulus.
- $\eta_{r1}t \equiv$ rock visco-elastic coefficient.

6.2. Proppant settlement

Novotny (1977) presented a proppant settlement model for fracture fluid based on a single particle in a Newtonian fluid. The terminal settling velocity could be calculated based on laminar, transition and turbulent flow.

For $N_{Re} \leq 2(Stokes - law \quad region)$,

$$C_D = \frac{24}{N_{Re}} \tag{20}$$

$$V_\infty = \frac{g(\rho_p - \rho)d^2}{18\mu} \tag{21}$$

For $2<N_{Re} < 500(Intermediate \quad region)$,

$$C_D = \frac{18.5}{N_{Re}^{0.6}} \tag{22}$$

$$V_\infty = \frac{20.34(\rho_p - \rho)^{0.71} d^{1.14}}{\rho^{0.29}\mu^{0.43}} \tag{23}$$

For $N_{Re} \geqslant 500(Newtons - law \quad region)$,

$$C_D = 0.44 \tag{24}$$

$$V_\infty = 1.74\sqrt{\frac{g(\rho_p - \rho)d}{\rho}} \tag{25}$$

where N_{Re} is the Reynolds number, $C_D \equiv$ drag coefficient on a sphere, $rho \equiv$ density of fluid in gm/cc, $\rho_p \equiv$ proppant density in gm/cc, $\mu \equiv$ viscosity in poises, g is the gravitational constant of 980 cm/sec2, d is the proppant diameter in cm, & $v_\propto \equiv$ velocity of a proppant particle in an infinite media in cm/sec.

Novotny (1977) also provided the justification for non-Newtonian fluids, wall effects and slurry concentrations. The fluid rheological property plays a large role in proppant transportation. Water (Britt, 2012; Britt et al., 2006), gel (Harris and Heath, 2006), foam (Valko and Economides, 1997), etc. were studied as fracturing fluids. Harris and Heath (2006) addressed the fact that proppant types also affect proppant transport, since the reaction of certain proppants and fluids might change the fluid rheology.

Barree and Conway (1994) suggested that proppant transport should incorporate bulk flow mechanics (fluid movement in the fracture). From the calculated vertical and lateral bulk fluid velocity and empirical fluid and proppant velocity relationship, the proppant velocity resulting from the fluid effect can be calculated. The overall proppant velocity arises from the combination of fluid bulk flow and particle settling. Tomac and Gutierrez (2015) emphasized that the proppant settling relations cannot be used in conditions with rough and narrow hydraulic fractures and high fluid viscosities, since the particle interaction during settling, temperamental upward and fluid counterflow may cause proppant trajectories that defy gravity.

Previous studies (Barboza et al., 2021; Fei et al., 2020; Hosseini and Khoei, 2020; Isah et al., 2021; Suri et al., 2020) have relied on the assumption of uniform fracture geometry. Smith et al. (2001) found that conditions corresponding to a layered modulus (i.e., stacked formations having different layers with varying moduli) cause width nonuniformities in fractures that affect proppant placement. Chun et al. (2021) identified through experiments that fracture width nonuniformities and height growth have major effects on proppant transport.

As the pumped proppant packs and settles in the hydraulic fracture, the fracturing process ends, and the production stage starts. During the production stage, the low conductivity of the uppropped zone, caused by the nonuniform proppant distribution inside a single fracture, tends to diminish production by 50% (Zanganeh et al., 2015). Furthermore, the nonuniform distribution of proppant among fracture clusters during fracturing operations can also cause significant reductions in well productivity (Li et al., 2021; Yu et al., 2015).

As well production starts, a series of physical and chemical processes happen and change the characteristics of the hydraulic fracture. Van-Batenburg et al. (1999) noted that the fluid flow in the fractures affects the packed proppant local stability, causing proppant flowback and open channel development in the fracture. Moreover, several authors have reported that the fracture porosity and permeability decrease during the production stage (Lee et al., 2010; Lehman et al., 1999; Sanematsu et al., 2015). Several causative mechanisms have been proposed, including stress changes (Bhandari et al., 2021), chemical reactions and precipitation (Khan et al., 2021), temperature/stress-enhanced dissolution (Bandara et al., 2018; Voltolini, 2021), rearrangement of the packing structure (Liu et al., 2021), etc. The decrease in permeability in the fractures significantly decreases the well recovery (Yu et al., 2015; Zanganeh et al., 2015).

6.3. Proppant Compaction and Deformation

Hydraulic fracture network is initially created using powerful pumping pressures, and once the fracturing is completed for a particular location, the fluids tend to dissipate into the rock formations as well as flow back, causing fluid pressure reduction. Later on, as the production proceeds, and reservoir pressure is reduced, the fracture closing pressure from the earth stresses increases. Chen et al. (2017) observed that the Hertz (1896) contact model is used to characterize proppant compaction, where the maximum vertical displacement for two proppant grains can be expressed as equation 26.

$$u_z = \frac{\left(1-\nu^2\right)}{EE^*} \cdot \left(\frac{3}{4}\pi\sigma_e\right)^2 \tag{26}$$

- where R ≡ radius; ν & E are Poisson's ratio, & modulus of elasticity of the half-space; and the effective stress is σ_e.

Based on the Hertz (1896) contact model, Li et al. (2015) considered a multilayer proppant with rhombohedron packing; the total fracture width reduction resulting from proppant compaction can be calculated as equations 27&28.

$$W_d = 3.78RP_c^{\frac{2}{3}}\left(n_2-1\right)\left(\frac{1-u_p^2}{E_p}\right)^{\frac{2}{3}} \tag{27}$$

$$n_2 = ceil\left(\frac{w_f}{\sqrt{3}\cdot C\cdot R}\right) \tag{28}$$

- where ceil(x) ≡ ceiling function given by ($ceil(x) = |x|+1$). C is the sphericity of the proppants, R is the proppant grain radius, and E and ν are the elastic modulus and Poisson ratio of the proppant, respectively. In addition, w_f is the fracture width of the rhombohedron packing before compaction, and Pc is the formation pressure.

Proppant grains can break into smaller parts under high compressive pressure, which further reduces the fracture width and blocks the fracture pores, thus decreasing the fracture conductivity. A proppant fragment study was conducted by Zheng and Tannant (2019). They applied a 3d discrete element model (PFC3D from Itasca (2014) Consulting Group) to simulate proppant particle breakage. In their model, particle deformation is considered to take place once the octahedral shear stress in a particle is greater than the particle strength.

$$Particle \quad deformation \quad criterion: \sigma_i > \sigma_{s_{(D)}} \tag{29}$$

- where σ_i is the octahedral shear stress and σ_s is the diameter-dependent stress threshold.

After the criterion is reached, the original particles are replaced by 4 smaller particles, and volume conservation still holds. Their results verified that the permeability and porosity decrease with proppant fragmentation, thus causing the fracture conductivity to decrease.

6.4. Proppant Dissolution and Precipitation

In addition to physical proppant compaction, stress-enhanced dissolution of the proppant increases the density of grain packing, and reprecipitation of mineral

The density of the grain packing increases as a result of an increase in the density of the proppant which results from physical proppant compaction and stress-enhnaced dissolution of the proppants. The mineral re-precipitation further occludes pores, thus decreasing the fracture conductivity (Lee et al., 2010; Luo et al., 2019; Yasuhara et al., 2003). The corresponding dissolution and precipitation of quartz are described in the three sections 6.4.1,6.4.2&6.4.3 listed below;

6.4.1. Dissolution mass flux

$\frac{dM_{diss}}{dt}$ is given by;

$$\frac{dM_{diss}}{dt} = \frac{3\pi \cdot V_m^2 (\sigma_a - \sigma_c) k + \rho_g d_c^2}{4RT} \quad (30)$$

- where V_m is the solid molar volume, σ_a = is the grain to grain pressure which must exceed the hydrostatic pore pressure, k ≡ constant of dissolution for the solid, ρ_g ≡ grain density, d_c ≡ contact diameter , R ≡ Universal gas constant, T ≡ system temperature, and σ_c is the critical stress for the initiation of the pressure solution.

6.4.2. Diffusive mass flux

$\frac{dM_{diff}}{dt}$ is given by;

$$\frac{dM_{diff}}{dt} = \frac{2\pi \cdot \omega \cdot D_b}{ln\left(\frac{d_c}{2\varepsilon}\right)} \cdot \left(C_{int} - C_{pore}\right) \quad (31)$$

- D_b ≡ coefficient of diffusion , ε is the immeasurably small length $\left(\frac{1}{1000} \times \textit{ contact area diameter}\right)$, d_c is the grain tograin contact diameter, and (Cint)x = ε and (Cpore)x = $\frac{d_c}{2}$ are the interface and pore space concentrations respectively. ω ≡ thickness of the water film that will be trapped at the interface.

6.4.3. Precipitation mass flux

$\frac{dM_{prec}}{dt}$ is given by;

$$\frac{dM_{prec}}{dt} = V_p \frac{A}{M} \cdot k_c \cdot \left(C_{pore} - C_{eq}\right) \quad (32)$$

- where V_p is the volume of the pore space, A ≡ surface area of the relative grains, M ≡relative fluid, k_c ≡ precipitation rate constant of the dissolved mineral, & C_{eq} ≡ dissolved quartz equilibrium solubility.

6.5. Un-uniform proppant distribution

In the ideal case, the proppant distribution in the fracture is uniform, but this scenario is atypical. Smith et al. (2001) found that conditions corresponding to a layered modulus (i.e., layered formations with different layers having different moduli) cause width nonuniformities in the fracture that affect the proppant distribution. Huang et al. (2021a) identified through experiments that fracture width nonuniformities and height growth have major effects on proppant transport. Yue et al. (2020) noted that the injected proppant gradually settles and accumulates in a ramp shape inside the fracture. Proppant also accumulates at any fracture intersections. All the above factors cause the nonuniformity of the proppant distribution inside the fracture. This in turn affects the fracture closing process. The uneven distribution of proppant has a direct impact on the production performance; thus, some scholars have constructed direct reservoir models to identify the relations. Zanganeh et al. (2015) assigned a low conductivity in the unpropped fracture section and claimed that this low conductivity diminished production by 50%. Furthermore, the nonuniform distribution of proppant among fracture clusters during fracturing operations can also cause significant reductions in well productivity (Yu et al., 2015).

6.6. Numerical modeling from micro-scale to reservoir-scale

Complementary to the basic analytical methods discussed above, numerical modeling can consider more complex conditions and processes, such as material heterogeneity and bedding anisotropy, non-ideal proppant shapes and distributions, mixed brittle-ductile shale behavior, and proppant crushing. Numerical modeling can also be used for upscaling from nano and micro-scale behavior to reservoir fracture closure behavior. This involves multi-scale modeling of fractured porous and granular media (Hu and Rutqvist, 2021; Zheng et al., 2020) to adequately capture compaction of proppant filled fracture that can include stages of proppant redistribution, embedment and crushing (Voltolini and Ajo-Franklin, 2020). In this contexts, recent work in Voltolini et al. (2021) and Katende et al. (2021) show how indentation tests can be evaluated in terms of Mohr-Coulomb plasticity that can then be applied for modeling proppant embedment and fracture closure at the reservoir scale.

Figure 26 presents results of micro-mechanical modeling of indentation of a spherical, proppant like, indenter into an anisotropic very ductile shale (Voltolini et al., 2021). The modeled complex micro-mechanical behavior around the indenter, including ductile deformation under the indenter and brittle fracture propagation along bedding was observed from x-ray micro-tomography. In Katende et al. (2021), core-scale and micro-indentation tests were applied to determine cohesion and friction angle of Caney shale required for modeling proppant embedment. Parameters for creep compaction can be determined from laboratory creep experiments at the core-scale, or by indentation and fracture flow through experiments (Nakagawa and Borglin, 2019; Zhang et al., 2015). Recent modeling of the long-term fracture creep closure for Caney shale properties predicts that clay rich units could experience substantial time-depend proppant embedment and fracture closure (Benge et al., 2021). Modeling of production would involve multiphase fluid flow and geomechanics, considering oil, gas, and water components, as well as elasto-plastic closure of fractures (Han et al., 2016; Liu et al., 2018; Shuang et al., 2020). In formations with high clay content, the modeling would need to include creep embedment and its impact on fracture permeability (Benge et al., 2021; Ding et al., 2020; Luo et al., 2020a). Such analysis maybe expanded to modeling time-dependent processes using coupled thermo-hydro-mechanical-chemical modeling in which the evolution of chemical compositions of the fluids can play a significant role for the long-term production behavior. Future research along those lines would require coupling of multiphase fluid flow and geomechanics models with reactive transport models that have been applied for example in nuclear waste disposal in shale and caprock sealing (Rutqvist et al., 2014; Xiao et al., 2020; Zheng et al., 2014). The validation of such complex models against laboratory and field observations is essential for more accurate prediction of the long-term.

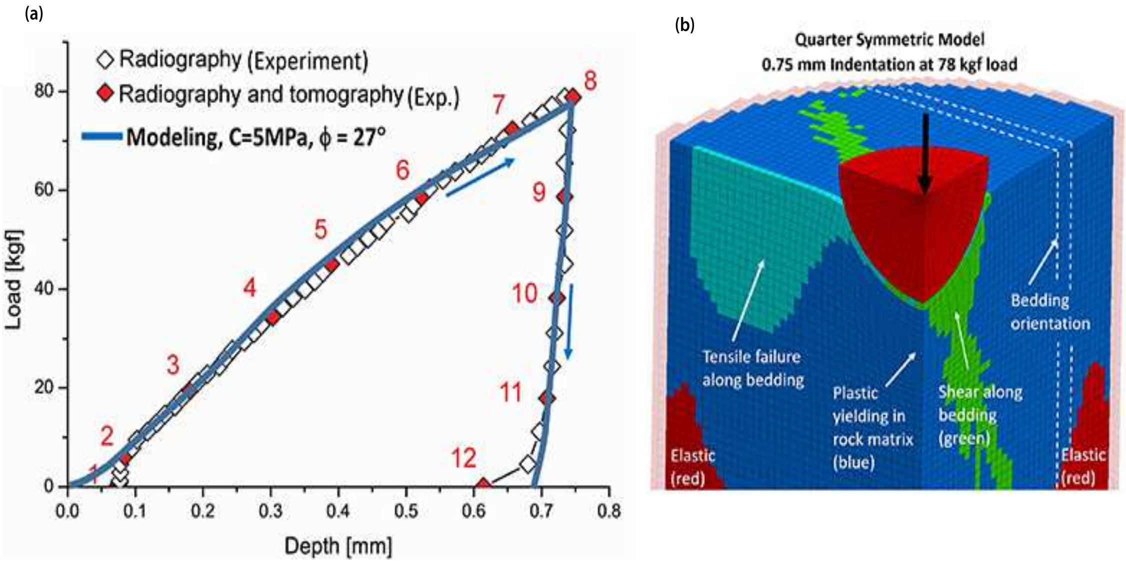

Figure 26: The modeling of indentation tests showing a mixed brittle-ductile behavior of plastic compaction below the indenter and brittle fracturing along the bedding. (a) comparison of modeled and experimental load-indentation curve, and (b) modeling results of ductile plastic compaction and brittle fracturing at the peak load. (modified from Voltolini et al. (2021))

7. Summary, Conclusions, and Recommendations

Hydraulic fracturing of unconventional shale reservoirs require use of proppants. Traditionally, quartz sand was the top choice as proppant. Recently, due to large demand, other sources of sand are also considered, as well as manufactured ceramic proppants, although the cost is prohibitive in the case of ceramics. The reservoir pressure and temperature are outside of the influence of engineering design, and as such dictate what type of fluids, proppants and completions design as well as production and reservoir management, will be applied in any given field. Mechanical and chemical stability of proppant is not only determined by its composition, but the size and shape of particles, and the composition of both, engineered and in situ geofluids, to which proppants will be exposed during their lifecycle.

Based on the assessment of proppant embedment in shale reservoirs, this review proposes best practices such as to optimize hydraulic fracturing and minimize proppant embedment from practical and economic perspectives. In addition, the review outlines next steps for addressing proppant embedment and environmental concerns related to hydraulic fracturing of shales.

- Specifically, it is imperative to refine the fracturing fluid and hydraulic fracturing treatment processes because imperfections in these procedures affect creep deformation, permeability, and proppant wetting characteristics.
- Rock properties combined with the proppant characteristics to a significant degree determine the embedment depth. The creation of an effective treatment design requires that operators possess a thorough apprehension of the mechanical and mineralogical characteristics of the shale formation.
- Characterization of the rheological behaviors of various fracturing fluids is central to ability of operators to tailor existing fluids and develop new hydraulic fracturing fluids with a broader array of applications.
- The use of proppants coated with various materials such as nanoparticles, graphene, and polymers, can potentially prevent fines generation preventing formation damage and maintaining well productivity.
- Modeling of proppant behavior should always be val-

idated against experimental studies and field observations and theoretical predictions can be advanced only through a more nuanced understanding of the rheology of fracturing fluids.

These are some of the gaps and future avenues of research and opportunities for collaborative technological development, which requires an interdisciplinary approach of science, engineering in academia, government, and private sector.

Nomenclature

k	Permeability
I	Illite
S	Smectite
N_2	Nitrogen
CO_2	Carbondioxide
PAM	Polyacrylamide
KCL	Potassium Chloride
LWC	Low Weight Ceramic
HSP	High Strength Proppant
RCP	Resin Coated Proppant
CCP	Ceramic Coated Proppant
ISP	Intermediate Strength Proppant
EUR	Estimated Ultimate Recovery
UCS	Unconfined Compressive Strength

Declaration of interests

The authors declare that they have no known competing conflicting interests or personal relationships that could have appeared to influence the work reported in this paper.

Acknowledgements

The authors of this paper would like to acknowledge that this study was made possible by Department of Energy(DOE) Award DE-FE0031776 from the Office of Fossil Energy. Funding for LBNL was provided by the U.S. Department of Energy, Office of Fossil Energy, through the National Energy Technology Laboratory and Oklahoma State University, under Award Number DE-AC02-05CH11231. We would like to thank Mr. E. Cline formerly at Chesapeake Energy, Mr. G. King from G. E, King Engineering & Mr. B. Dean from Continental Resources for constructive feedback on the article. The author would like to thank Dr. Mileva Radonjic without whose guidance this work would not have come to completion. The author is also grateful to the Petroleum Engineering PhD program in the School of Chemical Engineering at Oklahoma State University in Stillwater Oklahoma as the major PhD work has been conducted here with a research assistantship funded by Dr. Mileva Radonjic. The author would also like to thank; Mr. B. Anderson for his assistance in providing the Corelab API schematic, Mr. B. Chapman for his assistance with the visualization of the schematics for proppants, Mrs. Lisa O'Connel for providing optical micro-graphs from the Proppant Consortium, Mrs. Ashley. Rich for providing proppant optical micrographs from PropTester Inc, and Mr. D. Kevin for his assistance with the GIS. The authors would also like to thank Mrs. L. Whitworth and Mr. B. Johnson from the Venture 1 facility at Oklahoma State University for their assistance in acquiring SEM and EDS data.

Table 2: Summary of previous studies investigating proppant embedment

Author	**Methodology**	**Formation Name**	**Model used**	**Observations**
Liu et al. (2021)	• Finite Element Modeling.	——	• Utilized a model based on Li et al. (2015) findings; $$h = 1.04D_1(K^2p)^{\frac{2}{3}}\left[\left(\frac{1-\nu_1^2}{E_1}\right)^{\frac{2}{3}} + \left(\frac{1-\nu_2^2}{E_2}\right)^{\frac{2}{3}}\right] + D_2\frac{p}{E_2}$$ – h is the embedment depth, D_1&D_2 are diameters of the proppant, E_1&E_2 are the proppant elastic modulus, p is the effective stress, ν_1&ν_2 are the poisons ratio.	• Diameter of proppants had insignificant effect on the optimum proppant packing ratio. • Underestimation of proppant concentration was due to proppant embedment negligence.
Ding et al. (2020)	Finite Element Modeling	• Sandstone	• Hypothesised a model based on Hertz (1896) contact theory $$\frac{d}{R} = \left(\frac{3\pi q}{4\left[\frac{1}{\left(\frac{1-\nu_1^2}{E_1}\right)+\left(\frac{1-\nu_2^2}{E_2}\right)}\right]}\right)^{\frac{2}{3}}$$ – d is the contact depth, E_1&E_2 are the proppant elastic modulus, q is the effective stress, ν_1&ν_2 are the poisons ratio.	• Proppant embedment had a detrimental effect on production.
Zhi and Elsworth (2020)	Experimental methodology combined with Numerical Modeling	• Coal and Shale Samples	• Derived a semi-nalytical model to anticipate indentation and propped permeability evolution.	• When the variable stress hardening effect was neglected, proppant embedment was overestimated.

Table 2 continued: Summary of previous studies investigating proppant embedment

Author	Methodology	Formation Name	Model used	Observations
Bandara et al. (2020c)	• Experimental study to investigate crushing and embedment of proppant packs using sintered bauxite ceramic, resin coated sand and natural sand as proppants.	• Steel pedestals of 54mm in diameter.	$Proppant\ embedment(H) = Total\ deformation - Proppant\ deformation - Rock\ deformation - Proppant\ pack\ deformation$	• All proppants exhibited significant pack hardening. • Albeit sand proppants are easier to be obtained in terms of cost, RCP and CCP showed great proppant crushing and embedment tests.
Chen et al. (2020)	Finite Element Modeling	• Formation characteristics of a geothermal reservoir.	• Hypothesised a model based on Hertz (1896) contact theory $$\delta = \left[\frac{3P_{e,c} l_{pr}^2 R}{4E^*}\right]^{\frac{2}{3}} \frac{1}{R}$$ – δ is the contact depth, $P_{e,c}$ is the effective stress, E^* effective youngs modulus for the proppant and rock formation, R is the proppant radius, l_{pr} distance between two adjacent proppants	• The higher the proppant distribution density, the higher the heat extraction rate and the reduction in ammassed thermal energy and break through time.
Perez et al. (2020)	Experiments& Modeling	Shale	Integrated geomechanical workflow	• Fluid design and proppant selection must be optimised considering the geo–mechanical conditions.
Luo et al. (2020b)	Modeling	——	$$\varepsilon(t) = \frac{\sigma}{E_{r0}} + \frac{\sigma}{E_{r1}}\left(1 - e^{\frac{-E_{r1}}{\eta_{r1}} t}\right)$$ • $\varepsilon(t) \equiv degree\ of\ embedment$, $\sigma = exerted\ compressive\ stress$, $E_{r1} \equiv Modulus\ of\ elasticity$	• Proppant grain arrangement significantly influences fracture conductivity and this decreases as the effect of fines migration, crushing of proppants, formation damage and dissolution of proppants.

Table 2 continued: Summary of previous studies investigating proppant embedment

Author	**Methodology**	**Formation Name**	**Model used**	**Observations**
Osiptsov et al. (2020)	Coupled finite element modeling	——	$$e_h = b_0 + b_1\left[1.04D_1\left(K^2p\right)^{\frac{2}{3}} \times\left[\left(\frac{1-\nu^2}{E}+\frac{1-\nu_s^2}{E_s}\right)^{\frac{2}{3}}-\left(\frac{1-\nu^2}{E}\right)^{\frac{2}{3}}\right]+D_2\frac{p}{E}\right]$$ • e_h is the embedment depth, b_0, b_1, D_1&D_2 are parameters describing the embedment. K ≡ piezoconductivity coeficient, p ≡ pressure, E ≡ equivalent elastic modulus of elasticity, E_s ≡ modulus of elasticity of the rock material, ν ≡ poisson ration & ν_s ≡ rock material poisson ration.	• Proppant pack compaction greatly influences fracture conductivity whereas the decrease in fracture aperture due to proppant embedment has an insignificant effect on well production.
Li et al. (2020)	Computational modeling	Shale	• Used the Chen et al. (2017) hypothesis; $h = \eta(\sigma_e)^\lambda$ and h ≡ embedment, η&λ are fitting parameters and σ_e is the effective stress.	• High density proppant embedment reduces fracture deformation as the effective stress increases.
Voltolini and Ajo-Franklin (2020)	• Experimental study supported by insitu X-Ray microtomography – Proppants used are; 1. Sand obtained from Ottawa a proxy for an ideal frac sand 2. Ceramic proppants	• Three shale formations were used; 1. Eagleford shale 2. Marcellus shale 3. Niobrara shale	——	• When quartz grains are intact, induced fracturing and partial embedment of the proppants is seen in all shales.
Yun et al. (2020)	Computational modeling	Geothermal Reservoir	• Used the Hertz (1896) hypothesis; $$\delta = \left[\frac{3P_{e,c}l_{pr}^2R}{4E^*}\right]^{\frac{2}{3}}\frac{1}{R}$$ – δ is the contact depth, $P_{e,c}$ is the effective stress, E^* effective youngs modulus for the proppant and rock formation, R is the proppant radius, l_{pr} distance between two adjacent proppants	• Thermal breakthrough time varies with proppant distribution. • An increase in the propped fracture spacing increased the geothermal development efficiency.

Table 2 continued: Summary of previous studies investigating proppant embedment

Author	**Methodology**	**Formation Name**	**Model used**	**Observations**
Wang and Elsworth (2020)	Computational modeling	——	$$w_e(x,z) = \begin{cases} w_a\left(\frac{3\pi}{4E}\right)^2\left[\frac{16\eta E'^2}{9\pi^3 c_p} ln\left(\frac{w_{r0}(x,z)\overline{\varphi}_{r0}(x,z)}{w_r(x,z)}\right)\right]^{\frac{2}{3}}, & w_r(x,z) \leq w_{r0}(x,z)\overline{\varphi}_{r0}(x,z) \\ 0, & w_r(x,z) \geq w_{r0}(x,z)\overline{\varphi}_{r0}(x,z) \end{cases}$$ • w_a is the asperity width, E is the equivalent young's modulus of elasticity, $w_r(x,z)$ is the fracture aperture, $\overline{\varphi}_{r0}(x,z)$ is the residual proppant concentration.	• Ultra light weight proppants exhibited great performance with gases compared to sands.
Haoze et al. (2020)	Orthogonal experimentation	Coal bed methane reservoir	$$\omega_{pb} = \omega_p - \omega_{p1} - (\omega_b - \omega_{b1})$$ • ω_{pb} is the embedding depth, ω_p is the deformation value of the block under proppant embedment, ω_{p1} is the deformation of the proppant test block at 1MPa, ω_b is the deformation value of the block without proppant placement, ω_{b1} is the deformation of the proppant test block at 1MPa.	• Increase in proppant mesh values increases characteristics of fracture proppant assemblies do increase. • Higher proppant placement may cause fracture damage.
Xu et al. (2019, 2020)	Computational modeling to validate experimental data	Shale	$$h_{em} = u_m - u_p$$ • h_{em} is the embedment depth, u_m is the displacement between the fracture and proppant when there is closure pressure, u_p is the displacement at the contact part of the fracture and proppant.	• There is a non-linear variation in fracture conductivity due to change in mechanical properties of shale.
Fan et al. (2019, 2020)	Discrete element modeling supported by experimental data	——	$$\frac{d}{D} = B^{\frac{1}{2}}\left(\frac{L}{D^2}\right)^{\frac{m}{2}}$$ • d = embedment diameter impress on fractured wall(m), D = proppant diameter, L = load exerted on a proppant surface, B and m are rock fitted coefficients for experimental data.	• Adding more proppants into the fracture alleviates proppant embedment leading to fracture propagation.
Tang et al. (2019)	Experimental	Sandstone	——	• Proppant embedment increased with the increase in shear stress.

Table 2 continued: Summary of previous studies investigating proppant embedment

Author	Methodology	Formation Name	Model used	Observations
Zheng et al. (2020)	Discrete element modeling supported by experiments	Montney siltstone	——	• Proppants with the smallest size resulted in the least proppant embedment.
Elsarawy and Nasr-El-Din (2019)	Experimental	• Eagle Ford shale • Marcellus shale.	——	• Proppant porosity under stress had a direct proportionality to the concentration of proppants and it was opposite to proppant size.
Nakagawa and Borglin (2019)	Experimentation supported by in-situ visualisation	Marcellus shale	——	• Brittleness and high calcite content of shale causes proppant crushing.
Zhong et al. (2019)	Experimentation	1. Longmaxi shale 2. Wufeng shale	——	• Fracture conductivity decreases as the closure pressure increases for both formations.
Karazincir et al. (2018, 2019)	Experimentation	1. Grey Berea 2. Castlegate 3. Berea Buff	——	• Near the fractured face, there was a loss in permeability due to proppant embedment.
Chen et al. (2018)	Computational modeling	——	$d_{c1} = \left(\frac{3.3\pi\sigma_y}{4E'}\right)^2 R$ • d_{c1} = maximum depth of embedment, R = radius of the proppant, σ_y = compressive stress, E' = effective young's modulus of elasticity.	• An increase in proppant concentration had no effect on the contact stress and the degree of embedment.
Mittal et al. (2018)	Experimentation	1. Eagle Ford Shale 2. Vaca Muerta Shale	——	• Proppant embedment had a great dependence on mineralogy.

Table 2 continued: Summary of previous studies investigating proppant embedment

Author	Methodology	Formation Name	Model used	Observations
Pimenov and Kanevskaya (2017)	Mathematical modeling	——	$$u_i(x) = \sum_{l=1}^{m} B_s^{il}(x) D_s^l + \sum_{l=1}^{m} B_n^{il}(x) D_n^l + \int_V G_{ik}(x,z) \triangledown p_{f_k}(z) dV(z)$$ • $u_i(x=$ displacement; $B_s^{il}(x) \& B_n^{il}(x)$ = influence coefficients for displacements; $D_s \& D_n$ =tangential and normal displacement coefficients, $G_{ik}(x,z)$ = Greens function.	• Proppant embedment is minimised by evaluating the change in the well productivity.
Ghanizadeh et al. (2016)	Rigorous core analysis supported by imaging	Montney shale	——	• Propped fracture permeability was higher than the combination of unpropped fracture and matrix permeability.
Mueller and Amro (2015)	Mathematical modeling supported by indentation hardness experiments	1. Marcellus shale 2. Eagle Ford shale 3. Mancos shale	$$u_z = \frac{D}{2} - \sqrt{\left(\frac{D^2}{4} - \frac{d^2}{4}\right)}$$ • u_z = depth of embedment, d = indentantion diameter, D = indenter diameter/proppant diameter.	• Fluid–rock interaction reduced the surface hardness and increased the depth of embedment of all shales.
Corapcioglu et al. (2014)	Experimentation	Niobrara shale	——	• Rock-fluid interactions decreased the youngs modulus while proppant embedment and crushing became inevitable.
Kurz et al. (2013)	Experimentation	Bakken shale	——	• Fracture conductivity was a function of the; proppant type, formation strength, embedment and spalling.
Denney (2012)	Experimentation	Eagle Ford	——	• Samples with the highest carbonate content showed a reduced young's modulus and the highest embedment.

Table 2 continued: Summary of previous studies investigating proppant embedment

Author	Methodology	Formation Name	Model used	Observations
Akrad et al. (2011)	Experimentation	1. Bakken shale 2. Barnett shale 3. Eagle Ford shale 4. Haynesville shale	——	• Exposure to fracturing fluids reduced the youngs modulus leading to embedment in all formations.
Neumann et al. (2010)	Experimental	Quissam Formation(tight limestone)	——	• The use of the right proppant may prevent flowback, crushing and embedment.
Wen et al. (2007)	Experimental	1. Siltstone 2. Conglomerate 3. Dolomitic mudstone	——	• Proppant embedment leads to great fracture damage.
Abass et al. (2006)	Experimentation	Carbonate	——	• Rock-fluid interactions caused embedment.
Nguyen et al. (2005)	Experimental	Unconsolidated sandstone	——	• Proppant packs reduced fines migration.
Lacy et al. (1998)	Computational modeling supported by laboratory experiments.	Sandstone	——	• When the brittle hardness and young's modulus decreases, embedment becomes a problem.
Volk et al. (1981)	Experimental	Tight sandstone	——	• When the proppant coverage decreased, the rate of fracture closure increased.

Bibliography

H. H. Abass, A. A. Al-Mulhem, M. H. Alqam, and M. R. Khan. Acid Fracturing or Proppant Fracturing in Carbonate Formation? A Rock Mechanics View. pages 1–9. Society of Petroleum Engineers, SPE Annual Technical Conference and Exhibition, 24-27 September, San Antonio, Texas, USA, 2006. doi: 10.2118/6813-MS.

Y. N. Abousleiman, M. H. Tran, S. Hoang, C. P. Bobko, A. Ortega, and F.-J. Ulm. Geomechanics Field and Laboratory Characterization of the Woodford Shale: The Next Gas Play. pages 1–14. Society of Petroleum Engineers, SPE Annual Technical Conference and Exhibition, 11-14 November, Anaheim, California, U.S.A., 2007. doi: 10.2118/110120-MS.

M. Ahamed, M. Perera, L. Dong-yin, P. Ranjith, and S. Matthai. Proppant damage mechanisms in coal seam reservoirs during the hydraulic fracturing process: A review. *Fuel*, 253:615–629, 2019. doi: 10.1016/j.fuel.2019.04.166.

O. M. Akrad, J. L. Miskimins, and M. Prasad. The Effects of Fracturing Fluids on Shale Rock Mechanical Properties and Proppant Embedment. pages 1–12. SPE Annual Technical Conference and Exhibition, 30 October-2 November, Denver, Colorado, USA, Society of Petroleum Engineers, 2011. doi: 10.2118/146658-MS.

E. Alagoz and M. M. Sharma. Investigating Shale-Fluid Interactions and Its Effect on Proppant Embedment Using NMR techniques. *American Rock Mechanics Association*, pages 1–8, 2021.

S. Almond, G. Penny, and M. Conway. Factors Affecting Proppant Flowback with Resin Coated Proppants. pages 1–16. Society of Petroleum Engineers, SPE European Formation Damage Conference, 15-16 May, The Hague, Netherlands, 1995. doi: 10.2118/30096-MS.

B. Alramahi and M. Sundberg. Proppant Embedment And Conductivity of Hydraulic Fractures In Shales. pages 1–6. 46th U.S. Rock Mechanics/Geomechanics Symposium, 24-27 June, Chicago, Illinois, American Rock Mechanics Association, 2012.

M. Arshadi, A. Zolfaghari, M. Piri, G. A. Al-Muntasheri, and M. Sayed. The effect of deformation on two-phase flow through proppant-packed fractured shale samples: A micro-scale experimental investigation. *Advances in Water Resources*, 105:108–131, 2017. doi: 10.1016/j.advwatres.2017.04.022.

M. B. Asadi, M. Dejam, and S. Zendehboudi. Semi-analytical solution for productivity evaluation of a multi-fractured horizontal well in a bounded dual-porosity reservoir. *Journal of Hydrology*, 581(124288), 2020. doi: 10.1016/j.jhydrol.2019.124288.

A. I. Assem and H. A. Nasr-El-Din. Interactions Between Mud Acid and Sand Proppants. pages 1–11. Society of Petroleum Engineers, SPE North Africa Technical Conference and Exhibition, 14-16 September, Cairo, Egypt, 2015. doi: 10.2118/175833-MS.

R. Atteberry, R. Tucker, and J. Ritz. Application Of Sintered Bauxite Proppants To Stimulation Of Low Permeability South Texas Gas Reservoirs. pages 1–11. Symposium on Low Permeability Gas Reservoirs, 20-22 May, Denver, Colorado, Society of Petroleum Engineers, 1979. doi: 10.2118/7924-MS.

J. Bai, Y. Kang, Z. Chen, L. You, M. Chen, and X. Li. Changes in retained fracturing fluid properties and their effect on shale mechanical properties. *Journal of Natural Gas Science and Engineering*, 855(103163), 2020. doi: 10.1016/j.jngse.2020.103163.

K. Bandara, P. Ranjith, A. Haque, W. Wanniarachchi, W. Zheng, and T. Rathnaweera. An experimental investigation of the effect of long-term, time-dependent proppant embedment on fracture permeability and fracture aperture reduction. *International Journal of Rock Mechanics and Mining Sciences*, 144:1–22, 2021. doi: 10.1016/j.ijrmms.2021.104813.

K. M. A. S. Bandara, P. G. Ranjith, T. D. Rathnaweera, M. S. A. Perera, and W. Kumari. Thermally-induced mechanical behaviour of a single proppant under compression: Insights into the long-term integrity of hydraulic fracturing in geothermal reservoirs. *Measurement*, pages 76–91, 2018. doi: 10.1016/j.measurement.2018.01.053.

K. M. A. S. Bandara, P. G. Ranjith, and T. D. Rathnaweera. Laboratory-scale study on proppant behaviour in unconventional oil and gas reservoir formations. *Journal of Natural Gas Science and Engineering*, 78(103329), 2020a. doi: 10.1016/j.jngse.2020.103329.

K. M. A. S. Bandara, P. G. Ranjith, and T. D. Rathnaweera. Extensive analysis of single ceramic proppant fracture mechanism and the influence of realistic extreme reservoir conditions on proppant mechanical performance. *Journal of Petroleum Science and Engineering*, page 107586, 2020b. doi: 10.1016/j.petrol.2020.107586.

K. M. A. S. Bandara, P. G. Ranjith, T. D. Rathnaweera, W. A. M. Wanniarachchi, and S. Q. Yang. Crushing and embedment of proppant packs under cyclic loading: An insight to enhanced unconventional oil/gas recovery. *Geoscience Frontiers*, pages 1–15, 2020c. doi: 10.1016/j.gsf.2020.02.017.

B. R. Barboza, B. Chen, and C. Li. A Review on Proppant Transport Modelling. *Journal of Petroleum Science and Engineering*, pages 1–13, 2021. doi: 10.1016/j.petrol.2021.108753.

R. Barree and M. Conway. Proppant Holdup, Bridging, and Screenout Behavior in Naturally Fractured Reservoirs. pages 1–7. Society of Petroleum Engineers, SPE Production and Operations Symposium, 24-27 March, Oklahoma City, Oklahoma, 2000. doi: 10.2118/67298-MS.

R. Barree and M. Conway. Experimental and Numerical Modeling of Convective Proppant Transport. pages 1–16. Society of Petroleum

Engineers, SPE Annual Technical Conference and Exhibition, 25-28 September, New Orleans, Louisiana, 1994. doi: 10.2118/28564-MS.

R. D. Barree, R. J. Duenckel, and B. T. Hlidek. Proppant Sieve Distribution - What Really Matters? pages 1–14. SPE Hydraulic Fracturing Technology Conference and Exhibition, 5-7 February, The Woodlands, Texas, USA, Society of Petroleum Engineers, 2019. doi: 10.2118/194382-MS.

R. Beckwith. Proppants: Where in the World. pages 1–5. Journal of Petroleum Technology, Society of Petroleum Engineers, 2011. doi: 10.2118/0411-0036-JPT.

M. Benge, Y. Lu, A. Katende, J. Rutqvist, D. Crandall, A. Haecker, G. King, J. Renk, M. Radonjic, and A. Bunger. Connecting Geomechanical Properties with Potential for Proppant Embedment and Production Decline for the Emerging Caney Shale, Oklahoma. pages 1–6. Society of Petroleum Engineers, Unconventional Resources Technology Conference held in Houston, Texas, USA, 26-28 July 2021, 2021.

M. R. Besler, J. W. Steele, T. Egan, and J. Wagner. Improving Well Productivity and Profitability in the BakkenA Summary of Our Experiences Drilling, Stimulating, and Operating Horizontal Wells. pages 1–13. Society of Petroleum Engineers, SPE Annual Technical Conference and Exhibition held in Anaheim, California, U.S.A., 1114 November 2007., 2007. doi: 10.2118/110679-MS.

A. R. Bhandari, P. B. Flemings, and R. Hofmann. The dependence of shale permeability on confining stress and pore pressure. *Journal of Natural Gas Science and Engineering*, 92:1–16, 2021. doi: 10.1016/j.jngse.2021.1040081.

S. Bilgen and I. Sarikaya. New horizon in energy: Shale gas. *Journal of Natural Gas Science and Engineering*, 35, Part A:637–645, 2016. doi: 10.1016/j.jngse.2016.09.014.

D. Boardman and J. Puckette. Stratigraphy and Paleontology of the Upper Mississippian Barnett Shale of Texas and Caney Shale of Southern Oklahoma. OGS Open-File Report No. 6, 2006. Oklahoma Geological Survey, Norman Oklahoma.

J. M. Bremer, B. Mibeck, B. L. Huffman, C. D. Gorecki, J. A. Sorensen, D. D. Schmidt, and J. A. Harju. Mechanical and Geochemical Assessment of Hydraulic Fracturing Proppants Exposed to Carbon Dioxide and Hydrogen Sulfide. pages 1–9. Canadian Unconventional Resources and International Petroleum Conference, 19-21 October, Calgary, Alberta, Canada, Society of Petroleum Engineers, 2010. doi: 10.2118/136550-MS.

L. Britt. Fracture stimulation fundamentals. *Journal of Natural Gas Science and Engineering*, 8:34–51, 2012. doi: 10.1016/j.jngse.2012.06.006.

L. K. Britt, M. B. Smith, Z. A. Haddad, J. P. Lawrence, S. T. Chipperfield, and T. J. Hellman. Waterfracs: We Do Need Proppant After All. pages 1–15. Society of Petroleum Engineers, SPE Annual Technical Conference and Exhibition, 24-27 September, San Antonio, Texas, USA, 2006. doi: 10.2118/102227-MS.

A. Buenrostro, A. Harbi, A. Arevalo, and J. Carmona. Channel Fracturing Technology to Successfully Deploy Proppant Fracturing Stimulation Under Limited BHP Window for Completion Integrity. pages 1–11. Society of Petroleum Engineers, SPE Middle East Oil and Gas Show and Conference, 18-21 March, Manama, Bahrain, 2019. doi: 10.2118/195086-MS.

J. M. Burgers. Het atoommodel van Rutherford-Bohr. *Royal Netherlands Academy of Arts and Sciences.*, 1918. doi: http://ilorentz.org/history/proefschriften/sources/Burgers_1918.pdf.

H. B. Carroll and B. Baker. Particle Size Distributions Generated By Crushed Proppants And Their Effects On Fracture Conductivity. pages 1–11. Symposium on Low Permeability Gas Reservoirs, 20-22 May, Denver, Colorado, Society of Petroleum Engineers, 1979. doi: 10.2118/7923-MS.

D. Chen, Z. Ye, Z. Pan, Y. Zhou, and J. Zhang. A permeability model for the hydraulic fracture filled with proppant packs under combined effect of compaction and embedment. *Journal of Petroleum Science and Engineering*, 149:428–435, 2017. doi: 10.1016/j.petrol.2016.10.045.

M. Chen, S. Zhang, M. Liu, X. Ma, Y. Zou, T. Zhou, N. Li, and S. Li. Calculation method of proppant embedment depth in hydraulic fracturing. *Petroleum Exploration and Development*, 45(1):159–166, 2018. doi: 10.1016/S1876-3804(18)30016-8.

X. Chen, P. Eichhubl, J. E. Olson, and T. A. Dewers. Effect of Water on Fracture Mechanical Properties of Shales. *Journal of Geophysical Research-Solid Earth*, 124(3):2428–2444, 2019. doi: 10.1029/2018JB016479.

Y. Chen, H. Wang, T. Li, Y. Wang, F. Ren, and G. Ma. Evaluation of geothermal development considering proppant embedment in hydraulic fractures. *Renewable Energy*, 153:985–997, 2020. doi: 10.1016/j.renene.2020.02.063.

C. Cheng and A. P. Bunger. Rapid simulation of multiple radially growing hydraulic fractures using an energy-based approach. *International Journal of Numerical and Analystical Methods in Geomechanics*, 2015. doi: 10.1002/nag.2471.

T. Chun, D. Zhu, Z. Zhang, S. Mao, and K. Wu. Experimental Study of Proppant Transport in Complex Fractures with Horizontal Bedding Planes for Slickwater Fracturing. *SPE Production and Operations*, 36(01):1–13, 2021. doi: 10.2118/199877-PA.

D. Chuprakov, L. Belyakova, A. Iuldasheva, A. Alekseev, D. Syresin, M. Chertov, P. Spesivtsev, F. I. S. Suarez, I. Velikanov, L. Semin, and D. Bannikov. Proppant Flowback: Can We Mitigate the Risk? pages 1–27. Society of Petroleum Engineers, SPE Hydraulic Fracturing Technology Conference and Exhibition, 4-6 February, The Woodlands, Texas, USA, 2020. doi: 10.2118/199748-MS.

D. Chuprakov, A. Iuldasheva, and A. Alekseev. Criterion of proppant pack mobilization by filtrating fluids: Theory and experiments. *Journal of Petroleum Science and Engineering*, page 107792, 2021. doi: 10.1016/j.petrol.2020.107792.

P. E. Clark. Transport of Proppant in Hydraulic Fractures. *Society of Petroleum Engineers*, pages 1–7, 2006. doi: 10.2118/103167-MS.

C. Clarkson, N. Solano, R. M. Bustin, A. Bustin, G. Chalmers, L. He, Y. Melnichenko, A. Radlinski, and T. Blach. Pore structure characterization of North American shale gas reservoirs using USANS/SANS, gas adsorption, and mercury intrusion. *Fuel*, 103:606–616, 2013. doi: 10.1016/j.fuel.2012.06.119.

C. R. Clarkson, J. L. Jensen, and T. Blasingame. Reservoir Engineering for Unconventional Reservoirs: What Do We Have to Consider? pages 1–45. Society of Petroleum Engineers, North American Unconventional Gas Conference and Exhibition, 14-16 June, The Woodlands, Texas, USA, 2011. doi: 10.2118/145080-MS.

C. Cooke. Conductivity of Fracture Proppants in Multiple Layers. pages 1–7. Journal of Petroleum Technology, Society of Petroleum Engineers, 1973a. doi: 10.2118/4117-PA.

C. E. Cooke. Fracturing With a High-Strength Proppant. pages 1–5. Journal of Petroleum Technology, Society of Petroleum Engineers, 1977. doi: 10.2118/6213-PA.

C. E. Cooke. Conductivity of Fracture Proppants in Multiple Layers. pages 1–7. Society of Petroleum Engineers, Journal of Petroleum Technology, September 1973b. doi: 10.2118/4117-PA.

C. E. Cooke, J. L. Gidley, and D. H. Mutti. Use of High-Strength Proppant for Fracturing Deep Wells. pages 1–8. SPE Deep Drilling and Production Symposium, 17-19 April, Amarillo, Texas, Society of Petroleum Engineers, 1977. doi: 10.2118/6440-MS.

H. Corapcioglu, J. Miskimins, and M. Prasad. Fracturing Fluid Effects on Young's Modulus and Embedment in the Niobrara Formation. pages 1–17. SPE Annual Technical Conference and Exhibition, 27-29 October, Amsterdam, The Netherlands, Society of Petroleum Engineers, 2014. doi: 10.2118/170835-MS.

G. Coulter and R. D. Wells. The Advantages of High Proppant Concentration in Fracture Stimulation. pages 1–5. Journal of Petroleum Technology, Society of Petroleum Engineers, 1972. doi: 10.2118/3298-PA.

A. C. F. Cripps. *Introduction to Contact Mechanics*. Springer, 2007. ISBN 978-0-387-68187-0.

M. E. Curtis, R. J. Ambrose, C. H. Sondergeld, and C. S. Rai. Transmission and Scanning Electron Microscopy Investigation of Pore Connectivity of Gas Shales on the Nanoscale. pages 1–10. Society of Petroleum Engineers, North American Unconventional Gas Conference and Exhibition, 14-16 June, The Woodlands, Texas, USA, 2011. doi: 10.2118/144391-MS.

M. E. Curtis, E. Goergen, J. Jernigen, C. H. Sondergeld, and C. S. Rai. High-Resolution Mapping of the Distribution and Connectivity of Organic Matter in Shales. pages 1–8. Society of Petroleum Engineers, SPE Annual Technical Conference and Exhibition, 27-29 October, Amsterdam, The Netherlands, 2014. doi: 10.2118/170787-MS.

D. K. Danso, B. M. Negash, T. Y. Ahmed, N. Yekeen, and T. A. O. Ganat. Recent advances in multifunctional proppant technology and increased well output with micro and nano proppants. *Journal of Petroleum Science and Engineering*, 196:1–22, 2021. doi: 10.1016/j.petrol.2020.108026.

M. Dejam. Tracer dispersion in a hydraulic fracture with porous walls. *Chemical Engineering Research and Design*, 150:169–178, 2019. doi: 10.1016/j.cherd.2019.07.027.

M. Dejam, H. Hassanzadeh, and Z. Chen. Semi-analytical solution for pressure transient analysis of a hydraulically fractured vertical well in a bounded dual-porosity reservoir. *Journal of Hydrology*, 565:289–301, 2018. doi: 10.1016/j.jhydrol.2018.08.020.

S. Deng, H. Li, G. Ma, H. Huang, and X. Li. Simulation of shaleproppant interaction in hydraulic fracturing by the discrete element method. *International Journal of Rock Mechanics and Mining Sciences*, 70:219–228, 2014. doi: 10.1016/j.ijrmms.2014.04.011.

D. Denney. Fracturing-Fluid Effects on Shale and Proppant Embedment. pages 1–3. Journal of Petroleum Technology, Society of Petroleum Engineers, 2012. doi: 10.2118/0312-0059-JPT.

E. Detournay and A. H. D. Cheng. Fundamentals of Poroelasticity. *Analysis and Design Methods*, pages 113–171, 1993. doi: 10.1016/B978-0-08-040615-2.50011-3.

D. Dewhurst, A. Bunger, M. Josh, J. Sarout, C. D. Piane, L. Esteban, and M. Clennell. Mechanics, Physics, Chemistry and Shale Rock Properties. pages 1–11. American Rock Mechanics Association, 47th U.S. Rock Mechanics/Geomechanics Symposium, 23-26 June, San Francisco, California, 2013. doi: https://www.onepetro.org/conference-paper/ARMA-2013-151.

B. Dewprashad, H. Abass, D. Meadows, J. Weaver, and B. Bennett. A Method To Select Resin-Coated Proppants. pages 1–8. Society of Petroleum Engineers, SPE Annual Technical Conference and Exhibition, 3-6 October, Houston, Texas, 1993. doi: 10.2118/26523-MS.

B. Dindoruk, R. R. Ratnakar, and J. He. Review of recent advances in petroleum fluid properties and their representation. *Journal of Natural Gas Science and Engineering*, pages 1–13, 2020. doi: 10.1016/j.jngse.2020.103541.

X. Ding, F. Zhang, L. Yang, and G. Q. Zhang. Modelling Proppant Embedment in Viscoelastic Formations with the Fractional Maxwell Model. pages 1–12. International Society for Rock Mechanics and Rock Engineering, ISRM International Symposium - 10th Asian Rock Mechanics Symposium, 29 October - 3 November, Singapore, 2018.

X. Ding, F. Zhang, and G. Zhang. Modelling of time-dependent proppant embedment and its influence on tight gas production. *Journal of Natural Gas Science and Engineering*, (103519), 2020. doi: 10.1016/j.jngse.2020.103519.

T. Dong, N. B. Harris, K. Ayranci, and S. Yang. The impact of rock composition on geomechanical properties of a shale formation: Middle and Upper Devonian Horn River Group shale, Northeast British Columbia, Canada. *AAPG Bulletin*, 101(2):177204, 2017. doi: 10.1306/07251615199.

T. Dong, N. B. Harris, L. J.Knapp, J. M. McMillan, and D. L. Bish. The effect of thermal maturity on geomechanical properties in shale reservoirs: An example from the Upper Devonian Duvernay Formation, Western Canada Sedimentary Basin. *Marine and Petroleum Geology*, 97:137–153, 2018. doi: 10.1016/j.marpetgeo.2018.07.007.

E. V. Dontsov and A. P. Peirce. The Effect of Proppant Size on Hydraulic Fracturing by a Slurry. pages 1–11. 48th U.S. Rock Mechanics/Geomechanics Symposium, 1-4 June, Minneapolis, Minnesota, Society of Petroleum Engineers, 2014.

H. Du, M. Radonjic, and Y. Chen. Microstructure and micro-geomechanics evaluation of Pottsville and Marcellus shales. *Journal of Petroleum Science and Engineering*, 2021. doi: 10.1016/j.petrol.2020.107876.

R. Duenckel, M. W. Conway, B. Eldred, and M. Vincent. Proppant Diagenesis–Integrated Analyses Provide New Insights Into Origin, Occurrence, and Implications for Proppant Performance. pages 1–14. SPE Production & Operations, Society of Petroleum Engineers, 2012. doi: 10.2118/139875-PA.

R. Duenckel, N. Moore, L. O'Connell, K. Abney, S. Drylie, and F. Chen. The Science of Proppant Conductivity Testing-Lessons Learned and Best Practices. pages 1–20. Society of Petroleum Engineers, SPE Hydraulic Fracturing Technology Conference, The Woodlands, Texas, USA, February 2016. Paper Number: SPE-179125-MS, 2016. doi: 10.2118/179125-MS.

R. J. Duenckel, M. W. Conway, B. Eldred, and M. C. Vincent. Proppant Diagenesis - Integrated Analyses Provide New Insights Into Origin, Occurrence, And Implications For Proppant Performance. pages 1–27. SPE Hydraulic Fracturing Technology Conference, 24-26 January, The Woodlands, Texas, USA, Society of Petroleum Engineers, 2011. doi: 10.2118/139875-MS.

R. Dusterhoft, P. Nguyen, and M. Conway. Maximizing Effective Proppant Permeability under High-Stress, High Gas-Rate Conditions. pages 1–16. Society of Petroleum Engineers, SPE Annual Technical Conference and Exhibition, 26-29 September, Houston, Texas, 2004. doi: 10.2118/90398-MS.

M. G. Edgin, B. Medina-Rodriguez, J. P. Kaszuba, J. C. Dewey, and V. Alvarado. Geochemical reactions and alteration of pore architecture in saturated shale after injection of stimulation fluid. *Fuel*, (120815):1–11, 2021. doi: 10.1016/j.fuel.2021.120815.

M. A. El-Kader, M. I. Abdoub, A. M. Fadl, A. A. Rabou, O. A. Desouky, and M. F. El-Shahat. Novel light-weight glass-ceramic proppants based on frits for hydraulic fracturing process. *Ceramics International*, 46(2), 2020. doi: 10.1016/j.ceramint.2019.09.173.

H. Elochukwu and K. K. KhaiKiat. Characterization of Baram and Tanjung sands as potential proppants. *Energy Geoscience*, 2(3):175–180, 2021. doi: 10.1016/j.engeos.2020.12.002.

A. M. Elsarawy and H. A. Nasr-El-Din. An Experimental Investigation of Proppant Diagenesis and Proppant-Formation-Fluid Interactions in Hydraulic Fracturing of Eagle Ford Shale. pages 1–25. SPE Trinidad and Tobago Section Energy Resources Conference, 25-26 June, Port of Spain, Trinidad and Tobago, Society of Petroleum Engineers, 2018. doi: 10.2118/191225-MS.

A. M. Elsarawy and H. A. Nasr-El-Din. Proppant Diagenesis in Carbonate-Rich Eagle Ford Shale Fractures. pages 1–13. SPE Drilling & Completion, Society of Petroleum Engineers, 2020. doi: 10.2118/200481-PA.

A. M. Elsarawy and H. A. Nasr-El-Din. A new method to measure propped fracture width and proppant porosity in shale fractures. *Journal of Petroleum Science and Engineering*, 181(106162), 2019. doi: 10.1016/j.petrol.2019.06.026.

T. Eren and V. S. Suicmez. Directional drilling positioning calculations. *Journal of Natural Gas Science and Engineering*, 73(103081), 2020. doi: 10.1016/j.jngse.2019.103081.

M. O. Eshkalak, S. D. Mohaghegh, and S. Esmaili. Geomechanical Properties of Unconventional Shale Reservoirs. *Journal of Petroleum Engineering*, pages 1–10, 2014. doi: 10.1155/2014/961641.

M. Fan, J. McClure, Y. Han, N. Ripepi, E. Westman, M. Gu, and C. Chen. Calculation method of proppant embedment depth in hydraulic fracturing. pages 1–17. SPE Journal, Society of Petroleum Engineers, 2019. doi: 10.2118/195588-PA.

M. Fan, Y. Han, M. Gu, J. M. amd Nino Ripepi, E. Westman, and C. Chen. Investigation of the Conductivity of a Proppant Mixture Using an Experiment/Simulation-integrated Approach. *Journal of Natural Gas Science and Engineering*, (103234), 2020. doi: 10.1016/j.jngse.2020.103234.

M. Fan, Z. Li, Y. Han, Y. Teng, and C. Chen. Experimental and Numerical Investigations of the Role of Proppant Embedment on Fracture Conductivity in Narrow Fractures. *SPE Journal*, 26(1):1–13, 2021. doi: 10.2118/204222-PA.

W. Fei, Q. Chen, X. Lyu, and S. Zhang. Fracturing-Fluid Flowback

Simulation with Consideration of Proppant Transport in Hydraulically Fractured Shale Wells. *ACS Omega*, 5(16):94919502, 2020. doi: 10.1021/acsomega.0c00714.

L. P. Frash, J. Hampton, M. Gutierrez, A. Tutuncu, J. W. Carey, J. Hood, M. Mokhtari, H. Huang, and E. Mattson. Patterns in complex hydraulic fractures observed by true-triaxial experiments and implications for proppant placement and stimulated reservoir volumes. *Journal of Petroleum Exploration and Production Technology*, pages 2781–2792, 2019. doi: 10.1007/s13202-019-0681-2.

S. J. Frederic, F. Sanfilippo, J.-M. Embry, M. White, and J. B. Turnbull. The Sanding Mechanisms of Water Injectors and their QUantification in Terms of Sand Production: Example of the Buuzard Field (UKCS). pages 1–13. Society of Petroleum Engineers, SPE Annual Technical Conference and Exhibition, 30 October-2 November, Denver, Colorado, USA, 2011. doi: 10.2118/146551-MS.

L. Froute and A. R. Kovscek. Nano-Imaging of Shale Using Electron Microscopy Techniques. pages 1–12. Society of Petroleum Engineers, SPE/AAPG/SEG Unconventional Resources Technology Conference, 20-22 July, Virtual, 2020. doi: 10.15530/urtec-2020-3283.

A. Gaurav, E. Dao, and K. K. Mohanty. Evaluation of ultra-light-weight proppants for shale fracturing. *Journal of Petroleum Science and Engineering*, 92-93:82–88, 2012. doi: 10.1016/j.petrol.2012.06.010.

A. Ghanizadeh, C. R. Clarkson, S. Aquino, O. H. Ardakani, and H. Sanei. Petrophysical and geomechanical characteristics of Canadian tight oil and liquid-rich gas reservoirs: II. Geomechanical property estimation. *Fuel*, 153:682–691, 2015. doi: 10.1016/j.fuel.2015.02.113.

A. Ghanizadeh, C. R. Clarkson, H. Deglint, A. Vahedian, S. Aquino, and J. Wood. Unpropped/Propped Fracture Permeability and Proppant Embedment Evaluation: A Rigorous Core-Analysis/Imaging Methodology. pages 1–29. Unconventional Resources Technology Conference, San Antonio, Texas, 1-3 August 2016, Society of Petroleum Engineers, 2016. doi: 10.15530/urtec-2016-2459818.

H. Ghofrani and G. M. Atkinson. Activation Rate of Seismicity for Hydraulic Fracture Wells in the Western Canada Sedimentary Basin. *Bulletin of the Seismological Society of America*, 2020. doi: 10.1785/0120200002.

S. Ghosh, C. S. Rai, C. H. Sondergeld, and R. E. Larese. Experimental Investigation of Proppant Diagenesis. pages 1–23. SPE/CSUR Unconventional Resources Conference Canada, 30 September2 October, Calgary, Alberta, Canada, Society of Petroleum Engineers, 2014. doi: 10.2118/171604-MS.

D. Gokaraju, A. Thombare, S. Govindarajan, A. Mitra, A. Guedez, and M. Aldin. Laboratory Investigation and Characterization of the Poroelastic Response of Ultra-Tight Formations. *International Petroleum Technology Conference*, pages 1–13, 2020. doi: 10.2523/IPTC-19686-ABSTRACT.

M. Gu, E. Dao, and K. K. Mohanty. Investigation of ultra-light weight proppant application in shale fracturing. *Fuel*, 150:191–201, 2015. doi: 10.1016/j.fuel.2015.02.019.

A. S. Gundogar, C. M. Ross, A. D. Jew, J. R. Bargar, and A. R. Kovscek. Multiphysics Investigation of Geochemical Alterations in Marcellus Shale Using Reactive Core-Floods. *Energy and Fuels*, pages 1–13, 2021. doi: 10.1021/acs.energyfuels.1c00588.

J. Guo and Y. Liu. Modeling of Proppant Embedment: Elastic Deformation and Creep Deformation. pages 1–7. SPE International Production and Operations Conference & Exhibition, 14-16 May, Doha, Qatar, Society of Petroleum Engineers, 2012. doi: 10.2118/157449-MS.

T. Guo, S. Zhang, L. Wang, W. Sui, and H. Wen. Optimization of proppant size for frac pack completion using a new equipment. *Journal of Petroleum Science and Engineering*, 96–97:1–9, 2012. doi: 10.1016/j.petrol.2012.08.007.

A. Gupta, C. Rai, and C. Sondergeld. Experimental Investigation of Propped Fracture Conductivity and Proppant Diagenesis. pages 1–18. Unconventional Resources Technology Conference, Society of Petroleum Engineers, 2019. doi: 10.15530/urtec-2019-363.

J. Han and J. Y. Wang. Fracture Conductivity Decrease Due to Proppant Deformation and Crushing, a Parametrical Study. pages 1–15. Society of Petroleum Engineers, SPE Eastern Regional Meeting, 21-23 October, Charleston, WV, USA, 2014. doi: 10.2118/171019-MS.

J. Han, J. Y. Wang, and V. Puri. A fully coupled geomechanics and fluid flow model for proppant pack failure and fracture conductivity damage analysis. *Journal of Natural Gas Science and Engineering*, 31:546–554, 2016. doi: 10.1016/j.jngse.2016.03.034.

J. Hao, H. Hao, Y. Gao, X. Li, M. Qin, and K. Wang. Effect of Sintering Temperature on Property of Low-Density Ceramic Proppant Adding Coal Gangue. *Materials Science–Ceramics and Glasses*, 26(1), 2020. doi: hhttps://doi.org/10.5755/j01.ms.26.1.19376.

L. Haoze, B. Huang, Q. Cheng, and X. Zhao. Optimization of proppant parameters for CBM extraction using hydrofracturing by orthogonal experimental process. *Journal of Geophysics and Engineering*, pages 1–13, 2020. doi: https://doi.org/10.1093/jge/gxaa009.

L. Haoze, B. Huang, Q. Cheng, X. Zhao, B. Chen, and L. Zhao. Mechanism of Single Proppant Pressure Embedded in Coal Seam Fracture. *Energy Fuels*, 35(9):77567767, 2021. doi: https://doi.org/10.1021/acs.energyfuels.0c04360.

P. C. Harris and S. Heath. Proppant Transport of Fracturing Gels is Influenced by Proppant Type. pages 1–10. Society of Petroleum Engineers, SPE Hydraulic Fracturing Technology Conference, 19-21 January, The Woodlands, Texas, 2006. doi: 10.2118/118717-MS.

H. He, L. Luo, and K. Senetakis. Effect of normal load and shearing velocity on the interface friction of organic shale Proppant simulant. *Tribology International*, 144, 2020. doi: 10.1016/j.triboint.2019.106119.

L. He, H. Mei, X. Hu, M. Dejam, Z. Kou, and M. Zhang. Advanced Flowing Material Balance To Determine Original Gas in Place of Shale Gas Considering Adsorption Hysteresis. pages 1–11. Society of Petroleum Engineers, SPE Reservoir Evaluation & Engineering, 2019. doi: 10.2118/195581-PA.

H. Hertz. Uber die beruhrung fester elastischer Korper (On the contact of rigid elastic solids). *London: Macmillan, New York, Macmillan and co.*, pages 1857–1894, 1896. doi: https://archive.org/details/cu31924012500306/page/n45/mode/2up.

B. Hlidek and R. Duenckel. High Viscosity Friction Reducers - Potential for Fracture Damage and Impact of Brines on Proppant Transport Capability. pages 1–26. SPE Hydraulic Fracturing Technology Conference and Exhibition, 4-6 February, The Woodlands, Texas, USA, Society of Petroleum Engineers, February 2020. doi: 10.2118/199736-MS.

S. Holditch and J. Ely. Successful Stimulation of Deep Wells Using High Proppant Concentrations. pages 1–5. Journal of Petroleum Technology, Society of Petroleum Engineers, 1973. doi: 10.2118/4118-PA.

N. Hosseini and A. R. Khoei. Numerical simulation of proppant transport and tip screen-out in hydraulic fracturing with the extended finite element method. *International Journal of Rock Mechanics and Mining Sciences*, 128(104247), 2020. doi: 10.1016/j.ijrmms.2020.104247.

L. Hou, D. Elsworth, and X. Geng. Swelling and embedment induced by sub- and super-critical-CO2 on the permeability of propped fractures in shale. *International Journal of Coal Geology*, (103496), 2020. doi: 10.1016/j.coal.2020.103496.

D. Hu, D. N. Benoit, P. Nguyen, and R. Gashimov. Quantitative Analysis of Proppant-Formation Interactions by Digital Rock Methods. pages 1–11. Society of Petroleum Engineers, SPE Annual Technical Conference and Exhibition, 26-28 September, Dubai, UAE, 2016. doi: 10.2118/181342-MS.

M. Hu and J. Rutqvist. Multi-scale Coupled Processes Modeling of Fractures as Porous, Interfacial and Granular Systems from Rock Images with the Numerical Manifold Method. *Rock Mechanics and Rock Engineering*, pages 1–19, 2021. doi: 10.1007/s00603-021-02455-6.

F. Huang, C. Dong, Z. You, and X. Shang. Detachment of coal fines deposited in proppant packs induced by single-phase water flow: Theoretical and experimental analyses. *International Journal of Coal Geology*, 239:1–13, 2021a. doi: 10.1016/j.coal.2021.103728.

J. Huang, W. Gong, L. Lin, C. Yin, F. Liu, H. Zhou, L. Bai, L. Song, and Z. Yang. In-situ Proppant: Beads, Microproppant, and Channelized-Proppant. pages 1–13. Society of Petroleum Engineers, Abu Dhabi International Petroleum Exhibition & Conference, 11-14 November, Abu Dhabi, UAE, 2019. doi: 10.2118/197638-MS.

X. Huang, L. Zhang, R. Zhang, X. Chen, Y. Zhao, and S. Yuan. Numerical simulation of gas-liquid two-phase flow in the micro-fracture networks in fractured reservoirs. *Journal of Natural Gas Science and Engineering*, pages 1–26, 2021b. doi: 10.1016/j.jngse.2021.104101.

P. T. Huckabee, M. C. Vincent, J. M. Foreman, and J. P. Spivey. Field Results: Effect of Proppant Strength and Sieve Distribution Upon Well Productivity. pages 1–12. SPE Annual Technical Conference and Exhibition, 9-12 October, Dallas, Texas, Society of Petroleum Engineers, 2005. doi: 10.2118/96559-MS.

C. C. Iferobia and M. Ahmad. A review on the experimental techniques and applications in the geomechanical evaluation of shale gas reservoirs. *Journal of Natural Gas Science and Engineering*, (103090), 2020. doi: 10.1016/j.jngse.2019.103090.

J. Iriarte and A. N. Tutuncu. Geochemical and Geomechanical Alterations Related to Rock-Fluid-Proppant Interactions in the Niobrara Formation. pages 1–16. Society of Petroleum Engineers, SPE International Conference and Exhibition on Formation Damage Control, 7-9 February, Lafayette, Louisiana, USA, 2018. doi: 10.2118/189536-MS.

A. Isah, M. Hiba, K. Al-Azani, M. S. Aljawad, and M. Mahmoud. A comprehensive review of proppant transport in fractured reservoirs: Experimental, numerical, and field aspects. *Journal of Natural Gas Science and Engineering*, pages 1–13, 2021. doi: 10.1016/j.jngse.2021.103832.

M. A. Islam and P. Skalle. An Experimental Investigation of Shale Mechanical Properties Through Drained and Undrained Test Mechanisms. *Rock Mechanics and Rock Engineering*, 46:13911413, 2013. doi: 10.1007/s00603-013-0377-8.

Itasca. Proppant in Fluid Filled Joints–Itasca Consulting Group, Inc. https://www.itascacg.com/learning/tutorials/proppant-in-fluid-filled-joints, 2014. Online; last accessed January 30, 2020.

D. J. Jacobi, J. J. Breig, B. LeCompte, M. Kopal, G. Hursan, F. E. Mendez, S. Bliven, and J. Longo. Effective Geochemical and Geomechanical Characterization of Shale Gas Reservoirs From the Wellbore Environment: Caney and the Woodford Shale. pages 1–11. Society of Petroleum Engineers, SPE Annual Technical Conference and Exhibition, 4-7 October, New Orleans, Louisiana, 2009. doi: 10.2118/124231-MS.

S. J. M. Jeffry, K. Trjangganung, A. A. Chandrakant, B. Madon, A. Katende, and I. Ismail. Selection of suitable acid chemicals for matrix stimulation: A Malaysian Brown field scenario. *Journal of Petroleum Science and Engineering*, 186(106689), 2020. doi: 10.1016/j.petrol.2019.106689.

L. Jia, K. Li, J. Zhou, Z. Yan, F. Wan, and M. Kaita. A mathematical model for calculating rod-shaped proppant conductivity under the combined effect of compaction and embedment. *Journal of Petroleum Science and*

Engineering, pages 11–21, 2019. doi: 10.1016/j.petrol.2019.05.034.

Z. Kang, Y. Zhao, and D. Yang. Review of oil shale in-situ conversion technology. *Applied Energy*, 269(115121), 2020. doi: 10.1016/j.apenergy.2020.115121.

O. Karazincir, Y. Li, K. Zaki, W. Williams, R. Wu, Y. Tan, P. Rijken, and A. Rickards. Measurement of Reduced Permeability at Fracture Face Due to Proppant Embedment and Depletion. pages 1–16. SPE Annual Technical Conference and Exhibition, 24-26 September, Dallas, Texas, USA, Society of Petroleum Engineers, 2018. doi: 10.2118/196204-MS.

O. Karazincir, Y. Li, K. Zaki, W. Williams, R. Wu, Y. Tan, P. Rijken, and A. Rickards. Measurement of Reduced Permeability at Fracture Face Due to Proppant Embedment and Depletion - Part II. pages 1–18. SPE Annual Technical Conference and Exhibition, 30 September - 2 October, Calgary, Alberta, Canada, Society of Petroleum Engineers, 2019. doi: 10.2118/196204-MS.

A. Katende, J. Rutqvist, M. Benge, A. Seyedolali, A. Bunger, J. Puckette, A. Rihn, and M. Radonjic. Convergence of micro-geochemistry and micro-geomechanics towards understanding proppant shale rock interaction: a Caney shale case study in southern Oklahoma, USA(Submitted for publication, June 15, 2021). 2021.

H. J. Khan, E. Spielman-Sun, A. D. Jew, J. Bargar, A. Kovscek, and J. L. Druhan*. A Critical Review of the Physicochemical Impacts of Water Chemistry on Shale in Hydraulic Fracturing Systems. *Environmental Science and Technology*, 55(3):13771394, 2021. doi: 10.1021/acs.est.0c04901.

A. Khanna, A. Kotousov, J. Sobey, and P. Weller. Conductivity of narrow fractures filled with a proppant monolayer. *Journal of Petroleum Science and Engineering*, 100:9–13, 2015. doi: 10.1016/j.petrol.2012.11.016.

M. R. Krishnan, Y. Aldawsari, F. M. Michael, W. Li, and E. H. Alsharaeh. Mechanically reinforced polystyrene-polymethyl methacrylate copolymer-graphene and Epoxy-Graphene composites dual-coated sand proppants for hydraulic fracture operations. *Journal of Petroleum Science and Engineering*, 2021. doi: 10.1016/j.petrol.2020.107744.

B. A. Kurz, D. D. Schmidt, and P. E. Cortese. Investigation of Improved Conductivity and Proppant Applications in the Bakken Formation. pages 1–13. SPE Hydraulic Fracturing Technology Conference, 4-6 February, The Woodlands, Texas, USA, Society of Petroleum Engineers, 2013. doi: 10.2118/163849-MS.

L. L. Lacy, A. Rickards, and D. Bilden. Fracture Width and Embedment Testing in Soft Reservoir Sandstone. pages 1–5. SPE Drilling & Completion, Society of Petroleum Engineers, 1998. doi: 10.2118/36421-PA.

R. F. LaFollette and P. S. Carman. Proppant Diagenesis: Results So Far. pages 1–14. SPE Unconventional Gas Conference, 23-25 February, Pittsburgh, Pennsylvania, USA, Society of Petroleum Engineers, 2010. doi: 10.2118/131782-MS.

L. Lawal and M. Mahmoud. Poisson's Ratio, Porosity and Aspect Ratio as Geomechanical Index of Shale Brittleness. pages 1–8. International Petroleum Technology Conference, International Petroleum Technology Conference, 13-15 January, Dhahran, Kingdom of Saudi Arabia, 2020. doi: 10.2523/IPTC-20283-Abstract.

B. LeCompte, J. A. Franquet, and D. Jacobi. Evaluation of Haynesville Shale Vertical Well Completions With a Mineralogy Based Approach to Reservoir Geomechanics. pages 1–14. Society of Petroleum Engineers, SPE Annual Technical Conference and Exhibition, 4-7 October, New Orleans, Louisiana, 2009. doi: 10.2118/124227-MS.

D. Lee, D. Elsworth, H. Yasuhara, J. Weaver, and R. Rickman. An Evaluation of the Effects of Fracture Diagenesis On Fracture Treatments: Modeled Response. pages 1–12. International Society for Rock Mechanics and Rock Engineering, ISRM International Symposium - 10th Asian Rock Mechanics Symposium, 29 October - 3 November, Singapore, 2009.

D. S. Lee and H. Yasuhara. An evaluation of the effects of fracture diagenesis on hydraulic fracturing treatment. *Geosystems Engineering*, pages 113–118, 2013. doi: 10.1080/12269328.2013.780762.

D. S. Lee, D. Elsworth, H. Yasuhara, J. D. Weaver, and R. Rickmand. Experiment and modeling to evaluate the effects of proppant-pack diagenesis on fracture treatments. *Journal of Petroleum Science and Engineering*, 74(1–2):67–76, 2010. doi: 10.1016/j.petrol.2010.08.007.

T. Lee, D. Park, C. Shin, D. Jeong, and J. Choe. Efficient production estimation for a hydraulic fractured well considering fracture closure and proppant placement effects. *Energy Exploration and Exploitation*, 34 (4), 2016. doi: www.jstor.org/stable/90007421.

B. Legarth, E. Huenges, and G. Zimmermann. Hydraulic fracturing in a sedimentary geothermal reservoir: Results and implications. *International Journal of Rock Mechanics and Mining Sciences*, 42(7-8):61028–1041, 2005. doi: 10.1016/j.ijrmms.2005.05.014.

L. V. Lehman, M. A. Parker, M. E. Blauch, R. Haynes, and A. Blackmon. Proppant Conductivity What Counts and Why. pages 1–11. SPE Mid-Continent Operations Symposium, 28-31 March, Oklahoma City, Oklahoma, Society of Petroleum Engineers, 1999. doi: 10.2118/52219-MS.

J. Leimkuhler and G. Leveille. Unconventional Resources. *Society of Petroleum Engineers*, 08(1):1–3, 2012. doi: 10.2118/0112-026-TWA.

D. Li, F. He, W. Ou, J. Zhu, R. Li, and Y. Pan. Mechanism of multi-stage sand filling stimulation in horizontal shale gas well development. *Natural Gas Industry B*, 5(4):326–336, 2018. doi: 10.1016/j.ngib.2018.06.001.

J. Li, B. Li, Z. Wang, C. Ren, K. Yang, and S. Chen. An Anisotropic Permeability Model for Shale Gas Recovery Considering Slippage Effect and Embedded Proppants. *Natural Resources Research*, pages 1–24,

2020. doi: 10.1007/s11053-020-09660-0.

J. Li, P. Liu, S. Kuang, and A. Yu. Visual lab tests: Proppant transportation in a 3D printed vertical hydraulic fracture with two-sided rough surfaces. *Journal of Petroleum Science and Engineering*, (107738), 2021. doi: 10.1016/j.petrol.2020.107738.

K. Li, Y. Gao, Y. Lyu, and M. Wang. New Mathematical Models for Calculating Proppant Embedment and Fracture Conductivity. pages 1–12. Society of Petroleum Engineers, SPE Journal, 2015. doi: 10.2118/155954-PA.

M. Li, G. Yin, J. Xu, J. Cao, and Z. Song. Permeability evolution of shale under anisotropic true triaxial stress conditions. *International Journal of Coal Geology*, 165:142–148, 2016. doi: 10.1016/j.coal.2016.08.017.

F. Liang, M. Sayed, G. A. Al-Muntasheri, F. F. Chang, and L. Li. A comprehensive review on proppant technologies. *Petroleum*, 2(1):2639, 2016. doi: 10.1016/j.petlm.2015.11.001.

M. S. Liew, K. U. Danyaro, and N. A. W. A. Zawawi. A Comprehensive Guide to Different Fracturing Technologies: A Review. *Energies*, 13 (13):1–20, 2020. doi: 10.3390/en13133326.

H. Liu, P. Bedrikovetsky, Z. Yuan, J. Liu, and Y. Liu. An optimized model of calculating optimal packing ratio for graded proppant placement with consideration of proppant embedment and deformation. *Journal of Petroleum Science and Engineering*, 196(107703), 2021. doi: 10.1016/j.petrol.2020.107703.

Y. Liu, J. Y. Leung, and R. Chalaturnyk. Geomechanical Simulation of Partially Propped Fracture Closure and Its Implication for Water Flowback and Gas Production. pages 1–6. Society of Petroleum Engineers, SPE Res Eval & Eng 21 (02): 273290., 2018. doi: 10.2118/189454-PA.

X. Luo, Y. Qi, J. Li, P. Huang, S. Wang, X. Ren, and P. Zhang. Convection heat transfer and friction characteristics of liquid CO2-N2 foam fracturing fluid using C4F9OCH3 as frother. *Journal of Petroleum Science and Engineering*, (106461), 2019. doi: 10.1016/j.petrol.2019.106461.

Z. Luo, N. Zhang, L. Zhao, F. Liu, P. Liu, and N. Li. Modeling of pressure dissolution, proppant embedment, and the impact on long-term conductivity of propped fractures. *Journal of Petroleum Science and Engineering*, (106693), 2020a. doi: 10.1016/j.petrol.2019.106693.

Z. Luo, N. Zhang, L. Zhao, F. Liu, P. Liu, and N. Li. Modeling of pressure dissolution, proppant embedment, and the impact on long-term conductivity of propped fractures. *Journal of Petroleum Science and Engineering*, (106693), 2020b. doi: 10.1016/j.petrol.2019.106693.

Q. Lyu, J. Shi, and R. P. Gamage. Effects of testing method, lithology and fluid-rock interactions on shale permeability: A review of laboratory measurements. *Journal of Natural Gas Science and Engineering*, (103302), 2020. doi: 10.1016/j.jngse.2020.103302.

X. Lyu, F. Liu, P. Ren, and C. Grecos. An Image Processing Approach to Measuring the Sphericity and Roundness of Fracturing Proppants. *in IEEE Access*, 7:16078–16087, 2019. doi: 10.1109/ACCESS.2019.2894500.

H. Ma, C. Bao, Y. Tian, and G. Li. Effects of Feldspar Content on Microstructure and Property for High-Strength Corundum-Mullite Proppants. *Transactions of the Indian Ceramic Society*, 2020a. doi: 10.1080/0371750X.2019.1699863.

W. Ma, J. Perng, and I. Tomac. Experimental investigation of proppant flow and transport dynamics through fracture intersections. *Geomechanics for Energy and the Environment*, pages 1–18, 2020b. doi: 10.1016/j.gete.2020.100232.

X. Ma and M. D. Zoback. Static and Dynamic Response of Bakken Cores to Cyclic Hydrostatic Loading. *Rock Mechanics and Rock Engineering*, 51:19431953, 2018. doi: 10.1007/s00603-018-1443-z.

K. D. Mahrer. A review and perspective on far-field hydraulic fracture geometry studies. *Journal of Petroleum Science and Engineering*, 24(1): 13–28, 1999. doi: 10.1016/S0920-4105(99)00020-0.

M. Maslowski and M. Labus. Preliminary Studies on the Proppant Embedment in Baltic Basin Shale Rock. *Rock Mechanics and Rock Engineering*, pages 1–13, 2021. doi: 10.1007/s00603-021-02407-0.

M. Maslowski, P. Kasza, and K. Wilk. Studies on the effect of the proppant embedment phenomenon on the effective packed fracture in shale rock. *Acta Geodynamica et Geomaterialia*, 15(02):105115, 2018. doi: 10.13168/AGG.2018.0012.

J. C. Maxwell. *The Scientific Papers of James Clerk Maxwell*. Cambridge University Press, 1890. ISBN 9780511710377.

H. Melcher, M. Mayerhofer, K. Agarwal, E. Lolon, O. Oduba, J. Murphy, R. Ellis, K. Fiscus, R. Shelley, and L. Weijers. Shale Frac Designs Move to Just-Good-Enough Proppant Economics. pages 1–27. SPE Hydraulic Fracturing Technology Conference and Exhibition, 4-6 February, The Woodlands, Texas, USA, Society of Petroleum Engineers, 2020. doi: hhttps://doi.org/10.2118/199751-MS.

F. M. Michael, M. R. Krishnan, W. Li, and E. H. Alsharaeh. A Review on Polymer-Nanofiller Composites in Developing Coated Sand Proppants for Hydraulic Fracturing. *Journal of Natural Gas Science and Engineering*, page 103553, 2020. doi: 10.1016/j.jngse.2020.103553.

J. L. Miskimins and M. Alotaibi. The Impacts of Proppant Sorting and Dune Shape on Slickwater Hydraulic Fracturing Conductivity. pages 1–11. SPE/AAPG/SEG Asia Pacific Unconventional Resources Technology Conference, 18-19 November, Brisbane, Australia, Unconventional Resources Technology Conference, 2019. doi: 10.15530/AP-URTEC-2019-198208.

A. Mittal, C. S. Rai, and C. H. Sondergeld. Proppant-Conductivity Testing Under Simulated Reservoir Conditions: Impact of Crushing, Embedment, and Diagenesis on Long-Term Production in Shales. pages 1–12. SPE Journal, Society of Petroleum Engineers, 2018. doi: hhttps:

//doi.org/10.2118/191124-PA.

C. Montgomery and R. Steanson. Proppant Selection: The Key to Successful Fracture Stimulation. pages 1–10. Journal of Petroleum Technology, Society of Petroleum Engineers, 1985. doi: 10.2118/12616-PA.

M. Mueller and M. Amro. Indentaion Hardness for Improved Proppant Embedment Prediction in Shale Formations. pages 1–14. SPE European Formation Damage Conference and Exhibition, 3-5 June, Budapest, Hungary, Society of Petroleum Engineers, 2015. doi: 10.2118/174227-MS.

B.-S. Naima, F. DeBenedictis, M. Usie, and S. Bhaduri. A New-Intermediate Strength Proppant Additive to Combat Asphaltene Deposition for Delivering Long Term Flow Assurance. pages 1–13. Society of Petroleum Engineers, SPE International Conference and Exhibition on Formation Damage Control, 19-21 February, Lafayette, Louisiana, USA, 2020. doi: 10.2118/199283-MS.

S. Nakagawa and S. E. Borglin. Laboratory In-Situ Visualization of Long-Term Fracture Closure and Proppant Embedment in Brittle and Ductile Shale Samples. *American Rock Mechanics Association*, 2019. doi: https://www.onepetro.org/conference-paper/ARMA-2019-1996.

L. Neumann, P. Fernandes, M. Rosolen, V. Rodrigues, J. S. Neto, C. Pedroso, A. Mendez, and D. Torres. Case Study of Multiple-Hydraulic-Fracture Completion in a Subsea Horizontal Well, Campos Basin. pages 1–12. SPE Drilling & Completion, Society of Petroleum Engineers, 2010. doi: 10.2118/98277-PA.

P. D. Nguyen, R. G. Dusterhoft, and B. Clarkson. Control of Formation Fines to Provide Long-Term Conductivity in Weak, Unconsolidated Reservoirs. pages 1–17. Society of Petroleum Engineers, Offshore Technology Conference, 2-5 May, Houston, Texas, 2005. doi: 10.4043/17039-MS.

K. Nimerick, S. McConnell, and M. Samuelson. Compatibility of Resin–Coated Proppants With Crosslinked Fracturing Fluids. pages 1–5. Society of Petroleum Engineers, SSPE Production Engineering, 1992. doi: 10.2118/20639-PA.

L. Ning, S. Zhang, X. Ma, Y. Zou, S. Li, and Z. Zhang. Thermal effect on the evolution of hydraulic fracture conductivity: An experimental study of enhanced geothermal system. *Journal of Petroleum Science and Engineering*, 187(106814), 2020. doi: 10.1016/j.petrol.2019.106814.

M. Nobakht, R. Ambrose, C. R. Clarkson, J. E. Youngblood, and R. Adams. Effect of Completion Heterogeneity in a Horizontal Well With Multiple Fractures on the Long-Term Forecast in Shale-Gas Reservoirs. pages 1–9. Society of Petroleum Engineers, Journal of Canadian Petroleum Technology, 2013. doi: 10.2118/149400-PA.

L. Norman, J. Terracina, M. McCabe, and P. Nguyen. Application of Curable Resin-Coated Proppants. pages 1–7. Society of Petroleum Engineers, SPE Production Engineering, 1992. doi: 10.2118/20640-PA.

E. J. Novotny. Proppant Transport. pages 1–12. Society of Petroleum Engineers, SPE Annual Fall Technical Conference and Exhibition, 9-12 October, Denver, Colorado, 1977. doi: 10.2118/6813-MS.

A. A. Osiptsov, I. A. Garagash, S. A. Boronin, K. I. Tolmacheva, K. E. Lezhnev, and G. V. Paderin. Impact of Flowback Dynamics on Fracture Conductivity. *Journal of Petroleum Science and Engineering*, pages 1–24, 2020. doi: 10.1016/j.petrol.2019.106822.

T. T. Palisch, R. J. Duenckel, M. A. Chapman, S. Woolfolk, and M. C. Vincent. How to Use and Misuse Proppant Crush Tests – Exposing the Top 10 Myths. pages 1–15. Society of Petroleum Engineers, SP-SPE Hydraulic Fracturing Technology Conference, 19-21 January, The Woodlands, Texas, 2009. doi: 10.2118/119242-MS.

Z. Pan, Y. Ma, N. N. Danesh, L. D. Connell, R. Sander, D. I. Down, and M. Camilleri. Measurement of Shale Anisotropic Permeability and Its Impact on Shale Gas Production. pages 1–14. Society of Petroleum Engineers, PE Asia Pacific Unconventional Resources Conference and Exhibition, Brisbane, Australia, 2015. doi: 10.2118/176955-MS.

O. Perez, F. E. Fragachan, M. Omer, and J. Huang. Emerging Fluid Design with Enhanced Proppant Carrying Capacity: An Integrated Geomechanical Workflow. pages 1–12. International Petroleum Technology Conference, International Petroleum Technology Conference, 13-15 January, Dhahran, Kingdom of Saudi Arabia, 2020. doi: 10.2523/IPTC-20108-MS.

A. A. Pimenov and R. D. Kanevskaya. Mathematical Modeling of Proppant Embedment and Its Effect on Conductivity of Hydraulic Fracture. pages 1–8. SPE Russian Petroleum Technology Conference, 16-18 October, Moscow, Russia, Society of Petroleum Engineers, 2017. doi: 10.2118/187934-MS.

L. Qingyun, A. D. Jew, G. E. B. Jr, J. R. Bargar, and K. Maher. Reactive Transport Modeling of Shale-Fluid Interactions after Imbibition of Fracturing Fluids. *Energy& Fuels*, 2020. doi: 10.1021/acs.energyfuels.9b04542.

M. Radonjic, G. Luo, Y. Wang, M. Achang, J. Cains, A. Katende, J. Puckette, M. Grammer, and G. E. King. Integrated Microstructural Characterisation of Caney Shale, OK. pages 1–11. Society of Petroleum Engineers, SPE Reservoir Evaluation & Engineering, 2020. doi: 10.15530/urtec-2020-2947.

H. L. Ramandi, M. A. Pirzada, S. Saydam, C. Arns, and H. Roshan. Digital and experimental rock analysis of proppant injection into naturally fractured coal. *Fuel*, 286(Part1):1–7, 2021. doi: 10.1016/j.fuel.2020.119368.

A. S. Ramlan, R. M. Zin, N. F. A. Bakar, and N. H. Othman. Recent Progress on Proppant Laboratory Testing Method: Characterisation, Conductivity, Transportation, and Erosivity. *Journal of Petroleum Science and Engineering*, (108871):1–10, 2021. doi: 10.1016/j.petrol.

2021.108871.

N. Raysoni and J. D. Weaver. Long-Term Proppant Performance. pages 1–8. Society of Petroleum Engineers, SPE International Symposium and Exhibition on Formation Damage Control, 15-17 February, Lafayette, Louisiana, USA, 2012. doi: 10.2118/150669-MS.

A. Rezaei, F. Siddiqui, B. Dindoruk, and M. Y. Soliman. A Review on Factors Influencing the Rock Mechanics of the Gas Bearing Formations. *Journal of Natural Gas Science and Engineering*, (103348), 2020. doi: 10.1016/j.jngse.2020.103348.

H. Rogers. Shale gas–the unfolding story. *Oxford Review of Economic Policy*, 27(1):117–143, 2011. doi: 10.1093/oxrep/grr004.

J. Rutqvist. Fractured rock stress-permeability relationships from in situ data and effects of temperature and chemical-mechanical couplings. *Geofluids*, 15(1-2), 2015. doi: 10.1111/gfl.12089.

J. Rutqvist, A. P. Rinaldi, F. Cappa, and G. J. Moridis. Modeling of fault reactivation and induced seismicity during hydraulic fracturing of shale–gas reservoirs. *Journal of Petroleum Science and Engineering*, 107: 31–34, 2013. doi: 10.1016/j.petrol.2013.04.023.

J. Rutqvist, L. Zheng, F. Chen, H.-H. Liu, and J. Birkholzer. Modeling of Coupled Thermo-Hydro-Mechanical Processes with Links to Geochemistry Associated with Bentonite-Backfilled Repository Tunnels in Clay Formations. *Rock Mechanics and Rock Engineering*, 47:167–186, 2014. doi: 10.1007/s00603-013-0375-x.

R. Sahai and R. G. Moghanloo. Proppant transport in complex fracture networks A review. *Journal of Petroleum Science and Engineering*, 182(106199), 2019. doi: 10.1016/j.petrol.2019.106199.

J. N. Sallis, D. M. Agee, P. D. Artola, C. Guimaraes, and V. Chaloupka. Proppant Flowback Prevention with Next Generation Fiber Technology: Implementation of an Innovative Solution for HPHT Hydraulic Fracturing in Indonesia. pages 1–8. International Petroleum Technology Conference, International Petroleum Technology Conference, 10-12 December, Kuala Lumpur, Malaysia, 2014. doi: 10.2523/IPTC-17979-MS.

C. Sambo, C. C. Iferobi, A. A. Babasafari, S. Rezaei, and O. A. Akanni. The Role of 4D Time Lapse Seismic Technology as Reservoir Monitoring and Surveillance Tool: A Comprehensive Review. *Journal of Natural Gas Science and Engineering*, 2020. doi: 10.1016/j.jngse.2020.103312.

P. Sanematsu, Y. Shen, K. Thompson, T. Yu, Y. Wang, D.-L. Chang, B. Alramahi, AliTakbiri-Borujeni, M. Tyagi, and C. Willson. Image-based Stokes flow modeling in bulk proppant packs and propped fractures under high loading stresses. *Journal of Petroleum Science and Engineering*, 135:391–402, 2015. doi: 10.1016/j.petrol.2015.09.017.

D. Schmidt, P. R. Rankin, B. Williams, T. Palisch, and J. Kullman. Performance of Mixed Proppant Sizes. pages 1–10. SPE Hydraulic Fracturing Technology Conference, 4-6 February, The Woodlands, Texas, USA, Society of Petroleum Engineers, 2014. doi: 10.2118/168629-MS.

S. Schubarth and D. M. Tayler. Investigating How Proppant Packs Change Under Stress. pages 1–7. SPE Annual Technical Conference and Exhibition, 26-29 September, Houston, Texas, Society of Petroleum Engineers, 2004. doi: 10.2118/90562-MS.

E. Sharma and S. Livescu. New Laboratory Lubricity Research on Coiled Tubing Operations in Open-Hole Wells and Sand- or Proppant-Filled Cased-Hole Wells. pages 1–14. Society of Petroleum Engineers, SPE/ICoTA Well Intervention Conference and Exhibition, 24-25 March, The Woodlands, Texas, USA, 2020. doi: 10.2118/199848-MS.

L. Shenggui, J. Huang, S. Tang, S. Shi, X. Wu, and X. Liu. Experimental Study on the Damage of Artificial Fracture Permeability in Coal during the Flow Back of Guar-Based Fracturing Fluid. *Geofluids*, (8302310): 1–13, 2020. doi: 10.1155/2020/8302310.

F. Shi. XFEM-based numerical modeling of well performance considering proppant transport, embedment, crushing and rock creep in shale gas reservoirs. *Journal of Petroleum Science and Engineering*, 201:1–13, 2021. doi: 10.1016/j.petrol.2021.108523.

R. J. Shor and M. M. Sharma. Reducing Proppant Flowback From Fractures: Factors Affecting the Maximum Flowback Rate. pages 1–11. Society of Petroleum Engineers, SPE Hydraulic Fracturing Technology Conference, 4-6 February, The Woodlands, Texas, USA, 2014. doi: 10.2118/168649-MS.

Z. Shuang, R. Manchanda, and M. M. Sharma. Modeling Fracture Closure with Proppant Settling and Embedment during Shut-In and Production. pages 1–16. SPE Drilling & Completion, Society of Petroleum Engineers, 2020. doi: 10.2118/201205-PA.

R. Sierra, M. Tran, Y. Abousleiman, and R. Slatt. Woodford Shale Mechanical Properties And the Impacts of Lithofacies. pages 1–10. 44th U.S. Rock Mechanics Symposium and 5th U.S.-Canada Rock Mechanics Symposium, 27-30 June, Salt Lake City, Utah, American Rock Mechanics Association, 2010.

A. Sinclair, J. Graham, and C. Sinclair. Improved Well Stimulation With Resin-Coated Proppants. pages 1–8. Society of Petroleum Engineers, SPE Production Operations Symposium, 27 February-1 March, Oklahoma City, Oklahoma, 1983. doi: 10.2118/11579-MS.

M. Smith, A. Bale, L. Britt, H. Klein, E. Siebrits, and X. Dang. Layered Modulus Effects on Fracture Propagation, Proppant Placement, and Fracture Modeling. pages 1–14. Society of Petroleum Engineers, SPE Annual Technical Conference and Exhibition, 30 September-3 October, New Orleans, Louisiana, 2001. doi: 10.2118/71654-MS.

D. J. Soeder. The successful development of gas and oil resources from shales in North America. *Journal of Petroleum Science and Engineer-*

ing, 163:399–420, 2018. doi: 10.1016/j.petrol.2017.12.084.

D. J. Soeder and S. J. Borglum. Unconventional tight oil and shale gas resources. *The Fossil Fuel Revolution: Shale Gas and Tight Oil*, 2:31–61, 2019. doi: 10.1016/B978-0-12-815397-0.00003-3.

H. Song, Z. Liang, Z. Chen, and S. S. Rahman. Numerical modelling of hydraulic fracture propagation in poro-viscoelastic formation. *Journal of Petroleum Science and Engineering*, 196(107640), 2021a. doi: 10.1016/j.petrol.2020.107640.

L. Song, H. Yuan, Y. Gong, C. He, H. Zhou, X. Wan, W. Qin, S. Yang, and X. Ren. High-strength and long-term durable hydrophobic polystyrene microsphere: a promising ultra-lightweight proppant for fracturing technology. *Polymer Bulletin*, pages 1–10, 2021b. doi: 10.1007/s00289-021-03683-0.

S. Songire, C. Prakash, and R. Belakshe. Effects of Resin-Fluid Interaction on Fracturing Fluid Stability, Proppant Flowback, and Preventive Control Methods. pages 1–18. Society of Petroleum Engineers, SPE Middle East Oil and Gas Show and Conference, 18-21 March, Manama, Bahrain, 2019. doi: 10.2118/194959-MS.

P. A. Sookprasong. In-Situ Closure Stress on Proppant in the Fracture: A Controversial New Thinking. pages 1–7. Society of Petroleum Engineers, Tight Gas Completions Conference, 2-3 November, San Antonio, Texas, USA, 2010. doi: 10.2118/136338-MS.

Y. Suri, S. Z. Islam, and M. Hossain. Proppant transport in dynamically propagating hydraulic fractures using CFD-XFEM approach. *International Journal of Rock Mechanics and Mining Sciences*, 131(104356), 2020. doi: 10.1016/j.ijrmms.2020.104356.

E. Sutra, M. Spada, and P. Burgherr. Chemicals usage in stimulation processes for shale gas and deep geothermal systems: A comprehensive review and comparison. *Renewable and Sustainable Energy Reviews*, 77:1–10, 2017. doi: 10.1016/j.rser.2017.03.108.

F. E. Syfan and R. W. Anderson. Lower Quality Natural Quartz Proppants Result In Significant Conductivity Loss and Reduction In Ultimate Recovery: A Case History. pages 1–16. SPE Annual Technical Conference and Exhibition, 30 October-2 November, Denver, Colorado, USA, Society of Petroleum Engineers, 2011. doi: 10.2118/146827-MS.

P. Tan, H. Pang, R. Zhang, Y. Jin, Y. Zhou, J. Kao, and M. Fan. Experimental investigation into hydraulic fracture geometry and proppant migration characteristics for southeastern Sichuan deep shale reservoirs. *Journal of Petroleum Science and Engineering*, (106517), 2020. doi: 10.1016/j.petrol.2019.106517.

Y. Tan, Z. Pan, J. Liu, X.-T. Feng, and L. D. Connell. Laboratory study of proppant on shale fracture permeability and compressibility. *Fuel*, 222: 83–97, 2018. doi: 10.1016/j.fuel.2018.02.141.

S. Tandon, Z. Heidari, A. Aderiigbe, J. Shi, and T. Fuss-Dezelic. A new method for mechanical damage characterization in proppant packs using nuclear magnetic resonance measurements. *Journal of Petroleum Science and Engineering*, 167:343–353, 2018. doi: 10.1016/j.petrol.2018.03.087.

Q. Tang, G. hui Xue, S. jie Yang, K. Wang, and X. min Cui. Study on the preparation of a free-sintered inorganic polymer-based proppant using the suspensions solidification method. *Journal of Cleaner Production*, 148, 2017. doi: 10.1016/j.jclepro.2017.02.001.

Y. Tang and P. G. Ranjith. An experimental and analytical study of the effects of shear displacement, fluid type, joint roughness, shear strength, friction angle and dilation angle on proppant embedment development in tight gas sandstone reservoirs. *International Journal of Rock Mechanics and Mining Sciences*, 107, 2018. doi: 10.1016/j.ijrmms.2018.03.008.

Y. Tang, P. G. Ranjith, and B. Wu. Experimental study of effects of shearing on proppant embedment behaviour of tight gas sandstone reservoirs. *Journal of Petroleum Science and Engineering*, pages 1–7, 2019. doi: 10.1016/j.petrol.2018.07.066.

J. E. Tasque, I. N. Vega, S. Marco, P. A. Raffo, and N. B. D'Accorso. Ultra-light weight proppant: Synthesis, characterization, and performance of new proppants. *Journal of Natural Gas Science and Engineering*, 85:1–10, 2021. doi: 10.1016/j.jngse.2020.103717.

J. Terracina. Effects of Proppant Selection on Shale Fracture Treatments. pages 1–3. Journal of Petroleum Technology, Society of Petroleum Engineers, 2011.

J. Terracina, M. Parker, R. Pongratz, and R. Poole. How to Reduce Proppant Flowback in High-Rate Wells. pages 1–10. Society of Petroleum Engineers, SPE Middle East Oil Show, 17-20 March, Manama, Bahrain, 2000. doi: 10.2118/68202-MS.

J. M. Terracina, J. M. Turner, D. H. Collins, and S. Spillars. EProppant Selection and Its Effect on the Results of Fracturing Treatments Performed in Shale Formations. pages 1–17. SPE Annual Technical Conference and Exhibition, 19-22 September, Florence, Italy, Society of Petroleum Engineers, 2010. doi: 10.2118/135502-MS.

I. Tomac and M. Gutierrez. Micromechanics of proppant agglomeration during settling in hydraulic fractures. *Journal of Petroleum Exploration and Production Technology*, 5:417434, 2015. doi: 10.1007/s13202-014-0151-9.

O. Torsaeter, J. Kleppe, and T. van Golf-Racht. Multiphase Flow in Fractured Reservoirs. *Advances in Transport Phenomena in Porous Media*, 128:551–629, 1987. doi: 10.1007/978-94-009-3625-6_12.

J. M. Trela, P. D. Nguyen, and B. R. Smith. Controlling Proppant Flow Back to Maintain Fracture Conductivity and Minimize Workovers: Lessons Learned from 1,500 Fracturing Treatments. pages 1–15. Society of Petroleum Engineers, SPE International Symposium and Exhibition on Formation Damage Control, 13-15 February, Lafayette, Louisiana, USA, 2008. doi: 10.2118/112461-MS.

A. Vafaie and I. R. Kivi. An investigation on the effect of thermal maturity and rock composition on the mechanical behavior of carbonaceous shale formations. *Marine and Petroleum Geology*, 116, 2020. doi: hhttps://doi.org/10.1016/j.marpetgeo.2020.104315.

P. Valko and M. Economides. Foam Proppant Transport. pages 1–6. SPE Production & Facilities, Society of Petroleum Engineers, 1997. doi: 10.2118/27897-PA.

D. van Batenburg, E. Biezen, and J. Weaver. Towards Proppant Back-Production Prediction. pages 1–8. Society of Petroleum Engineers, SPE European Formation Damage Conference, 31 May-1 June, The Hague, Netherlands, 1999. doi: 10.2118/54730-MS.

D. Van-Batenburg, E. Biezen, and J. Weaver. Towards Proppant Back-Production Prediction. pages 1–8. SPE European Formation Damage Conference, 31 May-1 June, The Hague, Netherlands, Society of Petroleum Engineers, 1999. doi: 10.2118/54730-MS.

M. C. Vincent and P. T. Huckabee. Using Field Results to Guide Proppant Selection in the Pinedale Anticline. pages 1–8. Rocky Mountain Oil & Gas Technology Symposium, 16-18 April, Denver, Colorado, U.S.A., Society of Petroleum Engineers, 2007. doi: 10.2118/108991-MS.

L. J. Volk, C. J. Raible, H. B. Carroll, and J. S. Spears. Embedment Of High Strength Proppant Into Low-Permeability Reservoir Rock. pages 1–15. SPE/DOE Low Permeability Gas Reservoirs Symposium, 27-29 May, Denver, Colorado, Society of Petroleum Engineers, 1981. doi: 10.2118/9867-MS.

M. Voltolini. In-situ 4D visualization and analysis of temperature-driven creep in an oil shale propped fracture. *Journal of Petroleum Exploration and Production Technology*, pages 1–10, 2021. doi: 10.1016/j.petrol.2021.108375.

M. Voltolini and J. Ajo-Franklin. Evolution of propped fractures in shales: The microscale controlling factors as revealed by in situ X-Ray microtomography. *Journal of Petroleum Science and Engineering*, (106861), 2020. doi: 10.1016/j.petrol.2019.106861.

M. Voltolini, J. Rutqvist, and T. Kneafsey. Coupling dynamic in situ X-ray micro-imaging and indentation: A novel approach to evaluate micromechanics applied to oil shale. *Fuel*, (120987):1–12, 2021. doi: 10.1016/j.fuel.2021.120987.

D. Wang, H. Wang, F. Li, M. Chen, and A. P.Bunger. Parameters affecting the distribution of pulsed proppant in hydraulic fractures. *Journal of Petroleum Science and Engineering*, 191(107125), 2020a. doi: 10.1016/j.petrol.2020.107125.

D. Wang, Z. You, R. L. Johnson, L. Wu, P. Bedrikovetsky, S. M. Aminossadati, and C. R. Leonardi. Numerical investigation of the effects of proppant embedment on fracture permeability and well production in Queensland coal seam gas reservoirs. *International Journal of Coal Geology*, 144:1–15, 2021. doi: 10.1016/j.coal.2021.103689.

J. Wang and D. Elsworth. Fracture Penetration and Proppant Transport in Gas- and Foam-Fracturing. *Journal of Natural Gas Science and Engineering*, (103269), 2020. doi: 10.1016/j.jngse.2020.103269.

J. Wang and D. Elsworth. Role of proppant distribution on the evolution of hydraulic fracture conductivity. *Journal of Petroleum Science and Engineering*, 166:249–262, 2018. doi: 10.1016/j.petrol.2018.03.040.

J. Wang, D. Elsworth, and M. K. Denison. Propagation, proppant transport and the evolution of transport properties of hydraulic fractures. *Journal of Fluid Mechanics*, 855:503–534, 2018a. doi: hhttps://doi.org/10.1017/jfm.2018.670.

J. Wang, D. Elsworth, and T. Ma. Conductivity Evolution of Proppant-Filled Hydraulic Fractures. pages 1–14. 52nd U.S. Rock Mechanics/Geomechanics Symposium, 17-20 June, Seattle, Washington, American Rock Mechanics Association, 2018b. doi: https://www.onepetro.org/conference-paper/ARMA-2018-111.

J. Wang, Y. Huang, Y. Zhang, F. Zhou, E. Yao, and R. Wang. Study of Fracturing Fluid on Gel Breaking Performance and Damage to fracture conductivity. *Journal of Petroleum Science and Engineering*, (107443), 2020b. doi: 10.1016/j.petrol.2020.107443.

J. Wang, Y. Huang, F. Zhou, and X. Liang. The influence of proppant breakage, embedding, and particle migration on fracture conductivity. *Journal of Petroleum Science and Engineering*, 193(107385), 2020c. doi: hhttps://doi.org/10.1016/j.petrol.2020.107385.

L. Wang, J. D. Fortner, and D. E. Giammar. Impact of Water Chemistry on Element Mobilization from Eagle Ford Shale. *Environmental Engineering Science*, 32(4):310–320., 2015. doi: 10.1089/ees.2014.0342.

Q. Wang and R. Li. Research status of shale gas: A review. *Renewable Energy and Sustainable Energy Reviews*, 74:715–720, 2017. doi: 10.1016/j.rser.2017.03.007.

J. D. Weaver, P. D. Nguyen, M. A. Parker, and D. W. van Batenburg. Sustaining Fracture Conductivity. pages 1–10. Society of Petroleum Engineers, SPE European Formation Damage Conference, 25-27 May, Sheveningen, The Netherlands, 2005. doi: 10.2118/94666-MS.

J. D. Weaver, D. W. van Batenburg, and P. D. Nguyen. Sustaining Conductivity. pages 1–14. Society of Petroleum Engineers, SPE International Symposium and Exhibition on Formation Damage Control, 15-17 February, Lafayette, Louisiana, USA, 2006. doi: 10.2118/98236-MS.

J. D. Weaver, M. Parker, D. W. van Batenburg, and P. D. Nguyen. Fracture-Related Diagenesis May Impact Conductivity. pages 1–10. Society of Petroleum Engineers, SPE Journal, 2007. doi: 10.2118/98236-PA.

J. D. Weaver, R. D. Rickman, and H. Luo. Fracture-Conductivity Loss Due to Geochemical Interactions Between Manmade Proppants and Formations. pages 1–12. SPE Eastern Regional/AAPG Eastern Section Joint

Meeting, 11-15 October, Pittsburgh, Pennsylvania, USA, Society of Petroleum Engineers, 2008. doi: 10.2118/118174-MS.

J. D. Weaver, R. Rickman, H. Luo, and D. Elsworth. Fracture-Conductivity Loss Caused By Geochemical Interactions Between Man-Made Proppants And Formations. pages 1–12. 43rd U.S. Rock Mechanics Symposium & 4th U.S. - Canada Rock Mechanics Symposium, 28 June-1 July, Asheville, North Carolina, American Rock Mechanics Association, 2009a.

J. D. Weaver, R. D. Rickman, H. Luo, and R. Logrhy. A Study of Proppant Formation Reactions. pages 1–16. Society of Petroleum Engineers, SPE International Symposium on Oilfield Chemistry, 20-22 April, The Woodlands. Texas, 2009b. doi: 10.2118/121465-MS.

J. D. Weaver, R. D. Rickman, and H. Luo. Fracture-Conductivity Loss Caused by Geochemical Interactions Between Man-Made Proppants and Formations. pages 1–9. SPE Journal, Society of Petroleum Engineers, 2010. doi: 10.2118/118174-PA.

G. Wei, T. Babadagli, H. Huang, L. Hou, and H. Li. A visual experimental study: Resin-coated ceramic proppants transport within rough vertical models. *Journal of Petroleum Science and Engineering*, (107142):1–13, 2020. doi: 10.1016/j.petrol.2020.107142.

M. Wei, Y. Duan, M. Dong, Q. Fang, and M. Dejam. Transient Production Decline Behavior Analysis for a Multi-Fractured Horizontal Well with Discrete Fracture Networks in Shale Gas Reservoirs. *Journal of Porous Media*, 22(3):343–361, 2019. doi: 10.1615/JPorMedia.2019028982.

Q. Wen, S. Zhang, L. Wang, Y. Liu, and X. Li. The effect of proppant embedment upon the long-term conductivity of fractures. *Journal of Petroleum Science and Engineering*, 55(3-4):37–45, 2007. doi: 10.1016/j.petrol.2006.08.010.

W. Wick, S. Taneja, I. Gupta, C. H. Sondergeld, and C. S. Rai. Chemically Induced Formation Damage in Shale. pages 1–11. Society of Petrophysicists and Well-Log Analysts, Petrophysics, 2020.

X. Wu, Z. Huo, Q. Ren, H. Li, F. Lin, and T. Wei. Preparation and characterization of ceramic proppants with low density and high strength using fly ash. *Journal of Alloys and Compounds*, 702, 2017. doi: 10.1016/j.jallcom.2017.01.262.

H. Xiao, Z. Li, S. He, X. Lu, P. Liu, and J. Li. Experimental study on proppant diversion transportation and multi-size proppant distribution in complex fracture networks. *Journal of Petroleum Science and Engineering*, page 107800, 2021. doi: 10.1016/j.petrol.2020.107800.

T. Xiao, H. Xu, N. Moodie, R. Esser, W. Jia, L. Zheng, J. Rutqvist, and B. McPherson. Chemical-Mechanical Impacts of CO2 Intrusion Into Heterogeneous Caprock. *Water Resources Research*, 56(11):1–8, 2020. doi: 10.1029/2020WR027193.

W. Xiong, M. Gill, J. Moore, D. Crandall, J. A. Hakala, and C. Lopano. Influence of Reactive Flow Conditions on Barite Scaling in Marcellus Shale during Stimulation and Shut-In Periods of Hydraulic Fracturing. *Energy & Fuels*, 34(11), 2020. doi: 10.1016/j.jngse.2020.103348.

J. Xu, Y. Ding, L. Yang, Z. Liu, R. Gao, H. Yang, and Z. Wang. Effect of proppant deformation and embedment on fracture conductivity after fracturing fluid loss. *Journal of Natural Gas Science and Engineering*, 71(102986), 2019. doi: 10.1016/j.jngse.2019.102986.

J. Xu, Y. Ding, L. Yang, Z. Liu, R. Gao, H. Yang, and Z. Wang. Conductivity analysis of hydraulic fractures filled with nonspherical proppants in tight oil reservoir. *Energy Science and Engineering*, pages 1–13, 2020. doi: 10.1002/ese3.517.

M. Yang, Y. Lu, Z. Ge, Z. Zhou, C. Chai, and L. Zhang. Optimal selection of viscoelastic surfactant fracturing fluids based on influence on coal seam pores. *Advanced Powder Technology*, 31(6):2179–2190, 2020. doi: 10.1016/j.apt.2020.03.005.

S. Yang, N. Harris, T. Dong, W. Wu, and Z. Chen. Mechanical Properties and Natural Fractures in a Horn River Shale Core from Well Logs and Hardness Measurements. pages 1–13. Society of Petroleum Engineers, EUROPEC 2015, 1-4 June, Madrid, Spain, 2015. doi: 10.2118/174287-MS.

S. Yang, N. B. Harris, T. Dong, W. Wu, and Z. Chen. Natural Fractures and Mechanical Properties in a Horn River Shale Core From Well Logs and Hardness Measurements. pages 1–12. Society of Petroleum Engineers, SPE Reservoir Evaluation & Engineering, 2018. doi: 10.2118/174287-PA.

Y. Yang, C. J. Robart, and M. Ruegamer. Analysis of U.S. Hydraulic Fracturing Design Trends. pages 1–14. Society of Petroleum Engineers, SPE Hydraulic Fracturing Technology Conference, 4-6 February, The Woodlands, Texas, USA, 2013. doi: 10.2118/163875-MS.

H. Yasuhara, D. Elsworth, and A. Polak. A mechanistic model for compaction of granular aggregates moderated by pressure solution. *JJournal of Geophysical Research: Solid Earth*, 76:1–15, 2003. doi: 10.1029/2003JB002536.

L. Yiman, T. Huang, Z. Pang, and C. Jin. Geochemical processes during hydraulic fracturing: a water-rock interaction experiment and field test study. *Geosciences Journal*, 21:753763, 2017. doi: 10.1007/s12303-017-0114-5.

W. Yu, T. Zhang, S. Du, and K. Sepehrnoori. Numerical study of the effect of uneven proppant distribution between multiple fractures on shale gas well performance. *Fuel*, 142:189–198, 2015. doi: 10.1016/j.fuel.2014.10.074.

M. Yue, Q. Zhang, W. Zhu, L. Zhang, H. Song, and J. Li. Effects of proppant distribution in fracture networks on horizontal well performance. *Journal of Petroleum Science and Engineering*, 187(106816), 2020. doi: 10.1016/j.petrol.2019.106816.

W. Yuepeng, X. Liu, L. Liang, and J. Xiong. Experimental study on the damage of organic-rich shale during water-shale interaction. *Journal of Natural Gas Science and Engineering*, (103103), 2020. doi: 10.1016/j.jngse.2019.103103.

C. Yun, H. Wang, T. Li, Y. Wang, F. Ren, and G. Ma. Evaluation of geothermal development considering proppant embedment in hydraulic fractures. *Renewable Energy*, 153:985–997, 2020. doi: 10.1016/j.renene.2020.02.063.

B. Zanganeh, M. Ahmadi, C. Hanks, and O. Awoleke. The role of hydraulic fracture geometry and conductivity profile, unpropped zone conductivity and fracturing fluid flowback on production performance of shale oil wells. *Journal of Unconventional Oil and Gas Resources*, pages 1–7, 2015. doi: 10.1016/j.juogr.2014.11.006.

F. Zeng, Y. Zhang, J. Guo, Q. Zhang, Z. Chen, J. Xiang, and Y. Zheng. Optimized completion design for triggering a fracture network to enhance horizontal shale well production. *Journal of Petroleum Science and Engineering*, 190(107043), 2020a. doi: 10.1016/j.petrol.2020.107043.

L. Zeng, N. Reid, Y. Lu, M. M. Hossain, A. Saeedi, and Q. Xie. Effect of the FluidShale Interaction on Salinity: Implications for High-Salinity Flowback Water during Hydraulic Fracturing in Shales. *Energy& Fuels*, 34(3):3031–3040, 2020b. doi: 10.1021/acs.energyfuels.9b04311.

J. Zhang and J. Hou. Theoretical conductivity analysis of surface modification agent treated proppant II Channel fracturing application. *Fuel*, 165(1):28–32, 2015. doi: 10.1016/j.fuel.2015.10.026.

J. Zhang, L. Ouyang, D. Zhu, and A. Hil. Experimental and numerical studies of reduced fracture conductivity due to proppant embedment in the shale reservoir. *Journal of Petroleum Science and Engineering*, (130):37–45, 2015. doi: 10.1016/j.petrol.2015.04.004.

L. Zhang, Z. Kou, H. Wang, Y. Zhao, M. Dejam, J. Guo, and J. Du. Performance analysis for a model of a multi-wing hydraulically fractured vertical well in a coalbed methane gas reservoir. *Journal of Petroleum Science and Engineering*, 166:104–120, 2018. doi: 10.1016/j.petrol.2018.03.038.

X. Zhao, E. He, J. Guo, Z. Haiyan, H. Wang, and W. He. The study of fracture propagation in pre-acidized shale reservoir during the hydraulic fracturing. *Journal of Petroleum Science and Engineering*, 184:106488, 2020. doi: 10.1016/j.petrol.2019.106488.

L. Zheng, J. Rutqvist, H.-H. Liu, J. T. Birkholzer, and E. Sonnenthal. Model evaluation of geochemically induced swelling/shrinkage in argillaceous formations for nuclear waste disposal. *Applied Clay Science*, 97-98:24–32, 2014. doi: 10.1016/j.clay.2014.05.019.

W. Zheng and D. D. Tannant. Influence of proppant fragmentation on fracture conductivity - Insights from three-dimensional discrete element modeling. *Journal of Petroleum Science and Engineering*, 177:1010–1023, 2019. doi: 10.1016/j.petrol.2019.03.015.

W. Zheng, D. D. Tannant, X. Cui, C. Xu, and X. Hu1. Improved discrete element modeling for proppant embedment into rock surfaces. *JActa Geotechnica*, 15:347364, 2020. doi: 10.1007/s11440-019-00819-5.

S. Zhi and D. Elsworth. Proppant embedment in coal and shale: Impacts of stress hardening and sorption. *International Journal of Coal Geology*, (103545), 2020. doi: 10.1016/j.coal.2020.103545.

Y. Zhong, E. Kuru, H. Zhang, J. Kuang, and J. She. Effect of Fracturing Fluid/Shale Rock Interaction on the Rock Physical and Mechanical Properties, the Proppant Embedment Depth and the Fracture Conductivity. *Rock Mechanics and Rock Engineering*, 52:10111022, 2019. doi: 10.1007/s00603-018-1658-z.

H. Zhuo, S. Deng, Z. Huang, C. Xia, Y. Zeng, and J. Jiang. Conductivity performance evaluation of fractures filled with proppant of different sizes in shale with LBM-DEM. *International Journal of Oil and Gas Technology*, 23(1), 2020. doi: 10.1504/IJOGCT.2020.104972.

M. Zoveidavianpoor, A. Gharibi, and M. Z. bin Jaafar. Experimental characterization of a new high-strength ultra-lightweight composite proppant derived from renewable resources. *Journal of Petroleum Science and Engineering*, 170:1038–1047, 2018. doi: 10.1016/j.petrol.2018.06.030.